FACULDADE DE ENGENHARIA DA UNIVERSIDADE DO PORTO

Exploring Sensors Fusion on the Design of Dependable Wearable Medical Electronic Systems

Cristina da Cunha Oliveira

Programa Doutoral em Engenharia Biomédica

Supervisor: José Machado da Silva

November 7, 2016

Exploring Sensors Fusion on the Design of Dependable Wearable Medical Electronic Systems

Cristina da Cunha Oliveira

Programa Doutoral em Engenharia Biomédica

November 7, 2016

Abstract

A new methodology for designing dependable medical systems is proposed. A systematic strategy for achieving dependability has been developed and demonstrated considering all the main blocks of a wearable medical system and its own requirements (reliability, safety/security, availability, maintainability, etc) and risks for dependability. A framework is defined to help identifying the main critical blocks of the system and perform a fault tree analysis.

The proposed methodology has been applied in the development of a new non-invasive aortic stent-graft monitoring system based on RFID technology, recurring to data fusion techniques and dependability analysis in order to obtain the best levels of performance, trust and functionality.

The abdominal aorta pressure monitoring system uses an inductive coupling interface to capture the pressure levels measured by a sensor cluster placed on the stent-graft. The processing of this set of signals with other physiological signals like the electrocardiogram (ECG) and arterial blood pressure (ABP) allows obtaining better resolution and decision trust with the acquired information in terms of fault identification in a wearable cardiovascular surveillance system.

After the identification of the main risks and threats for the correct functioning of the wearable monitoring system, specific design for testability and reconfiguration techniques can be developed. Regarding the cardiovascular system under analysis, a new fault detection and diagnosis method for the implanted pressure sensor was developed.

Data fusion techniques for the analysis and diagnosis of the captured vital signs complements the system. The data fusion was accomplished by employing several algorithms, notably fuzzy logic, artificial neural networks, decision trees and naive Bayes classifier, in order to correctly diagnose the patient and system status. All the tested algorithms are able to make a correct diagnosis, but the naive Bayes classifier allows obtaining the best results.

This approach can be used both for the identification of specific built-in self-test strategies, as well as for online diagnosis of anomalies which could be due to pathologies in the patient or malfunctions in the system.

Resumo

Na presente tese é proposta uma nova metodologia para o projeto de sistemas médicos com elevados níveis de dependabilidade. É estudada e implementada uma estratégia sistemática para alcançar elevados níveis de dependabilidade, considerando todos os principais blocos de um sistema médico vestível e os seus requisitos próprios (fiabilidade, segurança, disponibilidade, facilidade de manutenção, etc) e os riscos para a dependabilidade. É apresentada uma estrutura (*framework*) para análise da dependabilidade que auxilia o processo de identificação dos blocos mais críticos do sistema através da realização uma análise de árvore de falhas.

A metodologia proposta foi aplicada no desenvolvimento de um novo sistema de monitorização de próteses endovasculares não invasivo e baseado em tecnologia RFID, onde se recorre a técnicas de fusão de sinais e à análise de dependabilidade a fim de obter melhores níveis de desempenho, confiança e funcionamento.

O sistema de monitorização recorre a uma interface por acoplamento indutivo para capturar os níveis de pressão medidos por um *cluster* de sensores colocados nas paredes de uma prótese endovascular. O processamento conjunto destes sinais com outros sinais fisiológicos como o eletrocardiograma (ECG) e a pressão arterial (PA) permite obter melhor resolução e confiança de decisão perante a informação obtida, em termos de identificação de falhas na prótese endovascular e nos sensores de pressão num sistema de monitorização cardiovascular vestível.

O projeto de técnicas especificas de testabilidade e reconfiguração pode ser então desenvolvido, após a identificação dos principais riscos e ameaças para o correto funcionamento do sistema de monitorização vestível. Em relação ao sistema cardiovascular em análise, foi desenvolvido um novo método de deteção e diagnóstico de falhas do sensor de pressão implantado.

O sistema é complementado com técnicas de fusão de dados para a análise e diagnóstico dos sinais vitais capturados. A fusão de dados é realizada através da utilização de vários algoritmos, nomeadamente a lógica fuzzy, redes neuronais artificiais, árvores de decisão e classificador *naive* de Bayes, a fim de diagnosticar corretamente o estado do paciente e do sistema. Todos os algoritmos testados proporcionam um diagnóstico correto, mas o classificador *naive* de Bayes apresenta os melhores resultados.

Esta abordagem pode ser utilizada tanto para a identificação específica de estratégias de autoteste, bem como para o diagnóstico em-linha com o funcionamento de anomalias que possam ser devidas a patologias no paciente ou avarias no sistema.

Acknowledgments

First of all I would like to thank my supervisor Professor José Machado da Silva for all the support provided during the development of this thesis. I am also grateful for his scientific advice and knowledge and many insightful discussions and suggestions.

I am also thankful to FEUP and INESC TEC for providing all the necessary facilities, equipments and materials and therefore enabling the success of all the experimental work. Most of my work was carried out in the I223 lab from the Department of Electrical and Computer Engineering with a great team of researchers. We had many technical discussions and enjoyed each others accomplishments. I would like to thank my colleagues Nuno, Ruben, Bruno, Ganga and Fardin.

My sincere thanks to Professor Joaquim Gabriel Mendes from the Department of Mechanical Engineering for his assistance with the experiments using the hydraulic model, to Professor Cidália Botelho from the Department of Chemical Engineering for providing the means to make the simulated biological materials and Professor Luís Rocha and Alexandra Sepúlveda from the University of Minho for helping me with the measurements in the vacuum chamber.

I also would like to thank Antonio J. Salazar for his assistance with the impedance measurements, professor Miguel V. Correia for the support with the Biopac equipment, and Pedro Fonseca from LABIOMEP–University of Porto for the guidance on the acquisition and analysis of the EMG signal.

Last but not least, I would like to thank my family and friends, especially my husband Rui, my parents and my sister. The PhD work is quite demanding, time consuming and stressful but I could always count on their support and understanding.

This work has been carried-out in the framework of projects MIT-Pt/EDAM-EMD/0007/2008 and PTDC/EEI-ELC/1838/2012, with the support of the ERDF – European Regional Development Fund through the COMPETE Programme (operational programme for competitiveness) and national funds through FCT- Fundação para a Ciência e a Tecnologia (Portuguese Foundation for Science and Technology), and grant contract SFRH/BD/81476/2011.

Cristina da Cunha Oliveira

"Somewhere, something incredible is waiting to be known."

Carl Sagan

Contents

List of Figures

List of Tables

List of Acronyms and Symbols

Abbreviations

AAA	Abdominal Aortic Aneurysm
AAL	Ambient Assisted Living
ABP	Arterial Blood Pressure
A–CNTs	Aligned Carbon Nanotubes
ANN	Artificial Neural Network
BAN	Body Area Network
BIST	Built-in Self Test
BP	Blood Pressure
CAD	Coronary Artery Disease
CI	Confidence Interval
CMRR	Common Mode Rejection Ratio
CT	Classification Trees
DUT	Device Under Test
ECG	Electrocardiogram
EEG	Electroencephalography
ERU	Electronic Readout Unit
EVAR	Endovascular Endovascular Aneurism Repair
FEUP	Faculdade de Engenharia da Universidade do Porto
FIT	Failures In Time
FFT	Fast Fourier Transform
FL	Fuzzy Logic
FMEA	Failure Mode and Effects Analysis
FMECA	Failure Modes, Effects and Criticality Analysis
FN	False Negatives
FP	False Positives
FTA	Fault Tree Analysis
HCI	Hot Carrier Injection
HEC	Hydroxyethyl Cellulose
HR	Heart Rate
IBC	Intelligent Biomedical Clothing
IEC	International Electrotechnical Commission
IEV	International Electrotechnical Vocabulary
IP	Intellectual Property
MAP	Mean Arterial Pressure
MDT	Mean Down Time
MTBF	Mean Time Before Failure
MTTF	Mean Time To Failure
MVC	Maximum Voluntary Contraction

Abbreviations

NBC	Naive Bayes Classifiers
NBTI	Negative Bias Temperature Instability
PAD	Peripheral Artery Disease
PBTI	Positive Bias Temperature Instability
PC	Personal Computer
PDMS	Polydimethylsiloxane
PMA	Premarket Approval
PGA	Programmable Gain Amplifier
Q	Quality Factor
SCSs	Safety-critical Systems
SIL	Safety Integrity Level
SNR	Signal to Noise Ratio
SpO2	Oxygen Saturation
SRF	Self–resonant Frequencies
SVM	Support Vector Machine
TDDB	Time Dependent Dielectric Breakdown
TP	True Positives
TN	True Negatives
VNA	Vector Network Analyser
WHMS	Wireless Home Care Monitoring Systems
WLAN	Wireless Local Area Network
WPAN	Wireless Personal Area Network
WSN	Wireless Sensor Networks

Symbols	Unit	Meaning
C_s	F	Sensor's capacitance
f_{osc}	Hz	Oscillation frequency
L_s	H	Sensor's inductance
R_s	Ω	Sensor's resistance
Z_L	Ω	Impedance
μ		Mean
μC		Microcontroller
σ		Variance

Chapter 1

Introduction

Recent developments of electronics, informatics and telecommunications have contributed to improve the quality of the healthcare services offered in clinics, as well as on remote. In fact, this is particularly true with the new possibilities provided by telemedicine and telemonitoring of patients at distance.

Along with the progress of medical technologies, many countries are gradually becoming geriatric societies due to the rapid growth of the ageing population. This has increased the requirement for home health monitoring systems for securing independent lives of patients with chronic disorders or that have health care problems. The advances on sensors, wireless communications, and information technologies have promoted the rapid development of various wellness or disease monitoring systems, which enable extended independent living at home and improve the quality of life.

Traditionally, medicine for older adults has been based on an intervention basis (drugs, surgeries, prosthesis, etc.) to treat them. Nowadays, and regardless of the patients' age, the health care community is trying to focus on prevention, and wearable monitoring systems have been proposed to meet this task. Therefore diseases are intended to be prevented, rather than treated, by the continuous monitoring of vital signals, which provide information on the health status related with lifestyle and overall quality of life [1, 2, 3].

In parallel with the new possibilities being offered we found also the concern with the dependability of these systems. Biomedical electronic systems are safety-critical systems (SCSs) given that their failure could result in wrong diagnosis or treatments, or even the loss of lives.

1.1 Wearable Devices

The technological advances in sensors, low–power miniaturized microelectronic, and wireless networking enabled the design and proliferation of wireless sensor networks capable of autonomously monitoring and controlling environments applied to human health care. This can be achieved through a number of tiny wireless sensors strategically placed on the human body, creating what

became generally known as body area networks, which provide real–time feedback to medical personnel, alert when life threatening changes occur, and also communicate with the user in order to help himself maintaining an optimal health status, act on the level of awareness and allow better control of his own conditions [4, 5].

Remote health monitoring can be used only if the monitoring device is based on a comfortable sensing interface, easy to use and customizable. Its interface must allow continuous remote control in a natural environment without interference or discomfort for the users. The textile approach to embed sensing elements in clothing items allows lowering the cost of long–term monitoring of patients, as well as to easily customize the sensor configuration according to the needs of each individual [5]. By applying this concept it is possible to reduce health care costs maintaining high quality of care, shift the focus of health care expenditures from treatment to prevention, provide access to health care to a larger number of patients, reduce the length of hospital stays and address the elderly population and/or chronically ill patients issues. It also eases the access to specialized professionals through telemetry, thus decentralizing the provision of health care.

Because these wearable monitoring systems are to be used for medical purposes (continuous monitoring, diagnosis, etc.), their reliability and safety have to be perfectly controlled. Unfortunately, the complexity of these systems increases endlessly, making the existing dependability techniques developed for other safety-critical systems, such as aeronautics, space, and automotive fields, not totally appropriate for the medical field.

1.2 Research motivation

Nowadays there are several wearable medical monitoring systems available, all with different architectures, components, characteristics, and designs. Nevertheless all authors state that high levels of reliability, security, safety, availability and maintainability are required. Such high levels of dependability are difficult to achieve due to the complexity of these monitoring systems, which have different blocks and layers (sensors, acquisition system, software, networks, etc).

Conventional medical monitoring devices being used in hospitals are well established in terms of systems' architecture and functional behaviour. Moreover, if the monitoring system triggers an alarm, a trained health care practitioner, nurse or physician, will check if the patient has a real health problem or if it is a false alarm due to, e. g., the loosening of electrodes, disconnected cables, patient's sudden movement that caused a signal distortion, among others. False alarms in intensive care units (ICU) are more frequent than desired. ICU false alarm rates as high as 86% have been reported, with between 6% and 40% of ICU alarms having been reported to be true but clinically insignificant (requiring no immediate action) [6]. In fact, only 2% to 9% of alarms have been found to be important for patient management [7]. These false alarms can cause several issues such as: lead to a disruption of care, impacting both the patient and the clinical staff through noise disturbances, desensitization to warnings and slowing of response times, leading to decreased quality of care [8].

As for the case of wearable medical devices, whose main objective is a pervasive monitoring during the daily activities outside the health care facilities, there are no health technicians available to verify if an alarm produced by the monitoring system is accurate or whether an external event is causing a false alarm. Therefore, in order for wearable medical devices to succeed, a reliable real time diagnosis is mandatory.

1.3 Data Fusion

Data fusion techniques are often used to improve healthcare monitoring systems in mainly two aspects. The first is to increase the trust levels of the bio signals readings by reject or correct distorted vital sign signals, and the second is to provide additional information on the patient's condition by classifying the set of signals into normal or abnormal condition (e.g. arrhythmia, chest angina or stroke).

1.4 Research contributions

The main objective of this work was to develop a methodology to design dependable wearable medical systems. The approach proposed in this thesis aims at contributing to solve this problem by carefully studying the main components of wearable medical systems and model their behaviour. The obtained model allows for, in the one hand, to identify the most critical blocks or elements and guide the design of specific built-in test methods for the most sensitive parts of the system, and, on the other hand, to develop data analysis methods optimized to detect on-line the most likely to occur faults. The outcome of the system characterization and assessment of necessary test circuits methodology, is put to use by providing useful data about the monitoring system status. The understanding of how the monitoring system's deviation from its normal behaviour affects the bio signals is extremely important, since for instance a deviation on the sensors or amplifiers can cause an artefact and lead to a false diagnosis. The fusion of both the monitoring system signals and the patient vital signs is sought here to improve the functioning and diagnosis of medical wearable devices.

Medical and healthcare application systems demand high levels of dependability and trust of performance [9]. According to the IEC (International Electrotechnical Commission) IEV (International Electrotechnical Vocabulary) 191-02-03 standard "dependability (is) the collective term used to describe the availability performance and its influencing factors: reliability performance, maintainability performance and maintenance support performance". A system's dependability study includes the attributes analysis (e.g., availability, security and maintainability), risks (defects and failures), means (of prevention, detection and fault tolerance) and enables the objective of an efficient development of test and self-test methodologies.

The lack of a dependability model for the development of complex pervasive medical monitoring devices led to the need of developing such a model. The ultimate strategy for achieving dependability in medical wearable devices is summarized in fig. 1.1. A systematic and normalized

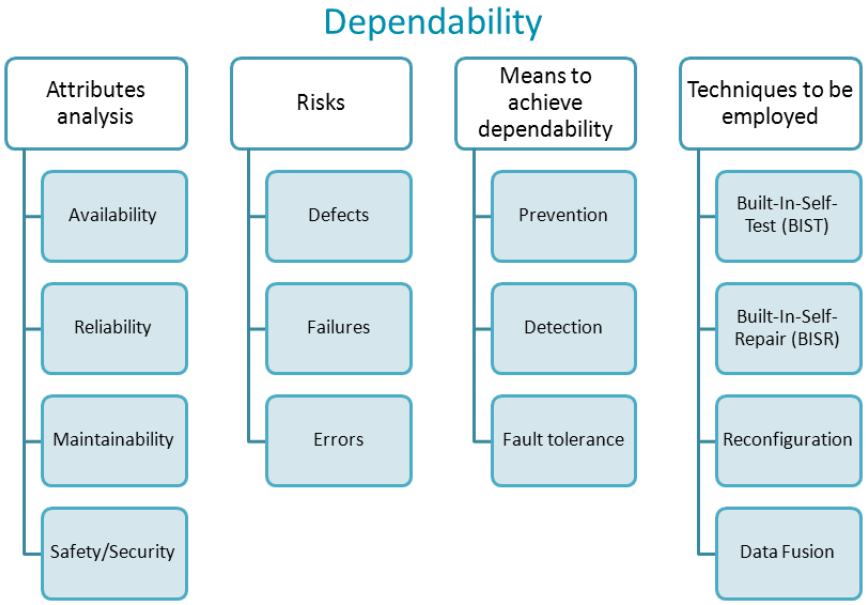

Figure 1.1: Dependability framework.

strategy for achieving dependability was studied and implemented, considering all the main blocks of a wearable medical system. Each block shows specific dependability requirements (reliability, safety/security, availability, maintainability, etc) and different risks. The methodology proposed here starts by identifying the main blocks of the system, perform a fault tree analysis (FTA), and a failure mode and effect analysis (FMEA). With the identification of the main risks, the dependability of the system is estimated based on mathematical and statistical models. Additionally, after this analysis, the main weaknesses and threats to the correct operation of the medical device can be diminished/eliminated after employing design for testability techniques and/or reconfiguration. The redesign of the circuits is complemented with data fusion techniques for the analysis and correction of the measured vital signs.

The design for dependability of medical devices methodology being proposed was applied on the development of a combined cardiac and aortic monitoring system, comprising a wearable cardiac monitor and an advanced telemetry system for post-EVAR surveillance (figure 1.2). To achieve that, implantable wireless pressure sensors which are biologically compatible and have suitable linearity and sensitivity, were produced [10]. An electronic readout unit (ERU) capable of energizing the pressure sensors and capture the pressure data is placed in the chest of the patient. This unit provides also the monitoring of a 12-lead ECG using textile dry electrodes [11]. The electronic unit and the electrodes are built in a customized clothing. Data is transmitted to a smartphone for further processing, data display, and eventual communication with a healthcare center. These developments were carried-out in the framework of research projects Sensecardiohealth and SIVIC[1] .

The main innovation and contributions can then be summarized as the following:

[1]Portuguese acronym for integrated cardiovascular surveillance system.

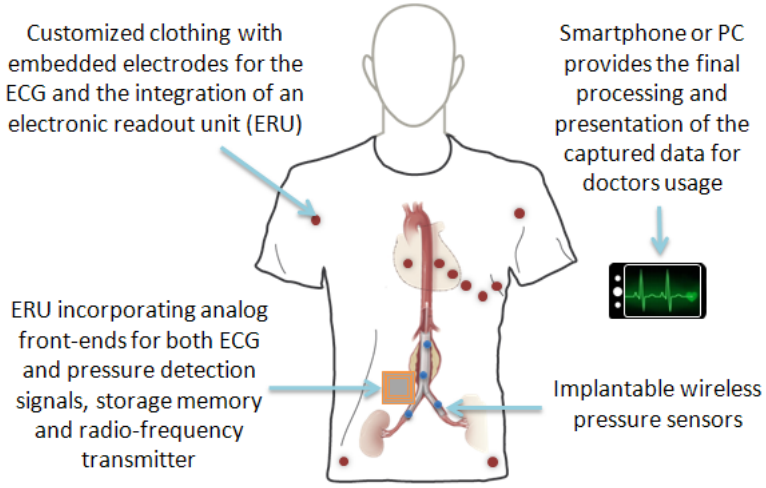

Figure 1.2: Wearable integrated cardiovascular monitoring system.

- Design and implementation of an inductive coupling based electronic system for reading the pressure in the abdominal aorta using locally implanted wireless pressure sensors;
- Use synchronous measure of the patient electrocardiogram (ECG) and intra-sac aneurysm pressure, in order to have a more robust and reliable monitoring;
- Characterization and validation of a model for LC pressure sensors;
- Development of a methodology for testing LC pressure sensors through inductive coupling;
- Characterization of textile antennas and ECG (electrocardiogram) detection electrodes;
- Definition of an approach to analyse the dependability/reliability of a medical system;
- Development of a data fusion algorithm for patient and system diagnosis.

1.5 Thesis Outline

This thesis continues in Chapter 2 with a summary of a state of the art on wearable monitoring systems for medical purposes. The advances on sensors, wireless communications and information technologies that have promoted a rapid development of various wellness or disease monitoring systems are reviewed and different systems that have been proposed to reduce health care costs, maintaining high quality of care, shift the focus of health care expenditures from treatment to prevention, provide access to health care to a larger number of patients, reduce the length of hospital stays and address the issue of specific requirements for elderly population and/or chronically ill patients, are presented. A description of the SIVIC system is also included with a description of the current status of the work, that includes the development of the telemetry system to energize the wireless pressure sensors and detect their response. .

Because these wearable monitoring systems are to be used for medical purposes, their dependability has to be perfectly controlled. Unfortunately, the complexity and the functional specificities of these systems make the existing dependability techniques, specifically developed for the aeronautics, space and automotive applications, not totally appropriate for the medical field [12]. Chapter 3 presents the attributes and risks for dependability in medical devices and the state of the art in this topic.

Chapter 4 describes the techniques that have been used in order to assure that a medical system shows the required levels of dependability. A fault detection system capable of diagnosing shifts on the sensors initial values and other possible faults for further calibration is presented. A section describing the textile electrodes for the ECG recording and their characterization is also included.

Chapter 5 presents the data fusion techniques, namely fuzzy logic, artificial neural networks, decision trees and naive Bayes classifiers, that were explored and employed in the SIVIC system to process the captured data to increase the trust levels with which diagnostics are made. Concerning the wearer condition, additional information is provided after classifying the set of signals into normal or abnormal (e.g., arrhythmia, tachycardia and bradycardia). As for the monitoring system, once an abnormal situation is detected in its operation or in the sensors, a set of tests is run to check if actually the wearer shows a degradation of his health condition or if the system is reporting erroneous values. Selected features from the vital signs and from quantities that characterize the system performance serve as inputs to the data fusion algorithms for Patient and System Status diagnosis purposes. The algorithms performance is evaluated based on their sensitivity, specificity and accuracy. It is shown that, based on these criteria, the naive Bayes classifier presents the best performance.

The last chapter (Chapter6) addresses the main conclusions of this thesis. A dependability analysis of a system under development employing techniques such as FMEA and FTA helps identifying which system blocks/components require testing circuits. The data provided by the testing circuits and the sensors for monitoring the patient condition are used to achieve high levels of dependability. The work presented herein shows how data fusion can be explored to improve the dependability of a cardiovascular monitoring wearable system, after providing a means to, on the fly, diagnosing whether deviations detected in the acquired signals are due to a disease or condition of the patient, or actually to a fault in the system. It is also a tool which can help, in the electronics design stage, the process of identifying test operations needed to improve a system's diagnosability.

Chapter 2

Wearable Medical Devices

Existing wearable health monitoring devices — ranging from simple pulse and activity monitors to portable Holter recorders and sophisticated implantable sensors — lack a wide acceptance among the general population and medical community despite their increasing numbers, variety and significant technological improvements over the last decade. This is mainly due to lack of confidence on the gathered data, that often needs further offline processing and analysis, the use of wired connections between sensors and the monitoring systems, which limit patients' activity (wires also influence negatively on the measured results), low level of comfort due to the wiring and batteries, systems' inflexibility, the absence of integration with third–party devices, and their intrinsic cost [4].

The medical community has raised concerns about the usefulness of these devices beyond being mere personal gadgets. Some physicians even question the validity of the captured data and the privacy issues that are involved.

Nevertheless, it has been recognized that the availability of these systems should not be underestimated. The markets for smart wearable technology (in particular fitness trackers, smart watches, connected headsets, smart glasses, personal trackers and wrist bands) are expected to still increase significantly this decade. There are predictions pointing for a growth of the devices for sports and fitness between $2k million and $5.1k million by 2018 [13]. The need to ensure that sensors remain in tight contact with the body and the ability of being washable without removing electronics, have prevented a wider acceptance of smart sports clothing, but again a five times increase in the market volume is expected between 2015 and 2020 reaching then about $500 million [13].

Also, within the personal medical and assisted living case there are signs that there is a growing desire from people to address their own health, but in this case the regulatory demands and the unavailability of services capable of dealing with very large quantities of data, have restricted the use and prescription of these systems as medical devices. Nevertheless, efforts are being made for the production of reliable, low cost and comfortable systems to be achieved. That is seen in the issuing of the Qualcomm Tricorder $10 million prize competition, run by the X-prize foundation [14], to be awarded to the first team *to design a product which can reliably measure five vital*

signs and diagnose 15 or more common diseases — deadline by early 2017. The global sales of Tricorder based products is expected to reach USD$ 100 million by 2020. Currently, some devices are already being produced and used on a non officially approved basis. The Scanadu ScoutTM device [15] allows measuring heart rate, body temperature, oxymetry, respiratory rate, blood pressure, ECG, and emotional stress. It is now being tested by more than 7 thousand people all over the world. Vandrico Inc. [16] reports a list of 56 devices being currently used for medical applications.

The spread of usage of embedded systems allows for reducing hospital patient costs and increase the health care quality level. Ambient assisted leaving and wireless home care monitoring systems (WHMS) have gained an increasing popularity among researchers, specially for the benefits they could deliver to the general population if some of these obstacles are overcome.

According to D. Gershbein and B. Palmer [17] :

> *When designed specifically for the end-user, in a local context, wearable and sensor technology could revolutionize the way we deliver services to populations at the last mile.*
>
> *A wearable built to address social good would ultimately need to follow a systemic, communitarian approach. It must be:*
>
> - *Cost-effective: Needs to have the capacity to be executed en masse in low-cost areas, with a demonstrated business case and need*
> - *Rugged and Durable: Waterproof, shockproof, weatherproof, heat resistant, easily stored, and built to last*
> - *Low-power: Run off a battery, have a long battery life (possibly using alternative energy), and be power efficient where there is no power*
> - *Scalable: Can be applied to varying environments and communities, sustained by a larger ecosystem, easily produced/developed, easy to use, easy to maintain/fixed by local skill force*
>
> *Wearable and sensor technology have the potential to deliver life-enhancing and life-saving services.*

In this section an overview of the state of the art on wearable monitoring systems, including a description of their characteristics, general architecture, some examples and future challenges is presented.

2.1 Characteristics and Architecture

Smart wearable embedded systems have gained an increasing importance in biomedical applications, such as, clinical analysis and patient monitoring. Nonetheless, they could not work unless medically significant data is first gathered from the patient to correlate and reach a final conclusion, thus denoting the necessity for a physical property to be measured. The term ”Smart” stems from the presence of active electronics including sensors, some form of audio or visual feedback, and a communication link, usually a wireless one.

2.1.1 Main Components

According to [18] any biomedical instrument should be composed by at least these four major blocks (see Figure 2.1):

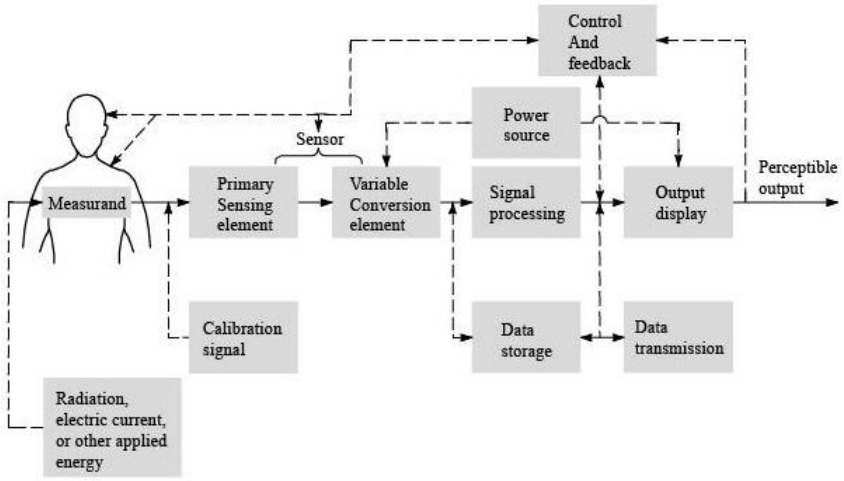

Figure 2.1: General architecture of biomedical instrumentation systems [18].

Measurand/physical properties

Several parameters like blood pressure, oxygen saturation (SpO2), blood glucose, heart rate and behaviour (ECG), temperature and respiration can be measured by home care systems. According to [19], all the information needed to reconstruct a body segment posture can also be effectively gathered by wearable sensors.

The information gathered from patients is only useful to the greatest extent in which it is related to the disease, condition or risk factor the patient is associated to; and can only be effectively employed if the data captured from sensors/transducers is accurate.

Sensors/transducers

According to IEEE, a transducer is a device that converts a physical magnitude of one form of energy into another form, generally on a one-to-one correspondence or according to a specified mathematical formula [20]. A sensor/transducer can be defined as a device that translates a physiological property into an electric signal and hence, a manipulable one.

Scilingo [21] concluded that "Experimental results showed that fabric electrodes and sensors can be adequately employed to acquire and monitor vital physiological and biomechanical signals, without loss of information", after evaluating the performance of wearable sensors versus normal acquisition ones. This information is critical for wearable systems, since it validates their use as usable sensors. If wearable systems could not deliver the performance done by regular sensors, their limitations would be higher and not necessarily would have reached their generally consent use.

Many wearable systems also have the ability to add or remove different types of pluggable medical transducers from the embedded system, making them customizable according to patient' own needs.

Data processing/transmission

In general, all the signals acquired from the sensors need some type of conditioning, such as, limitation, amplification, filtering, adaptation, conversion or any combination of them. These operations are usually performed in stages along the signal conditioning chain, and allow the wearable systems to better handle, process, and distribute the information from the physical signals.

Short–range wireless transmission standards allow appropriate data rates suitable to continuously transmit a sufficient set of patient vital status information. Bluetooth (IEEE 802.15.1), WLAN (IEEE 802.11), WPAN (IEEE 802.15.4 / ZigBee / 6LoWPAN) and WiMAX (IEEE 802.16e) are radio based standards using different frequency bands that meet the requirements. Wireless data transmission standards have also been developed specifically addressing the needs of medical systems, such as Wireless Medical Telemetry Service (WMTS) and Medical Implant Communication Service (MICS).

Several embedded medical systems have an architecture that includes an adaptable embedded system, a central server, and a connection to a health center where an expert diagnoser can provide remote assistance [22, 23].

The expert diagnoser is the health care professional who will run a series of examinations through the embedded system by accessing the central server over the Internet. The central server houses the software agents that run various diagnostic tests on the embedded system.

In smart home care, the home care monitoring systems (WHMS) collects data according to a physician's specifications, removing some of the cognitive burden from the patient and providing a continuous record to assist diagnosis. In–home tasks are also made easier, including remote device control, medicine reminders, object location and emergency communication.

Reliability and security issues also have to be considered on those platforms, both at computation and communication levels.

Output/display

As logical as it may sound, there is always a necessity to export the information gathered by the system to some kind of interface for easy interpretation for the diagnoser and/or the patient.

Regardless of the measurand taken into account, the sensors used, and the protocol for signal processing and transmission, there should always be a safe, reliable and easy way to assess the data, whether it is presented in visual, auditive or in any other form.

2.1.2 Characteristics

A wearable embedded system should be portable and non-intrusive. Tendentiously, it should be as light as possible and low-cost [23]. In continuous patient monitoring, the usability and comfort are important factors, making wireless communication one of the major trends in medical applications. Portability plays a major role, but it is not the only parameter that restricts mobility. Comfortability is as essential, because unless the user feels comfortable it is very unlikely he will be willing to use the system for long periods of time.

According to [22], the main characteristics a wireless home WHMS should present are:

- Interoperability, real–time data acquisition and analysis.
- Reliability and robustness.
- New node architectures.
- Patient and object tracking.
- Communication during obstructions and interference.
- Multimodal collaboration and energy conservation.
- Multitiered data management.

Extending the requirements mentioned above, some other aspects should also be considered as well, as is the case with battery life. It is an important specification not only because of energy conservation and efficiency requirements, but also because low-power capability increases the autonomy of the system.

Noise immunity should also be considered. Even though it relates closely to robustness and communication during obstructions, good design practices should always be employed in order to minimize the impact of such perturbations and thus increase the quality of the final product.

2.1.3 General Architecture

According to [22], a WHMS architecture should comprise the essential capabilities of each of the future medical applications:

- Integration with existing medical practices and technology;
- Real–time and long–term remote monitoring;
- Miniature wearable sensors;
- Assistance to the elderly and chronic patients.

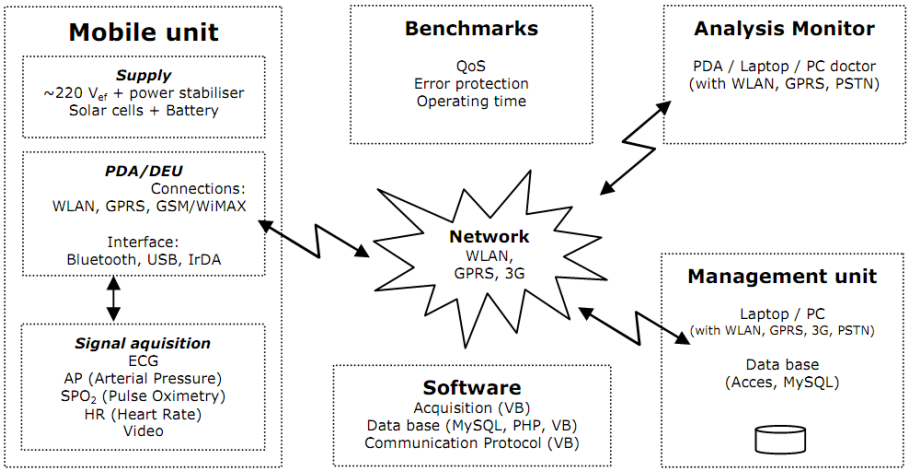

Figure 2.2: Block diagram of typical home-care embedded systems [22].

Figure 2.2 describes an example of a WHMS architecture. This system includes the mobile biosignals acquisition unit of the patient, the management unit for real time information recording and the monitor for analysis and inspection of the acquired data. The mobile unit is the embedded medical system and contains all the sensors and a wireless connection to the central server, the management unit for data recording, and also a connection to the health center–analysis monitor.

The key elements for the development and production of future embedded systems are the development of specific sensors, data transmission and embedded systems technologies [24].

2.2 Systems based on smart textiles

With the challenge of finding solutions to some of the problems mentioned above, the "Intelligent Biomedical Clothing" (IBC) concept was created. IBC usually refers to clothes with sensors — either enclosed between the layers of fabric or in the fabric itself — that are close to or in contact with the skin and can be piezoresistive yarns, optical fibers and/or coloured layers. IBCs are also understood as the integration into textile of sensors, actuators, computing and power source as a whole while being part of an interactive communication network [25].

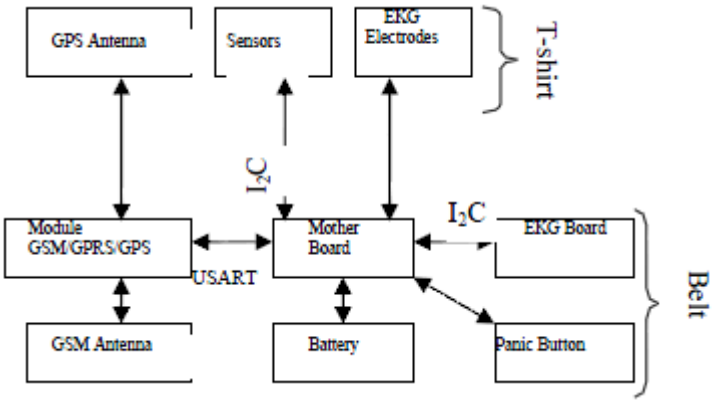

Figure 2.3: Architecture of the VTAMN: the partitioning between cloth and belt [26].

The VTAMN (Vêtement de Télé Assistance Médicale Nomade — Under cloth for Nomad Medical Teleassistance) project aims at measuring the activities and physiological parameters of subjects in their daily life with an original set up of sensors networked in a garment, distributed algorithms, presenting the possibility of launching alarms through a cell-phone and rescuing a person after a localization with a worn GPS.

Its architecture can be represented as in Figure 2.3, where 4 ECG surface electrodes, the coil of a pneumograph, 2 temperature sensors with their electronics, a fall detection module, wirings and interconnections buses are directly integrated into the garment.

The wiring for data and power supply is performed in a bus-like configuration called the "Body-LAN", using the I2C Bus, very convenient with its only 2 wires; the number of modules is easily extensible as the address of a component is transported with the data on the same wire. Also many IC and microcontrollers are compatible with this field bus. The turn coil of the pneumograph and the wires connected to the ECG electrodes follow separated paths. The opening of the undercloth is on the front side [26].

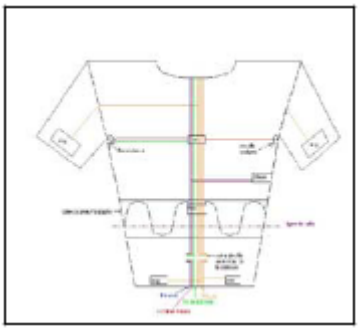

Figure 2.4: The wiring for the data path and power supply uses a bus-like model [26].

The WEALTHY is a wireless-enabled garment with embedded textile sensors for simultaneous acquisition and continuous monitoring of biomedical signs like ECG, respiration, EMG, and physical activity [25]. In the WEALTHY system, conductive and piezoresistive yarns are used to

manufacture a knitted garment possessing distributed functional regions. These are integrated and used as sensors, connections, and electrodes. The simultaneous recording of vital signs allows extrapolating parameters and the definition of new indices correlated to the whole set of recorded signals that may provide better information on the patients' status and contribute to make alert messages and personalized synoptic tables of patients' health [5].

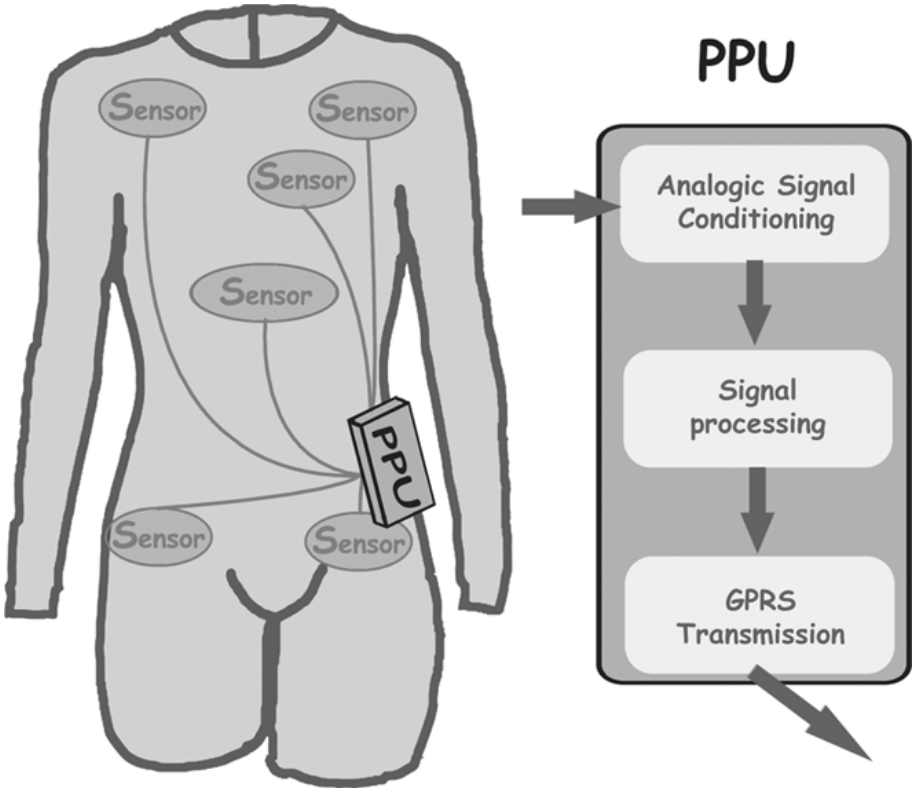

Figure 2.5: Overview of wearable WEALTHY's module [5].

MagIC is a sensorized vest including fully woven textile sensors for ECG and respiratory frequency detection and a portable electronic board for motion assessment, signal preprocessing, and Bluetooth connection for data transmission. In the MyHeart project the underlying concept relies on the use of tiny conductive wires knitted like normal textile yarns. In that way, the wearable system becomes more comfortable for the user, no wireless modules are needed for the sensors, and the whole system needs only one centralized on-body power supply, thus resulting in significant decrease of the overall system's size. One main device is used to control the on-garment bus and is also responsible for the synchronization and the power supply for all the on-body components.

The Medical Remote Monitoring of clothes (MERMOTH) project has produced a low cost, knitted, comfortable, and stretchable sensing garment that incorporates conductive and electrostrictive fabrics and yarns and dry electrodes, enabling the measurement of ECG, respiratory inductance plethysmography, skin temperature and activity through accelerometers. A PDA (Personal Digital Assistant) is connected to the microcontroller that is used to interface with the sensors on the garment, providing a radio frequency link to a local personal computer for display and

measurement interpretation.

SmartShirt is a wearable sensorized garment that measures human heart rhythm and respiration using a three lead ECG shirt. The conductive fiber grid and sensors are fully integrated in the garment [27].

The PROLIMB project aims at the development and design of a wearable electronic system, capture physical quantities associated with human locomotion of the most comfortable and non-invasive as possible, even for people with disorders and physical disabilities. The system is simple to handle and is not harmful to the patient. It can be usable as a piece of clothing and self-contained, enabling the monitoring of the most relevant variables, not only in a clinical setting or laboratory, but also for day-to-day patient with interference and minimal discomfort. The acquired signals include the linear and angular movements of the lower limbs, and myoelectric signals observed on the surface of the thigh and leg muscles. The observation of these quantities enables a multifactorial analysis of movement and consequently a more precise diagnosis and the ability to understand the role of different factors in a given pathology. The pathophysiological profile can be extracted to synthetically represent the relative importance of various factors in the locomotion of an individual. This procedure can help the clinician make decisions about the best therapy. The PROLIMB project addresses this issue by following a holistic approach, made possible by the involvement of research groups with strong activity in the fields of textile engineering, design and test in microelectronics and signal processing, in collaboration with physicians, in order to produce a sensor network that can be worn for acquiring and monitoring signals for characterizing magnitudes of locomotion of human lower limbs [28].

2.3 The SIVIC System

2.3.1 Overview

The measurement of aneurysms' intra-sac pressure has been reported as a reliable technique to monitor post-endovascular aneurysm repair (post-EVAR) of abdominal aortic aneurysms (AAA) using prosthetic grafts. The stent-graft is placed *in-situ* via insertion through the femoral arteries up to the aortic lumen to fit tightly in the bulged or ballooned AAA fraction [29]. This avoids the current aneurysm repair standard procedure based on open surgery, still mandatory in some cases, but much more invasive than the stent-graft approach.

The SIVIC[1] system, a combined cardiac and aortic monitoring system under development (Fig 2.7), provides the synchronous measurement of a patient's ECG (electrocardiogram) and pressure in the abdominal aortic aneurysm (AAA) sac, in order to obtain a more robust and reliable monitoring. Biologically compatible capacitive pressure sensors, which show suitable linearity and sensitivity [30], are used to capture the intra-sac AAA pressure and detect endoleaks.

[1] Portuguese acronym for integrated cardiovascular surveillance system.

Figure 2.6: Smart Shirt system: User requirements analysis [1].

The pressure monitoring system relies on an inductive coupling interface to capture the resonant frequencies of a cluster of *LC* sensors placed on the stent-graft wall[31]. An electronic readout unit (ERU) capable of energizing sensors and capture the pressure data is placed in the patient's chest. The antenna for energizing the sensors could be embroidered in a t-shirt that contains the ERU. Preliminary studies, namely electrical characterization, were conducted on textile antennas made in the Universidade da Beira Interior (see E). The ERU provides also the monitoring of a 12-lead ECG using textile dry electrodes [32]. The electronic unit and the electrodes are built in a customized clothing. Captured data is transmitted to a smartphone for further processing and diagnosis, data display, and eventually can also be transmitted by the smartphone to a healthcare center.

2.3.1.1 Endoleaks

Despite the advantages of the EVAR procedure compared with the open surgery, some post-surgery problems, such as endoleaks (figure 2.8), graft migration, stent fracture, and enlargement of the aneurysm sac may occur, which require regular monitoring/surveillance and behavioural analysis to avoid the rupture of AAAs and to prevent reinterventions [33]. The pressure in the walls and in the aneurysm sac is one of the most important indicators for supervising post-EVAR

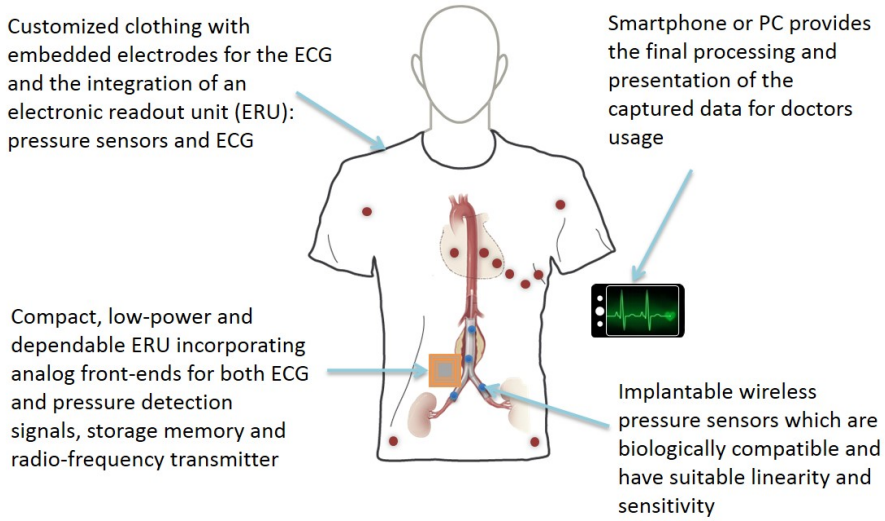

Figure 2.7: Wearable ECG data capture and transmitter module.

patients. Direct intra-sac pressure measurement outperforms imaging techniques in ascertaining either the complete AAA exclusion or the need for future interventions [34].

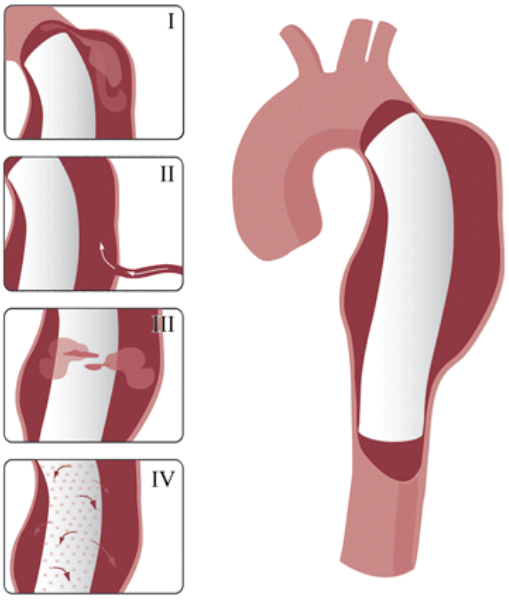

Figure 2.8: Types of endoleaks in a stent graft.

As reported in [35], a reduction in pulse pressure of 30% or more from the initial pressure measurement would be associated with a sealed sac and a less than 30% reduction in pulse pressure would indicate a type I (ineffective fixation at either end of the graft) or III (failure of the implanted graft including development of holes) endoleak. Taking angiography as the standard reference, for the detection of types I or III endoleaks at the completion of the procedure, pressure monitoring

allowed to detect 4 out of 5 (80%) of the leaks. As reported in [36], the clinical observation of mean arterial pressure is an important predictor of aneurysm expansion and of the occurrence of type II endoleaks, with the highest pressures recorded with increasing aneurysm diameters. Also, experimental results have showed that the pressure distribution in the aneurysm walls is not uniform being the higher pressures observed in the points of higher diameters.

2.3.1.2 Remote pressure monitoring systems

Remote aneurysm pressure monitoring systems [37] and results of clinical observation using these systems have been published [38], which show that the use of wirelessly accessed pressure sensors provide useful post-EVAR endovascular leaks observation and help guiding clinical therapy. Until now, two remote pressure sensors have been tested in clinical trials — the EndoSure Wireless Pressure Sensor (CardioMEMS, Atlanta, GA, USA) and the ImPressure AAA Sac Pressure Transducer (Remon Medical Technologies, Caesarea, Israel) [39]. The ImPressure sensor is hand sewed to the outside of a stent-graft and is activated by ultrasound waves from a hand-held probe, which charges the sensor that measures the surrounding pressure and transmits the data via acoustic waves back to the hand-held probe. In spite of ultrasound being safe and widely used for medical imaging, the measurement requires the use of an ultrasonic gel and direct contact between the skin and the transducer. Another drawback of this sensor is the impossibility of ultrasounds to travel through air or bone, which may lead to difficulties on communicating with the aneurysm sac. The EndoSure sensor consists of a simple resonant circuit and a sophisticated external antennae and receiver system. This sensor is delivered into the aneurysm sac through its own sheath (diameter 14 Fr/4.7 mm) during the procedure, which adds more complexity to the EVAR. Also, it has radiopaque markers to clearly define its location within the aneurysm sac and does not require direct contact of the reader with the skin. However, as the sensor is completely separated from the aortic endograft, there is no control on its position and it is not possible to use more than one sensor per patient due to the sensor's volume [37].

2.3.2 The developed endovascular aneurysm repair monitoring system

In the system being proposed the monitoring principle is based on the detection of pressure variations within the aneurysm sac by means of a cluster of passive pressure sensors attached to the stent-graft. Each sensor comprises a capacitor attached to an inductor forming together an *LC* resonant circuit whose oscillation frequency is sensitive to pressure variations. An external reader delivers energy and detects the sensor's resonance frequency through an inductive-coupling link. The use of different sensors placed on the same stent-graft provides a more accurate observation of the intra-sac pressure distribution, maximizes the system sensitivity to leakages, and increases the reliability of the monitoring process. The proposed monitoring system is composed of three major blocks (figure 2.9): the sensor cluster, the external reading system, and the signal retrieval and analysis.

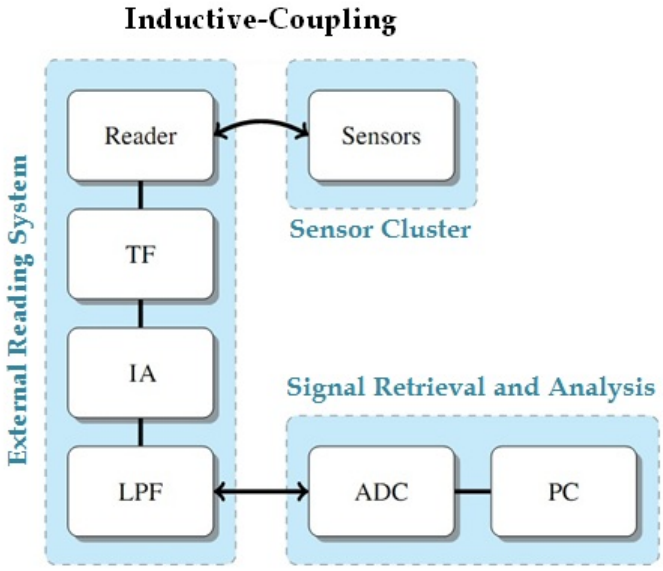

Figure 2.9: Block diagram of the telemetry system.

2.3.2.1 External Reading System

The external reading system (figure 2.10) includes a receiver capable of energizing the passive pressure sensors and detecting the sensors oscillation frequency, and a signal conditioning block composed of a transformer, amplifiers and a filter.

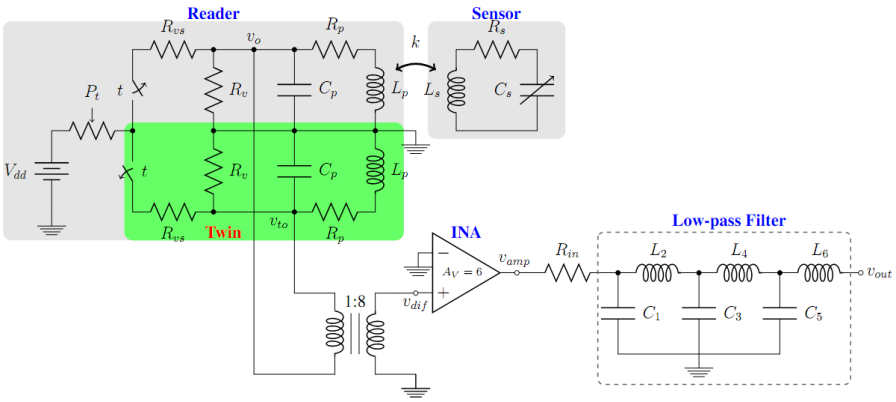

Figure 2.10: Schematic of the reader circuit.

The sensors and the receiver exchange information (the pressure dependent oscillation frequency) and energy (the external reader stimulates the sensors with a square waver) by means of inductive-coupling. To simplify the analysis of the circuit only one sensor is by now used in the model. Its components can be modelled as passive elements: a variable capacitor C_s, whose value changes with the applied pressure, connected to an inductor L_s, implementing a parallel resonant circuit. The schematic representation in figure 2.10 includes also resistors R_p and R_s which model parasitic series resistances, including those due to the skin effect.

$$f_{osc} = \frac{1}{2\pi\sqrt{(1-k^2)L_sC_s}}. \tag{2.1}$$

The oscillation frequency (equation 2.1) is defined after the sensor's capacitance and inductance, as well as the coupling factor k (equation 2.2) which depends on geometric factors: the reader's coil radius rr, the sensor's coil radius rs, and the distance between the antennas x, as depicted in the equation [40]. The k value can be estimated using data (exact positions and distances to the aorta) from imagiological exams that EVAR candidates typically take before the procedure [41].

$$k = \frac{r_s^2 r_r^2}{\sqrt{r_s r_r}(\sqrt{x^2+r_r^2})^3} \tag{2.2}$$

The value of resistance R_{vs}, which represents the voltage source v_{vs} internal resistance, is important for the maximization of the captured signal's amplitude. The C_p capacitance is necessary to maximize the transferred energy and the signal captured from the sensor. The developed circuit resorts to a twin circuit added to the first part of the reader, in order to provide a differential detection of the reflected oscillation. By duplicating the undesired noise signal the common-mode noise is also eliminated, increasing the output signal's quality and reducing the effect of the square wave harmonics. The sensors' oscillation frequency signal v_{dif} is obtained by subtracting the two signals in the receiver vo and vto using a transformer.

The transformer output signal needs to be further amplified with high slew-rate and bandwidth amplifiers. The instrumentation amplifier configuration is the best option in order to achieve high common-mode rejection ratio and high input impedance necessary to minimize noise. The amplified signal is applied to a low-pass passive filter to eliminate harmonics that could compromise the analogue to digital conversion dynamic range.

The reader circuit was implemented and tested, proving to be capable of energizing an LC network (a circuit with the same electrical characteristics of the pressure sensor) and capture the oscillation frequency with good accuracy [31, 42].

An alternative reader that is more compact and easier to implement in a wearable system, as well as, a semi-passive sensor circuit that were developed under the co-supervision of the author of this thesis, are presented in annex B.

2.3.2.2 Pressure sensors

Regarding the main pressure sensor specifications — namely dynamic range, resolution and accuracy — these can be retrieved from the maximum values of blood pressure in the human body and after the required accuracy and maximum errors admitted by the legislation for pressure measurement devices [43]. Taken into account that the cardiac cycle can reach as fast as 180 bpm (3 Hz), and that the change of rate is below 120 ms, the pressure monitoring needs a bandwidth of

around 80 Hz. The blood pressure in the aorta ranges typically from 60 to 150 mmHg (referring to atmospheric pressure). As for the measurement of the aortic aneurysm pressure, the sensor should have a dynamic range between 20 mmHg and 250 mm Hg, a 1 mmHg resolution, and an absolute accuracy below 5 mmHg [44].

The flexible capacitive sensors used in the present work were developed at U. Minho [10] using aligned carbon nanotubes (A–CNTs) embedded in a flexible substrate of polydimethylsiloxane (PDMS), a transparent, non-toxic and biocompatible silicone elastomer, forming a dielectric which is hermetically sealed at ambient pressure.

For evaluation and characterization purposes, the sensors were mounted inside a controlled pressure chamber (pressure range from vacuum – 0 kPa to atmospheric – 100 kPa) in order to measure the capacitive changes (a LCR meter was used to measure the flexible capacitor changes). Figure 2.11 shows the measured sensor capacitance versus pressure transfer characteristic. It can be seen that this characteristic fits very well that predicted by the analytic model and that it shows relatively good linearity, specially in the region close to the sensor's reference — atmospheric pressure. The pressures to be measured have been documented to be in the range of 40 mmHg ($\sim$ 105.3 kPa) for the diastolic pressure and 170 mmHg ($\sim$ 122.7 kPa) for the systolic pressure [35].

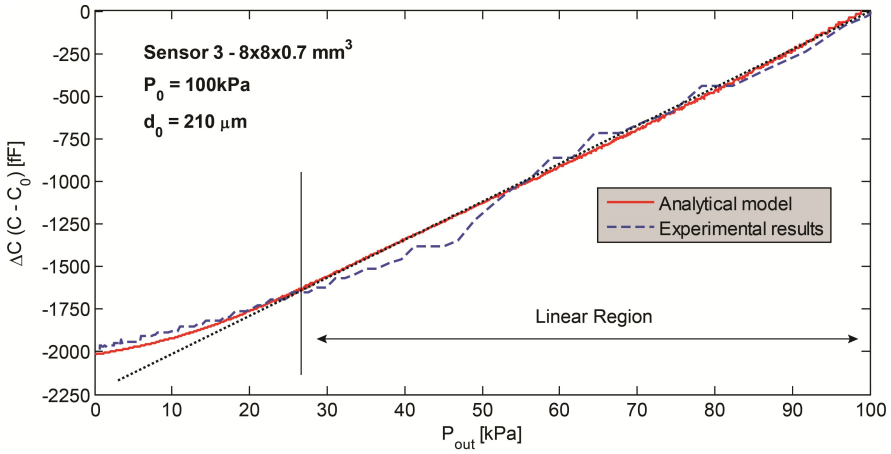

Figure 2.11: Transfer characteristic of one of the developed pressure sensors.

The inductors, which also operate as antennas, of the passive sensors (see Figure 2.12) were fabricated using a DuPont^{TM}Kapton$^{®}$ polyimide film in two different geometries (square and circle). For each geometry three antenna sizes were used in order to evaluate with different membrane (or dielectric) areas of the pressure sensor capacitor: 4 mm, 6 mm and 8 mm values were used for the square sides and circle diameters. The implemented antennas comprise two stacked inductors, one on the top layer and the other on the bottom layer of the polyimide film, which are connected with a via on the outer segment of each (figure 2.12).

The polyimide film has a thickness of 50 μm and the copper traces a thickness of 35 μm. All inductors are made with 0.1 mm trace widths with a space of 0.1 mm between them. The three arches which provide the interconnection between the inductor coils and the membranes have a 0.25 mm thickness and are spaced by 1.125 mm. The distance between the inner coil and the

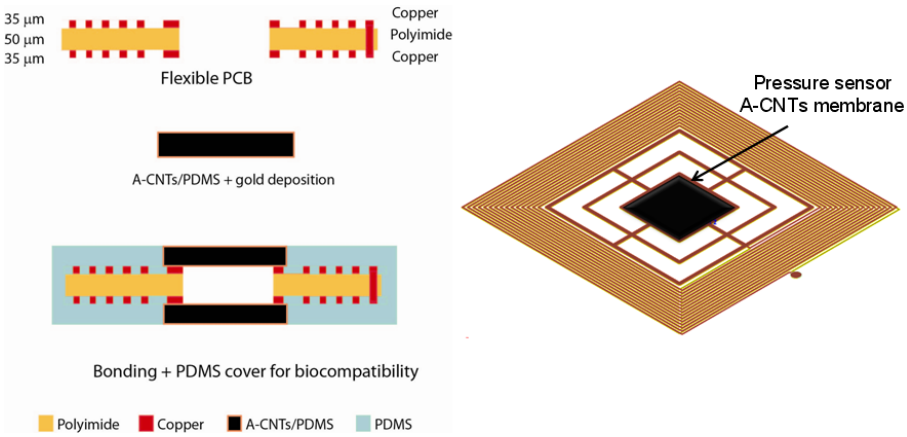

Figure 2.12: Overview of the passive *LC* structure.

largest arch is 0.15 mm for the square antennas and 0.25 mm for the circle antennas. Table 2.1 displays the outer and inner diameters dimensions, as well as the number of turns for each antenna.

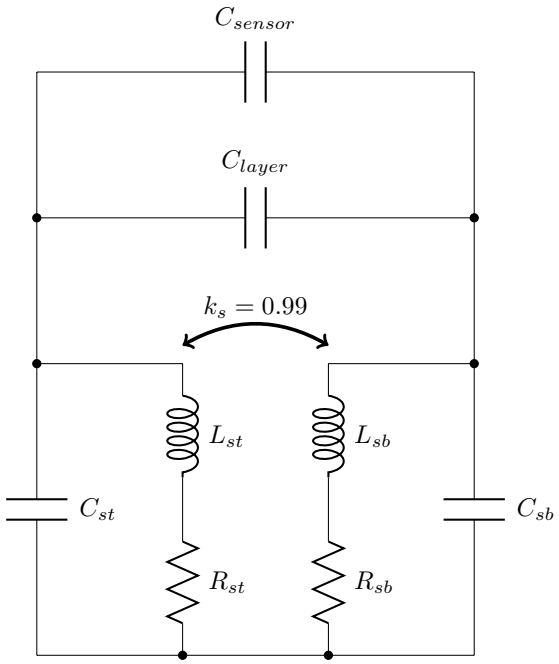

Figure 2.13: Electrical model of the pressure sensor (subscript t denotes top layer and b bottom layer).

Since the developed sensor shows a new structure, which is different from conventional CMOS or common printed circuit RFID tag antennas, it was needed to extract the respective electrical model (see figure 2.13). Each layer forms a resonant circuit comprising an inductance (L_st and L_sb), the series resistance (R_st and R_sb), and the parasitic capacitance due to the capacitance formed between the traces of the coils (C_st and C_sb). The parasitic capacitance established between the traces of the top and bottom layers C_{layer} is connected in parallel with the sensor's capacitance.

The calculated electrical parameters of the sensors are presented in table 2.2. The expressions

Table 2.1: Dimensions of the fabricated sensor antennas.

Parameters	C4	C6	C8	S4	S6	S8
Geometry	circle	circle	circle	square	square	square
d_{out} [mm]	16.3	17.5	18.8	16.3	17.5	18.5
d_{in} [mm]	10.5	12.5	14.5	10.3	12.3	14.3
N_{turns}	15	13	11	15	13	11
diel [mm]	4	6	8	4	6	8

for the calculations of planar spiral inductance presented in [45] were used for the estimation of the inductance L_s. The sensor capacitance C_{sensor}, the parasitic capacitance between the antenna's layers C_{layer} and the parasitic capacitance C_s were estimated using the expression for the parallel plate capacitor $C = \varepsilon \times \frac{area}{thickness}$ using copper's permittivity for the dielectric constant.

Table 2.2: Values of the electrical components of the sensors' model.

Parameters	C4	C6	C8	S4	S6	S8
L_s [μH]	4.62	4.30	3.74	5.41	5.04	4.45
R_s [Ω]	3.58	3.37	3.09	3.99	3.87	3.58
C_s [pF]	1.91	1.86	1.76	2.31	2.22	2.02
C_{layer} [pF]	19.15	18.57	17.48	33.63	32.30	29.44
C_{sensor} [pF]	2.23	5.01	8.90	2.83	6.38	11.33

The total inductance of the dual-layer planar inductor L_s is almost 4 times higher than a single layer inductor with the same dimensions $L_{total} \cong L_{st} + L_{sb} + 2M$. By design the current flows in the same direction on both layers. The proximity and the via between the inductors assures the mutual inductance M to be almost equal to L_s ($M = k_s\sqrt{L_{st}L_{sb}} \cong L_s$).

2.3.2.3 Results

Simulations

Simulations using Agilent ADS were performed to estimate the inductor's total inductance, self–resonant frequencies (SRF), and the natural oscillation frequency of the sensor f_{osc}. For characterization purposes, the sensors capacitance C_{sensor} was discarded from the model, and a S parameters simulation was performed to extract SRF and the total inductance of the antennas (@1MHz). For the determination of the sensor's oscillation frequency the circuit from figure 2.10 was simulated, using a transient analysis, after replacing the simple *RLC* sensor by the model in figure 2.13. The coupling k between the reader and the sensor was adjusted in a range of distances between 0 and 50 mm (in steps of 5 mm), considering the reader antenna to be a spiral square with a 50 mm diameter. The Fast Fourier Transform (FFT) of the signal observed on node v_{out} of the reader circuit was computed to extract the sensor's frequency.

A simulation of the variation of the sensors capacitance C_{sensor} in $\pm$ 1 pF was performed, considering a distance between the antennas of 10 mm, in order to assess how much the parasitic

layer capacitance mask the change in the sensor. Table 2.6 displays the variation of the sensors' resonant frequency with a change of 2 pF of the variable capacitor, which is the expect change of the sensor's membrane capacitance for the working pressure range (see Figure 2.11). The results from these simulations will be discussed and confronted with those obtained from experimental measurements in the next subsections.

Table 2.3: Simulation results of the sensors' resonant frequency variation.

f_{osc} [MHz]	C4	C6	C8	S4	S6	S8
C_{sensor} -1pF	8.04	7.95	8.07	5.68	5.71	5.93
C_{sensor}	7.86	7.79	7.92	5.60	5.64	5.86
C_{sensor} +1pF	7.69	7.63	7.78	5.52	5.57	5.79
Δf	0.352	0.323	0.286	0.154	0.139	0.139

Experimental evaluation

This section describes the procedures employed to experimentally characterize the sensors and the complete monitoring system, as well as the setups prepared for each measurement.

Sensor Antennas

Prior to the assembly of the A–CNTs membranes on the flex-PCB, the inductance (@1MHz) and the self-resonant frequency (SRF) of the antennas were measured with a vector network analyser (VNA). These values will be then compared with the values expected from the S parameters simulations in the next subsection.

Experimental results obtained using a vacuum chamber

The performance of the flexible sensors to different pressures and their use with the telemetric system, were evaluated using a vacuum chamber. Each sensor was subjected to different pressures by applying a pressure varying from 0 to 1 atm (vacuum to atmospheric pressure). The output of the reader circuit was recorded while commercial pressure sensors placed also inside the chamber were used to record reference values for comparison purposes. Results from the measurements with sensors C4, C6, S4 and S6 are presented in Figure 2.14.

Effect of distance and biological tissue in the frequency detection

Since the final application of the system is to read from sensors implanted inside the human body, further experiments were performed in order to assess the behaviour of the system in the presence of biological tissue between the antenna and the sensor. First, measurements using air as the medium between the reader and the sensor antennas were carried out for different distances ranging from 3 mm and 5 mm to 25 mm in steps of 5 mm. Afterwards a tissue emulating solution (phantom) with electrical characteristics (conductivity and permittivity) similar to the muscle tissue made according the recipes presented in [46] was employed (see Appendix C for the phantom

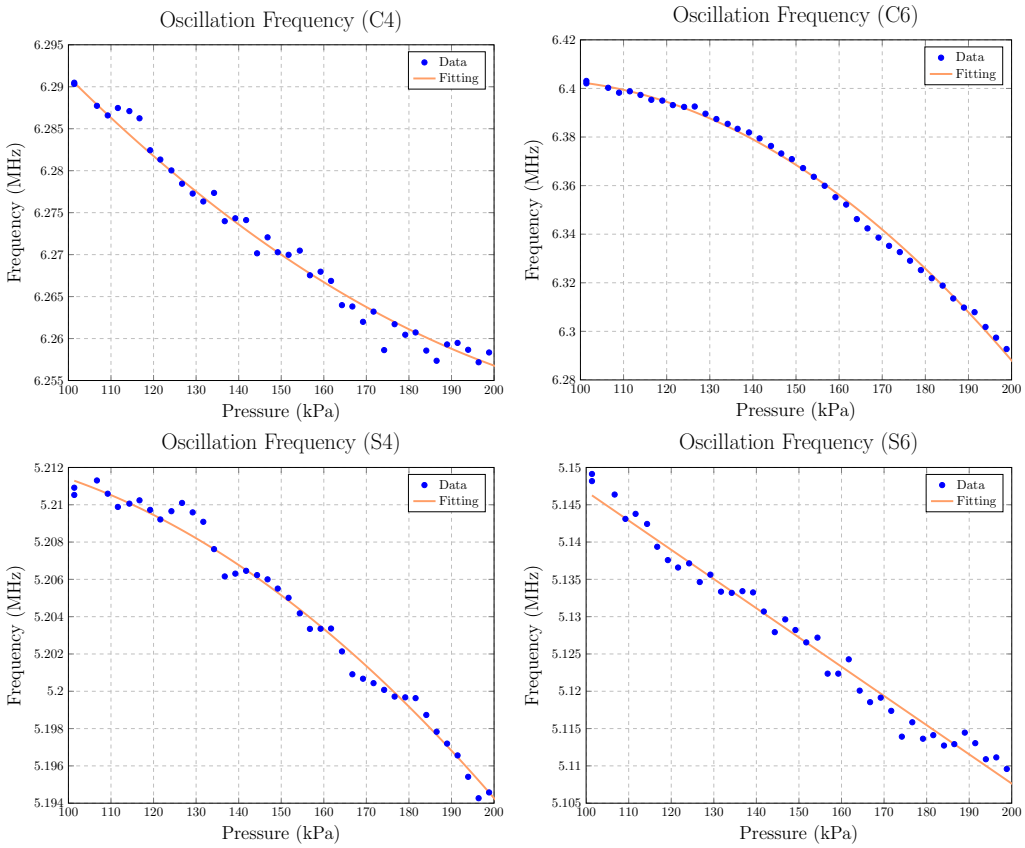

Figure 2.14: Sensors' oscillation frequencies measured with the telemetry system under pressure variations performed within a vacuum chamber.

recipe). The emulating solution was poured in a beaker in order to achieve the desired height, corresponding to the distance between the reader and the sensor. The reader antenna was placed under the beaker and the sensor was inserted in a hermetically sealed bag for protection and laid on top of the solution.

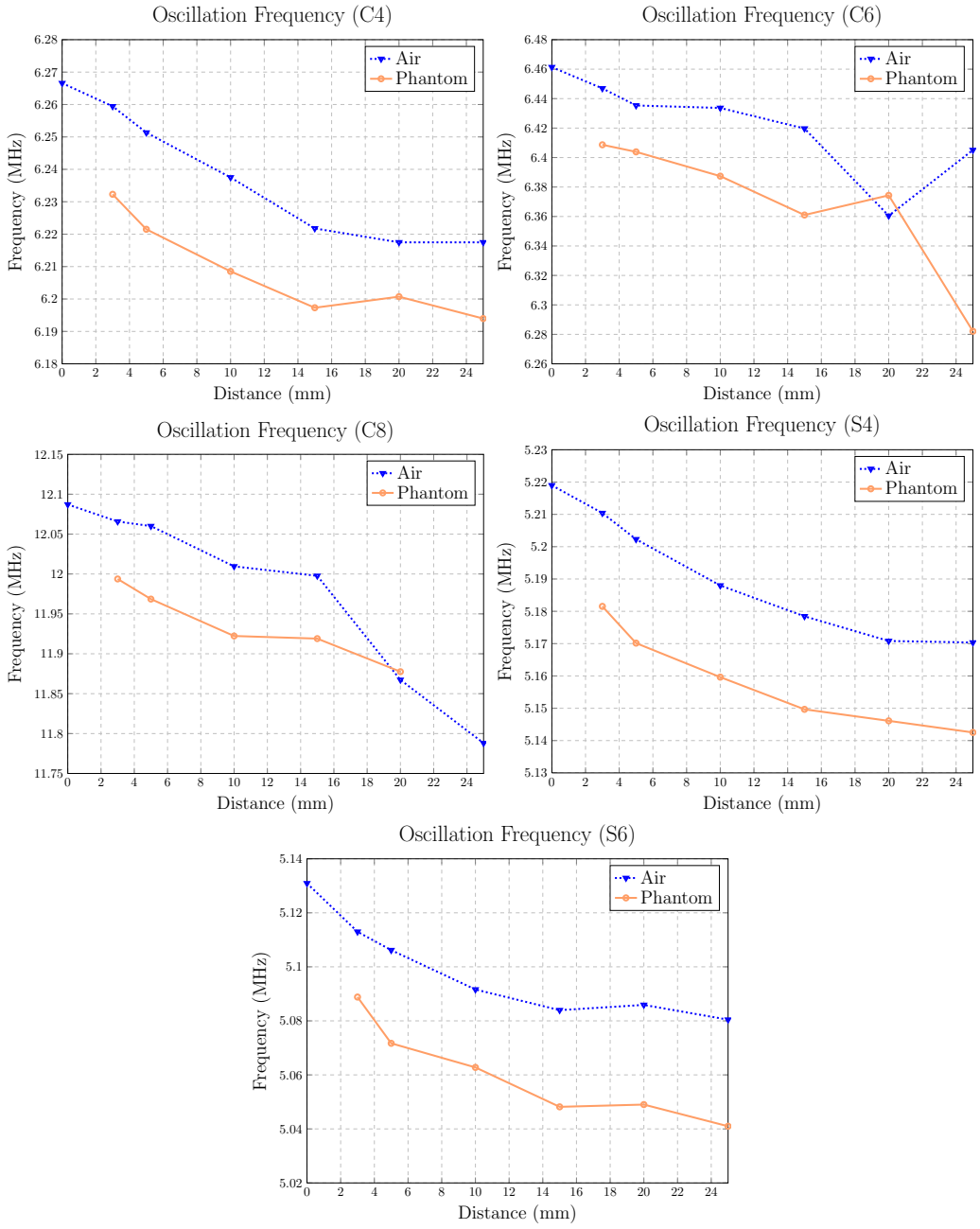

Figure 2.15: Frequencies measured with all the sensors using air and phantom as dielectric.

The curves presented in figure 2.15 show the variation of the measured oscillation frequencies of the different sensors, for a range of distances between the sensor and the reading antenna with air and phantom as the dielectric.

Hydraulic test bench

A hydraulic test bench that simulates the aorta was built to test the wireless pressure sensors and the reader system. This model includes the following elements:

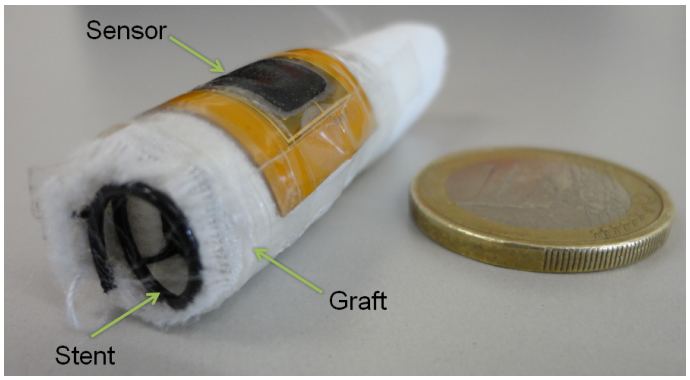

Figure 2.16: Stent-graft and the pressure sensor placed on top of the graft.

1. An electric 2/2-way solenoid valve, connected to the tap water, to simulate the cardiac cycle;
2. A tube to connect the valve to the aneurysm region;
3. An aneurysm region made with a flexible material;
4. A stent-graft made with a metal spiral to mimic the stent and a PET material to mimic the graft sewed and placed inside the aneurysm (figure 2.16);
5. A square 6x6 mm (S6) wireless pressure sensor placed on top of the stent–graft;
6. A commercial pressure sensor (MPXV5100GC6U from Freescale) placed in the tube right before the aneurysm region (a hole was made in the tube to place the sensor) connected to an acquisition board (NI DAQ USB-6008);
7. The wireless reader system with the reader antenna placed on the aneurysm region;

The complete setup is displayed in figure 2.17. The goal was to compare the performance given by the developed pressure sensor with that of a commercial sensor. Figure 2.18 displays the measured pressure and oscillation frequency during one trail. In this experiment the measurements started with the tap water closed, being then slowly opened and closed for 6 times to mimic the cardiac cycle.

Discussion of the results

This subsection discusses the telemetry system performance in terms of the accuracy of the sensor's electrical model, the effect of distance and biological tissue in the detected frequency

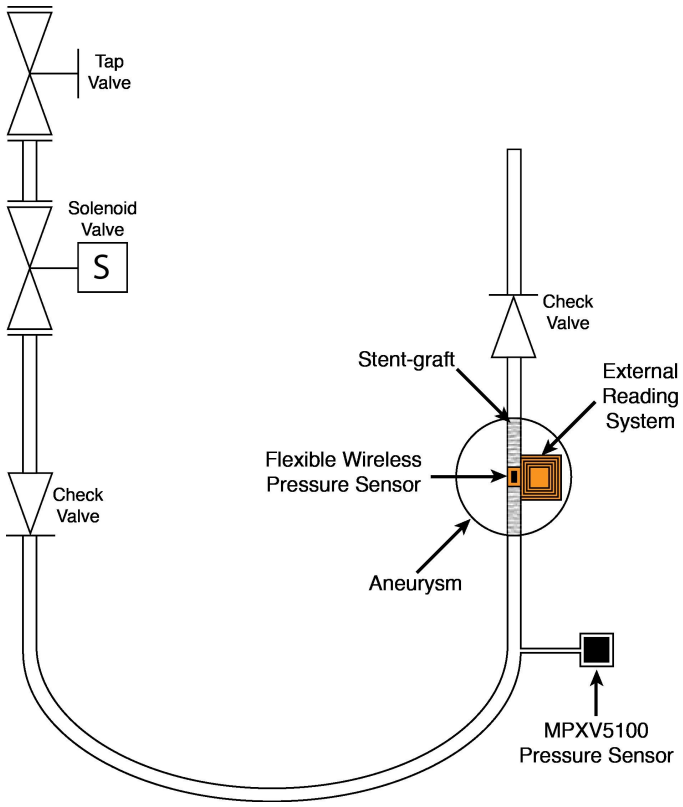

Figure 2.17: Diagram of the hydraulic test setup.

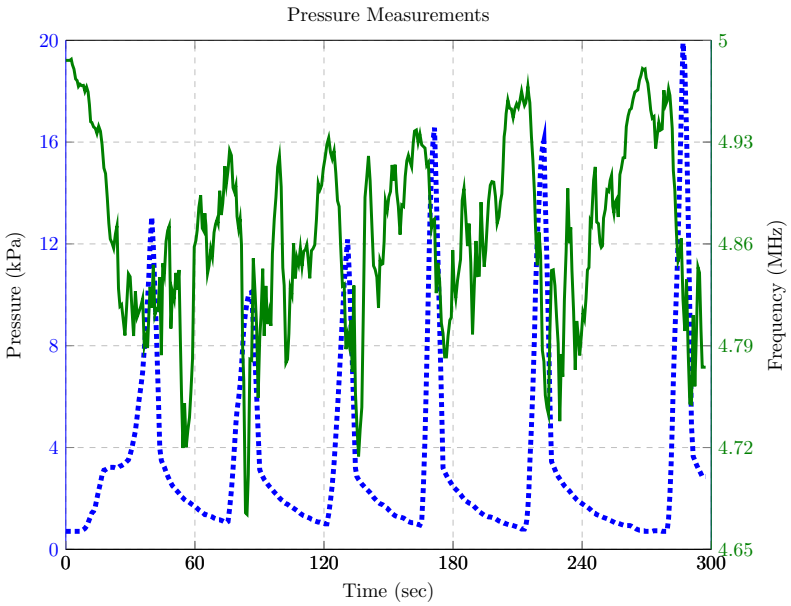

Figure 2.18: Measured pressure (continuous trace) and oscillation frequency (dashed trace) while the water tap valve was being opened and closed as in the cardiac cycle.

accuracy, the sensor's transfer characteristic curve and sensors performance in a hydraulic test bench.

Accuracy of the sensor's electrical model and the effect of distance and biological tissue in the detected frequency

Table 2.4 provides a comparison between the simulated and measured electrical parameters of the pressure sensors, such as the inductance, the SRF, and the sensors oscillation frequency after the assembly of the A–CNTs membranes.

The measured inductance values L_{meas} are lower than the values obtained after simulations L_{sim}. However, the antenna is not purely inductive since the overlap of the top and bottom coils introduces a significant parasitic capacitance, which is responsible for this difference, that is, it translates into a measured SRF of the antenna (SRF_{meas}) lower than the simulated value (SRF_{sim}).

Also, the measured oscillation frequency f_{meas}, for a distance of 10 mm between the sensor and the reading antenna, is lower than that expected from the simulated model f_{sim}, due to the fact that during the assembly of the A–CNTs onto the flex PCB using a special conductive glue, extra parasitic capacitance and resistance are inserted, which cannot be calculated.

Table 2.4: Simulated and measured parameters of the pressure sensors (inductance, SRF and oscillation frequency).

Results	C4	C6	C8	S4	S6	S8
L_{sim} [μH]	18.67	17.33	15.03	22.17	20.61	18.08
L_{meas} [μH]	15.05	13.36	—	18.08	16.12	12.78
SRF_{sim} [MHz]	8.28	8.72	9.63	5.82	6.15	6.86
SRF_{meas} [MHz]	7.89	7.96	—	6.23	6.33	7.36
f_{sim} [MHz]	7.86	7.79	7.92	5.60	5.64	5.86
f_{meas} [MHz]	6.32	6.43	12.01	5.19	5.09	—

The presence of the biological tissue causes a significant shifting of the received signal frequency. This can be due to the change of the medium permittivity to magnetic induction, also affected by the quality factor, as has been reported in [47],[48]. Regardless of this frequency shifting, found when comparing the detected signals in the presence and absence of the phantom, the detected signals showed signal-to-noise ratios and amplitude characteristics that allowed an easy detection of the sensor's resonant frequency, in the different cases.

Furthermore, the variation of the detected frequency tends to stabilize after the first 20 mm, meaning that the coupling coefficient k has little influence on the oscillation frequency for distances higher than 20 mm. It can be concluded that, since the distance between the abdominal section of the aorta where the stent–graft is meant to be placed and the anterior abdominal wall skin, is expected to be always higher than 20 mm [49], the system's performance will not be drastically compromised by the effect of the distance and the biological tissue.

Sensors' transfer characteristics

The transfer characteristics of the pressure sensors obtained with the telemetry system have a very defined shape, despite the presence of some small fluctuations seen with the smaller sensors (Figure 2.14).

The measured frequencies of sensors C4, C6 and S4 were fitted with a multiple linear least squares regression as a function of pressure $f_{osc}(p)$ (equation 2.3).

$$f_{osc}(p) = c_1 p^2 + c_2 p + c_3 p \tag{2.3}$$

The data from sensor S6 was fitted with a linear least squares regression due to its more linear behaviour (equation 2.4).

$$f_{osc}(p) = c_1 p + c_2 \tag{2.4}$$

Table 2.5 displays the regression coefficients.

Table 2.5: Regression coefficients for the frequency-pressure characteristic functions of each sensor.

Coeff.	C4	C6	S4	S6
c_1	1.591	-9.303	-0.926	-391.698
c_2	-821.228	1646.296	106.485	5185966.492
c_3	6357389.276	6330888.228	5210008.700	–

Sensor S6 presents the highest sensitivity in the region of interest, with a frequency variation of approximately 14.981 kHz between 100 kPa and 130 kPa. This result was expected since the square sensor has a A–CNT sensing membrane with larger area. The pressure inside the aneurysm sac is expected to be bellow 40 mmHg (105.33 kPa) in a successfully excluded AAA after the EVAR procedure. If there is an endoleak the aneurysm sac pressure rises to the levels of the patient arterial blood pressure, typically between 70 mmHg (109.33 kPa) diastolic and 200 mmHg (126.66 kPa)[34]. Hence, the purpose of our sensors is to distinguish between these two situations. Figure 2.19 displays the expected pressure in the aneurysm sac in the normal state (no endoleak), as well as in the presence of endovascular leakage, and compares them with the performance of sensor S6 for the region of interest. The noise of the sensor response plus the complete reading system (accuracy of the system) was measured for all the sensors, having a value of 2.28 Hz in average been obtained. These data shows that for this initial sensor version (not optimized and presenting large parallel capacitances that greatly reduce sensitivity) it would still be possible to detect endoleaks.

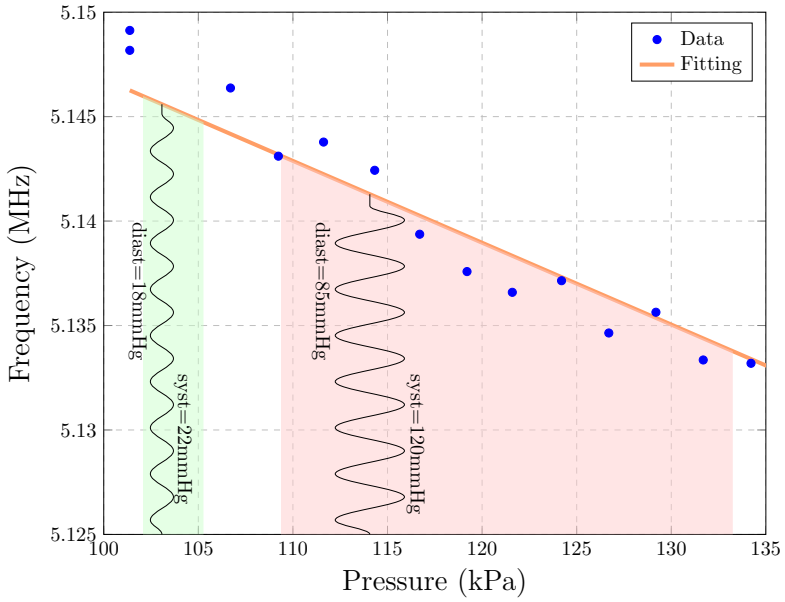

Figure 2.19: Transfer function of sensor S6 compared against the pressures expected in the aneurysm sac for a stent-graft without an endoleak (green range) and for a stent-graft with an endoleak (red range).

Sensors performance in a hydraulic test bench

Although a manual control of the water tap was used and thus there was some uncertainty in the pressure levels, still a variable pressure profile could be obtained that allows us to evaluate the sensor behaviour. Since the oscillation frequency is inversely proportional to the capacitance (equation 2.1), the highest oscillation frequencies correspond to the lowest pressures (when the water tap is closed). There is a slight delay between the measured pressure and the corresponding frequency shift, which is due to the location of the sensors. Since the water first passes by the commercial sensor and after by the aneurysm sac where the wireless pressure sensor is inserted, the pressure changes are first detected by the commercial sensor, as it is observable in figure 2.18. Also, the detected frequency seems to take longer to reach the values for lower pressures, in opposite to what happens within the commercial sensor that shows faster responses to lower pressures. As the aneurysm emulating sac accumulates water its flux goes from laminar to turbulent.

These proof–of–concept experiments demonstrate the suitability of the small, flexible, and passive sensor along with the readout telemetry system, to detect pressure variations in aneurysms.

Telemetry system calibration

The telemetry system is being improved in order to include a fault detection system, taking advantage of other physiological signals like the electrocardiogram (ECG) and arterial blood pressure (ABP), and resorting to measurements of the power and impedance seen from the reader

circuit to diagnose deviations in the *LC* values of the pressure sensor [50]. The reliability of the telemetry system can be further improved by placing a sensor with a fixed *LC* value, i.e. the value of C_s is not affected by the pressure inside the aortic sac, to be used as a reference. Taking the oscillation frequency given by this LC_{ref} and comparing with that given by equation 2.1, the deviation between the measured and expected frequencies can be used to calibrate the remaining sensors, whose responses are affected by the presence of human tissue and tilting. This calibration can be done right after the placing of the stent–graft.

2.3.3 ECG Data Acquisition and Transmission Unit

Wearable monitoring systems demand, to be viable, that high levels of dependability and autonomy are ensured in order the gathered data can be considered secure for medical diagnosis. Low-power consumption systems ensure longer operation time between recharges for the same battery capacity and tend to be more comfortable once bulky batteries are avoided. These are achieved after selecting the most power efficient devices available in the design phase and by means of adopting adaptive schemes to manage the power consumption when the device is operating in the field.

Figure 2.20 shows the 12-lead ECG data acquisition and transmission (DAT) module prototype that was developed. It is a circular board (30 mm ⌀) with an ECG acquisition analogue front-end based on the low-power Texas Instruments 24-bit ADS1298 chip and a PAN1740 Bluetooth Low Energy (BLE) module from Panasonic. The board includes also an I2C EEPROM and a DC-DC converter to supply a regulated 3.3 V. The PAN1740 is a small (9 x 9.5 x 1.8 mm) BLE single mode module based on the Dialog DA14580 SoC with an advertised power consumption of 4.9 mA when transmitting/receiving. This SoC includes a 32 bit ARM Cortex M0 microcontroller operating at a 16 MHz frequency, that is used to perform all the necessary processing operations, thus saving the cost of an external μC, the additional PCB area and power consumption. The EEPROM is used to save the application code during the developing phase. In the final version it can be removed and the code can be saved in the One-Time Programmable (OTP) memory present on the BLE module.

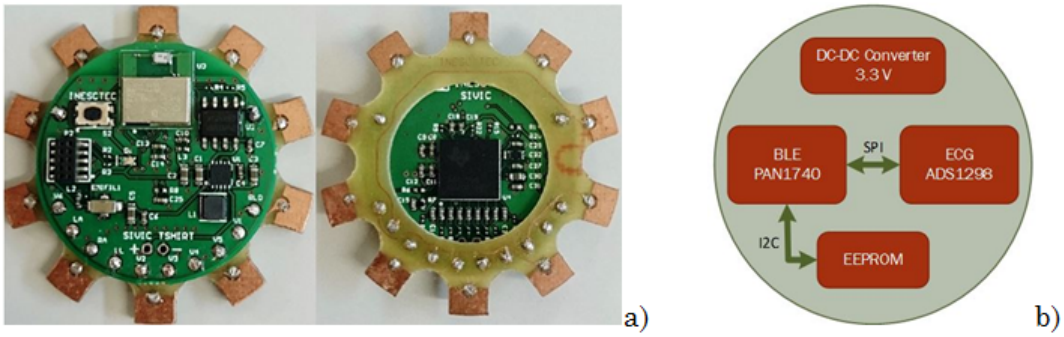

Figure 2.20: a) Photo of the 12-lead ECG module prototype (front and back sides); b) block diagram.

Besides the selection of low-power devices further research was carried out to minimize the power consumption involved in the data acquisition, processing and transmission of the captured data. Although 24-bit samples are captured from the ADS1298, only 16-bit resolution samples are used. This reduction in samples resolution provides a first approach to de-noising and reduces the power required for transmission.

In the running mode, the μC receives an interruption from the ADS1298 every 4 ms, indicating the presence of new samples. That initiates an SPI communication to get the samples from the 3 channels and save them in a buffer. For each T ms, where T can be defined, an application task is executed to check if the buffer size reached 120 bytes. When that is the case, data is copied to the BLE Attribute Protocol (ATT) database and a notification is sent to the mobile phone to initialize the data transmission procedure. The final ECG data processing operations (e. g., decompression, QRS and T-wave detection algorithms) are implemented in the mobile phone, which is, eventually, also responsible to transmit collected data to a data center for more complex diagnosis.

The DAT is set with a sampling frequency of 250 Hz, which provides a good balance in terms of data accuracy and power consumption. This frequency is adequate to ensure that phase noise does not impair the estimation of the R-wave fiducial point [51].

Wireless ECG monitoring systems with a high number of leads (e.g. 12-lead) are usually designed for clinical usage, being systems with a lower number of acquisition channels (e.g. 1 to 3 channels) commonly used in ambulatory cases [52, 53]. The SIVIC system was designed having in mind its use in both clinical and ambulatory scenarios, and thus the number of ECG data acquisition channels is reconfigurable between a single lead (1 channel) to twelve leads. Inputs not used to capture ECG signals can be used to acquire other biosignals.

The development of this readout unit included also the design of a custom socket which would allow for an easy attaching and detaching to and from the T-shirt. Figure 2.21 shows the 3D view of this socket and cover, how the electronic board is inserted, and a view of the final T-shirt including also the socket.

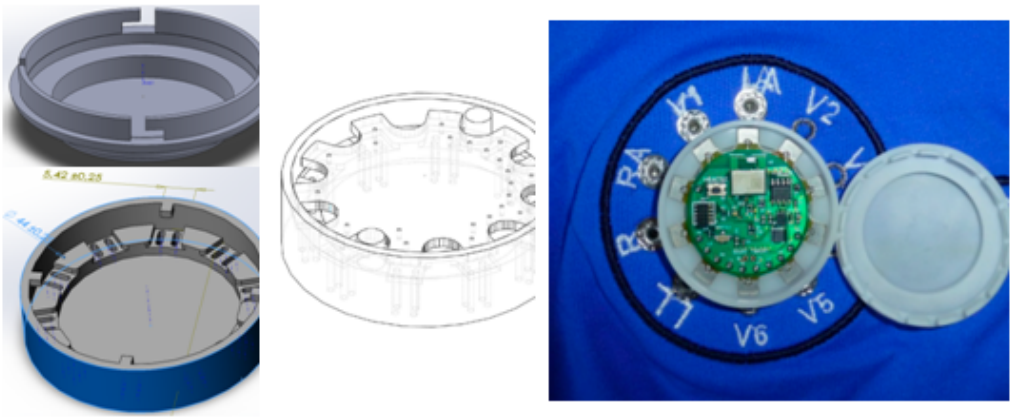

Figure 2.21: Custom socket designed to provide the attachment of the electronic readout unit to the T-shirt..

Figure 2.22.a) shows a prototype of the T-shirt with the cardiac monitoring SIVIC system. It integrates five snap fasteners in the configuration corresponding to the derivations of the triangle of Einthoven and Wilson leads I, II and III and the precordial V1. The T-shirt was fabricated using seamless knitting technology and is composed of two superimposed fabrics, integrating snap fasteners to attach the ECG electrodes. These interconnect to the DAT unit through embedded textile conductors and a custom designed socket. Five snaps are also available to connect to an external conventional Holter for comparison purposes.

a) b)

Figure 2.22: a) A SIVIC 5-leads unit and T-shirt prototype; b) Android application screenshot.

The T-shirt data acquisition board communicates with a smartphone via the Bluetooth Low Energy technology (BLE) protocol. Once the application (app) is started, the smartphone performs a scan to identify the Bluetooth devices in the environment. After the user selects the T-shirt board, the communication link is established and the smartphone starts receiving data frames. This application uses the androidplot library which provides dedicated functions to display graphical data as well as managing functions such as scrolling, definition of the window size, zooming, colours, etc.

To read data, the app uses a CSV parser. It allows distinguishing different rows and columns. At each line, the CSV parser assigns the values to decimal variables that can be subjected to filtering, for example to remove the baseline due to respiration or other interferences (Figure 2.23).

Figure 2.23: ECG plot in the smartphone before and after filtering.

Figure 2.22.b) shows ECG signals displayed on a smartphone, captured when a person wears the T-Shirt in a steady position and without any skin preparation. In this case the smartphone

receives three leads (LI, LII, V1) and from them calculates four more leads (LIII, aVR, aVL, aVF) [32].

```
protected int HeartBeat (int heartBeat, double avg,
double l2, double prePreviousL2 ){
if (l2-prePreviousL2>=0.7 && j>0 && cont_samples-
cont_samples3 >=10){
heartBeat++;
cont_samples3 = cont_samples;
}
return heartBeat;
}
```

Nevertheless, preliminary processing is performed, namely to detect the heart beating. To find heartbeats, a while loop analyses samples to see if rising edge are present, i. e., if the difference between the current sample and the previous ones is higher than 0.7 mV that is considered as a rising edge.

Each time a heartbeat is found the heart beating counter is updated. The heart beating rate in beats per minute is calculated periodically for diagnostics purposes. The buffer $diff[]$ provides the difference between successive heartbeat and allows detecting abnormal changes in the heart beating rate.

```
protected float DeltaQRS(int[] qrsBuffer, int heartBeat){
for(i=0;i<= heartBeat - 2 ;i++){
diff[i]=qrsBuffer[i+1]-qrsBuffer[i];
if (i == 0){
expectation = diff[i];
}
else{
expectation = (expectation + diff[i]);
}
}  expectation /= heartBeat-1;
return expectation;
}
```

2.4 Standards for medical devices

International standards ISO 14971, ISO 13485, and IEC 60601 mandate the documentation of a medical device manufacturer's risk management process. During the premarket approval (PMA) process for medical devices, including 510(k) and other PMA documentation requirements, a documented risk analysis process for the hardware, software, and electronic components used

in medical devices is required by the Federal Drug Administration (FDA). Risk management is reported under these requirements using a risk management file, which contains all of the documents, records, and other supporting materials produced by the risk management process, so that it is both traceable to functional and safety requirements and transparent to regulatory agencies [54].

Table 2.6: Several key international standards for medical device reliability and medical device software reliability.

Medical Device Standard	Definition
ISO 14971	Establishes the requirements of risk management for ensuring the safety and reliability of medical devices
IEC 60601	Identifies required safety standards for electromedical equipment
ISO/TR 80002	Applies the risk management requirements of ISO 14971 to medical device software
IEC 62304	Defines lifecycle requirements for medical device software to establish a framework for software development and maintenance
IEC 21 CFR Part 11	Requires that any software used to develop and manufacture medical devices meet certain standards for data security and integrity
IEC Verification and Validation	Defines testing procedures to ensure that medical device software specifications meet functional needs and fulfils its design specifications

2.4.1 ISO 14971

As an internationally recognized standard for medical device manufacturers, ISO 14971 establishes risk management as an essential part of ensuring the safety and reliability of medical devices. Derived from ISO 13485, which requires a documented product realization process, ISO 14971 specifies that this process should include risk management. This standard:

- specifies a framework manufacturers must use to identify the hazards associated with a medical device, including in vitro diagnostic medical equipment;
- requires companies to conduct and document a risk management process, which it defines fully as described above;
- applies to all stages of the product lifecycle, from its design and development through its decommissioning and disposal;
- calls for the evaluation and assessment of risks to patient, operator, and others; and extends to the equipment itself, other equipment, and the surrounding environment.

2.4.2 IEC 60601

This standard identifies required safety standards for electrical medical equipment, which may be defined as equipment connected to a power supply and used in diagnosis, treatment, or monitoring of a patient; which makes physical or electrical contact with the patient, transfers energy to or from the patient, and/or detects energy transfer to or from the patient. This standard also extends to accessories used with such equipment. This standard:

- sets specific requirements for electromagnetic compatibility, human factors such as the usability of devices, and specific types of applications such as devices used during surgery;
- defines hazards ranging from electrical shock, mechanical sources of harm, radiation, ignition or fire, and excessive energy output;
- requires the use of risk controls including safety by design, protective measures taken during manufacturing, and instructions or labelling information for safety;
- identifies performance requirements, that is, characteristics of a system which are required to maintain residual risk;
- mandates risk analysis activities for specific areas of product design, including protection against shock, protection against the entry of liquids, and the use of flammable materials.

2.5 Conclusions

Wearable technology has demonstrated its usefulness in several applications such as: examination and management of cardiovascular diseases, rehabilitation — in order to provide more precise assessments of human performance and help health care providers to optimize the nature of the rehabilitation interventions by tailoring them to the habitual environment of the patient—, biofeedback in Parkinson patients and for functional assessments in stroke patients [55].

Health-monitoring wearable systems include a vast and heterogeneous range of devices and WSN standards, in order to facilitate and promote their use in a wide range of applications. The development of these systems have involved the efforts or different researchers, developers and users. Their intrinsic interdisciplinary nature is an outcome of the functional characteristics of the applications related to health care and thus integrate biomedical engineering, microlelectronics, communications, and medical informatics. Also, knowledge in the fields of medicine, social sciences, psychology, economics, ethics, and law must be taken into account and be integrated into the development and deployment of wearable health-monitoring systems. Since most of these systems are still on prototype stages, developers have not yet faced deployment issues. The research focus on the next few decades will be to address the deployment issues such as service

organization, privacy, user needs, acceptance, system security and safety, and economic and financial issues. Systematic evaluations of the effectiveness and efficiency of wearable health care systems are considered crucial to ensure potential user acceptance. Along with these perspectives, several technical, as well as medical issues, have to be solved before definite clinical trials can be conducted. The most important challenges are the development of smart signal processing, data analysis and interpretation, communication standards interoperability, electronic components efficiency, and energy supply. To get the most out of the wearable technologies, research needs to be carried out by studying user requirements and developing a comprehensive approach to health and wellness services, instead of devices and applications that monitor only single diseases [56].

Based on these needs the SIVIC system was developed. The system is a combined cardiac and aortic monitoring system that provides the synchronous measurement of a patient's ECG and pressure in the abdominal aneurysm sac, in order to obtain a more robust and reliable monitoring. Wireless pressure sensors are used to capture the intra-sac aortic abdominal aneurysm pressure and detect endoleaks. An electronic readout unit (ERU) capable of energizing the pressure sensors and capture the pressure data is placed in the chest of the patient. This unit provides also the monitoring of a 12-lead ECG using textile dry electrodes. The electronic unit and the electrodes are built in a customized clothing. Data is transmitted to a smartphone for further processing, data display, and eventual communication with a healthcare center.

The next chapter will be focused on the dependability requirements for wearable medical devices. First the concepts of dependability will be introduced, namely the reliability, security, safety, availability and maintainability. Also techniques and strategies to improve the values of such dependability attributes will be studied and compared.

Chapter 3

Dependability

Medical application systems demand high levels of dependability and trust of performance [9]. According to the IEC (International Electrotechnical Commission) IEV (International Electrotechnical Vocabulary) 191-02-03 standard "dependability (is) the collective term used to describe the availability performance and its influencing factors: reliability performance, maintainability performance and maintenance support performance". A system's dependability study includes the attributes analysis (e.g., availability, security and maintainability), risks (defects and failures), means (of prevention, detection and fault tolerance) and enables the objective of an efficient development of test and self-test methodologies.

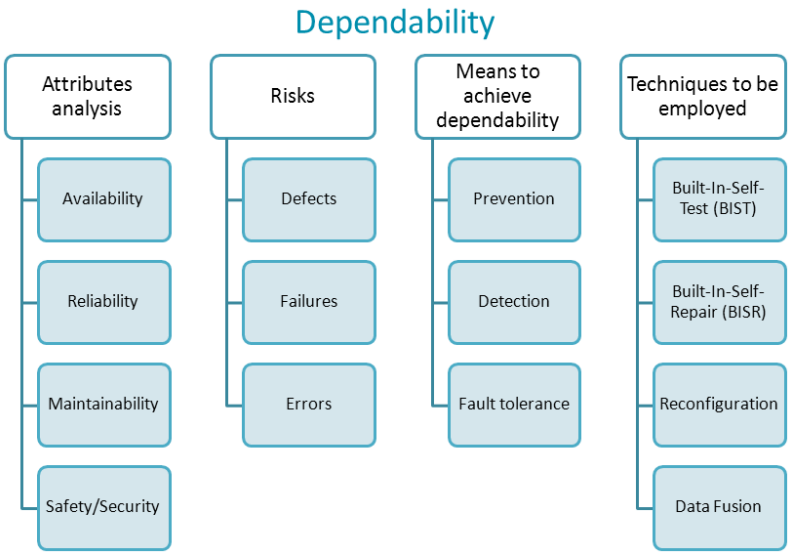

Figure 3.1: Dependability framework.

3.1 Dependability attributes

3.1.1 Reliability

Reliability is defined as the probability that an item can perform a required function under given conditions for a given time interval (t_1, t_2) and is often specified in terms of the Mean Time Before Failure ($MTBF$) or Failures In Time (FIT). It is generally assumed that the specified item is in a state to perform this required function at the beginning of the time interval.

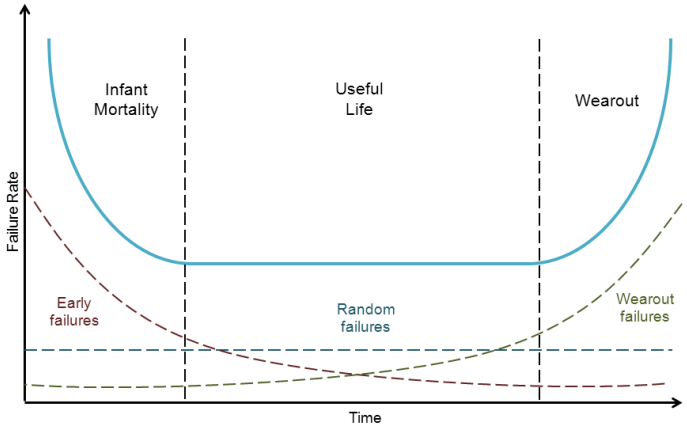

Figure 3.2: Reliability rate of a medical device.

The parts count method calculates the system or equipment failure rate under the single-use environment by using the following equation [57]:

$$\lambda_S = \Sigma_{i=1}^{n} \theta_i (\lambda_g Q_g)_i \tag{3.1}$$

where, λ_S is the system failure rate expressed in number of failures/10^6 hours.
n is the number of different generic component classifications.
Q_g is the generic component quality factor.
λ_g is the generic part failure rate expressed in failures/10^6 hours.
θ_i the generic part quantity for classification i.

The values of Q_g and λ_g are tabulated in [57].

Reliability is composed of three primary subdivisions, each with its own particular attributes: electronic reliability, mechanical reliability and software reliability.

3.1.1.1 Electronic reliability

Electronic reliability is a function of the age of a component or assembly. The failure rate is defined in terms of the number of malfunctions occurring during a period of time (figures 3.2and 3.3a). As is evident from figure 3.2, the reliability rate is divided into three distinct time periods: infant mortality, useful life and wear-out.

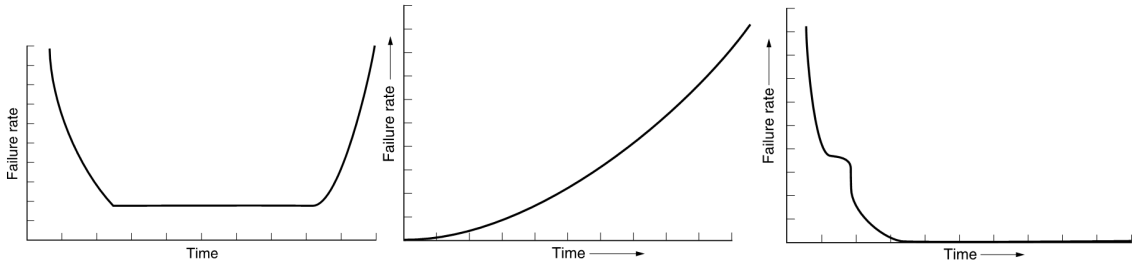

(a) Electronic reliability. (b) Mechanical reliability. (c) Software reliability.

Figure 3.3: Reliability rate [58].

Infant mortality is the beginning of the life of an electronic component or assembly. This period is characterized by an initial high failure rate, which decreases rapidly and then stabilizes. These failures are caused by gross, built-in flaws, due to faulty workmanship, bad processes, manufacturing deviations from the design intent or transportation damage. Examples of early failures include: poor welds or seals, poor solder joints, contamination on surfaces or in materials, voids, cracks, or thin spots on insulation or protective coatings [58]. Many of these failures can be prevented by improving the control over the manufacturing process or by screening components. Improvements in design or materials are necessary for these manufacturing deviations.

The useful life period of a component or assembly is the largest segment of the life cycle and is characterized by a constant failure rate. During this period, the failure rate reaches its lowest level and remains relatively constant. Failures occurring during this period are either stress related or occur by chance. These are the most difficult to repeat or analyse.

The final period in the life cycle occurs when the failure rate begins to increase rapidly. Wear-out failures are due primarily to deterioration of the design strength of the components or assemblies, as a consequence of operation and/or exposure to environmental stress. Such deterioration may result from: corrosion or oxidation, insulation breakdown or leakage, ionic migration of metals on surfaces or in vacuum, frictional wear or fatigue, shrinkage and cracking in materials. Replacing components prior to reaching this period through a preventive maintenance program can prevent wear-out failures [58].

3.1.1.2 Mechanical reliability

Mechanical reliability (figure 3.3b) differs considerably from electronic reliability in its reaction to the ageing of a component or assembly. Mechanical components or assemblies begin their life cycle at a failure rate of zero and experience a rapidly increasing failure rate. This curve approximates the wear-out portion of the electronics life curve.

Mechanical failures are due primarily to deterioration of the design strength of the component or assembly. Such deterioration may result from: frictional wear, shrinkage and/or cracking, fatigue, surface erosion, corrosion, creep, material strength deterioration. Optimization of mechanical reliability occurs with timely replacement of components or assemblies through preventive

maintenance, before the failure rate reaches unacceptably high levels [58].

3.1.1.3 Software reliability

The following definition of reliability is given by the IEEE Standard Glossary of Software Engineering Terminology: "The ability of a system or component to perform its required functions under stated conditions for a specified period of time". In the case of medical device software, that definition should be expanded to include the concepts of safety and efficacy as follows: The ability of a system or component to perform its required functions in a safe and effective manner, under stated conditions, for a specified period of time. The main point of this definition is that reliability, safety, and efficacy are inseparable requirements for medical device software. In order to apply this definition, the software developer must know exactly what the "required functions" of the particular medical device are. Sometimes such functional definitions are obvious, but in general they are not. Such knowledge requires the existence of a formal software specification. In addition, the software developer must know the "stated conditions". This means the environment in which the software is to operate must be fully defined. This may include whether the software will be operated during a stressful situation, the lighting and noise levels in the area of operation, and the technical knowledge of the user. "For a specified period of time" indicates that the reliability is being measured for a specific period of time, known as a mission time. This may be the length of a surgical case, the warranty period for the device, or the total operational life of the device. Software reliability differs considerably from both electronic and mechanical reliability in that software is not subject to the physical constraints of electronic and mechanical components. Software reliability consists of the process of preventing failures through structured design and detecting and removing errors in the coding. Once all "bugs" are removed, the program will operate without failure forever. However, practically, the software reliability curve may be as shown in figure 3.3c, with early failures as the software is first used and a long period of constant failures as bugs are fixed. Software failures are due primarily to: specification errors, design errors, typographical errors and omission of symbols [58].

3.1.2 Availability

The availability represents the readiness for correct service of the system and conversely the unavailability (1-availability) is the time over lifetime during which the system is being repaired. The availability can be related to Mean Time Betwwen Failures (MTBF) in repairable systems (or to Mean Time To Failure (MTTF) in the case of no repair options) in terms of the Mean Down Time (MDT) using equation (3.2)[59]:

$$Availability = \frac{MTBF}{MTBF + MDT} \tag{3.2}$$

3.1.3 Maintainability

Maintainability is another system design parameter that has an impact on the effectiveness of a system. It represents the ability of a system to undergo repair and modifications. Failures will occur no matter how reliable a system is. A system's ability to be maintained, that is, retained in or restored to an effective usable condition, is important to systems' effectiveness. Maintainability is a characteristic of system design, as is reliability [58].

3.1.4 Safety

Safety evaluates the occurrence or risk of injury, loss and danger to persons, property or the environment and can be described by the Safety Integrity Level (SIL) [60]. For implantable medical devices safety is a key element, since according to the European Council Directive 90/385/EEC on the approximation of the laws of the member states relating to active implantable medical devices [61] "The devices must be designed and manufactured in such a way that, when implanted ... their use does not compromise the clinical condition or the safety of patients. They must not present any risk to the persons implanting them or, where applicable, to other persons."

3.2 Dependability risks

A *fault* is an anomalous physical condition caused by a manufacturing problem, fatigue, external disturbance (intentional or un-intentional), design flaw. An *error* is the effect of activation of a fault and a *failure* is the over-all system effect of an error. In most cases a fault first causes an error in the service state of a component that is a part of the internal state of the system and the external state is not immediately affected. For this reason the definition of an error is: the part of the total state of the system that may lead to its subsequent service failure. It is important to note that many errors do not reach the system's external state and cause a failure. A fault is active when it causes an error, otherwise it is dormant [62].

Although dependability issues are more often addressed in sensors and actuators since they interact with the environment, front-end and back-end analogue electronics are of interest due to their higher sensitivity to parameter variations in comparison with digital circuits. Also sensors are often completely integrated with the front-end electronics. Despite very little information can be found on the dependability of analogue and mixed-signal circuits, it is one of the most critical parts of most critical systems, especially in the medical ones [63].

With the moving of designs into nanoscale technology levels, new deep submicron technologies circuits are subject to different degradation mechanisms like Negative Bias Temperature Instability (NBTI), Positive Bias Temperature Instability (PBTI), Hot Carrier Injection (HCI), and Time Dependent Dielectric Breakdown (TDDB). Several analogue operations require matched parameters and therefore any mismatch introduced by these degradation mechanisms can result in analogue circuit failures [60].

The commercial semiconductor industry in general, and implantable devices in particular, have historically benefited from the wide reliability margin available in early generation technologies. As long as no extrinsic defects were allowed to escape into a product population, failures due to material wearout were extremely unlikely. However, performance demands required to stay on the Moore's Law curve have increasingly reduced that margin, to the point that wearout due to some failure mechanisms is an important product consideration. Figure 3.4 gives a schematic illustration of this problem, showing new technology generations pushing the envelope out closer to the intrinsic failure point [64].

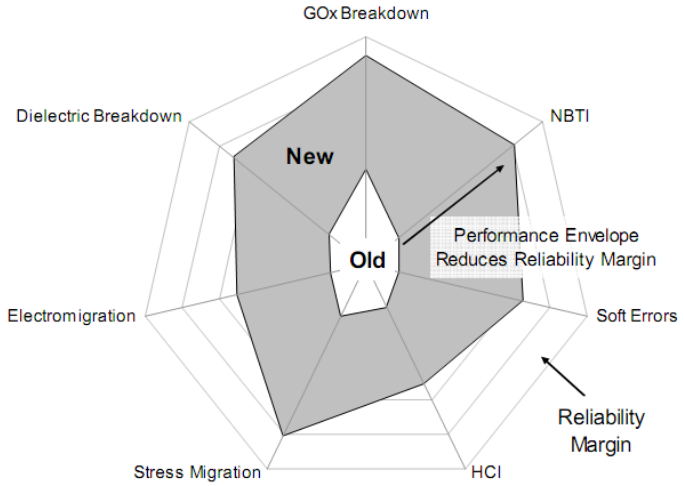

Figure 3.4: Schematic illustration of reduced reliability margin due to pushing of the performance limits. Failure due to wear-out occurs at the outside end of each axis [64].

3.3 Means to achieve dependability

Figure 3.1 summarizes the methodology to achieve dependability. This qualifier is composed by several attributes such as reliability, availability, security/safety, maintainability, which can have a different weight for each system, or even for each block inside a system. Therefore it is crucial to define the level of complexity of the dependability analysis, in order to account for the main attributes that influence the functioning of the system/block.

The first task in order to achieve a dependable system is to identify the risk that can compromise the correct operation of the system's components and perform a fault tree analysis for each block of the system: pressure sensor, external reading circuit, ECG acquisition circuit, microprocessors, and other elements of the system. The analysis is performed taking in consideration the most likely failure mechanisms and probability of working rates of each building element. One of the obstacles here arises from the difficulty of establishing dependencies among components or modules of the electronic system. Assuming independence between elements, when that is likely, helps for building the corresponding dependability hierarchy model.

3.3.1 Failure mode and effect analysis

Failure mode and effect analysis (FMEA) is a widely used tool to evaluate a design at the early stage from the reliability aspect. This criterion is extremely useful to identify the need for and the effects of a design change. FMEA requires the listing of all possible failure modes of each component on paper and their effects on the listed subsystems, etc. The method is known as failure modes, effects, and criticality analysis (FMECA) when criticalities or priorities are assigned to failure mode effects. A FMEA is a bottom-up approach that identifies each failure mode, beginning with the lowest-level components in the system, and examines the effects of their failures at higher levels of the system. In this way, a FMEA can trace the end effects of part failures through to system-level failure and the risks or hazards it can cause. A FMEA can also include an analysis of the criticality of each failure mode: an analysis method often referred to as a FMECA (Failure Mode, Effects, and Criticality Analysis) whereby potential failure modes are classified according to their severity or risk. A FMEA is an extremely flexible analysis tool, as it may apply to the product itself or to the process of using the medical device. Its flexibility makes this method ideal for meeting the standards imposed by medical device regulations. Some of the important characteristics of FMEA are as follows:

- it is an upward approach that starts at the detailed level;
- after examining failure effects of all components, the entire system is screened completely;
- it is an effective tool to identify weak spots in system design and indicate areas where further or detailed analysis are desirable;

This technique allows a systematic analysis of a product or a process at the early stages of development to initiate different avoiding measures.

Disadvantages of FMEA are the high effort of execution and the complexity of analysis, which increases significantly with the complexity of the analyzed system. A reduced effort of execution can be achieved by the use of an appropriate software support. Another disadvantage of FMEA is that complex causal chains cannot be mapped by the defined sequence to determine "error, fault effect, cause of error". The result of the FMEA only reflects the subjective assessment of the experts involved, and in particular the obtained risk priority number cannot be considered as an absolute measure of risk. The isolated application of FMEA does not lead to an objective quantification of risks and solutions to eliminate causes of errors. However, it allows a systematic and structured collection of explicit and implicit available knowledge about possible errors [65].

3.3.2 Fault tree analysis

Fault tree analysis (FTA) is — besides FMEA — one of the most common methods of quality management. The core of the method is the creation of a fault tree based on a previously performed system analysis. Based on one error, all possible failure combinations are collected that may have caused the error.

FTA begins by identifying an undesirable event, called the top event, associated with a system under consideration. Fault events which could cause the occurrence of the top event are generated and connected by logic operators such as AND and OR. The AND gate provides a TRUE (failed) output when all its inputs are TRUE (failures). In contrast, the OR gate provides a TRUE (failure) output when only one OR more of its inputs are true (failures). All in all, the fault tree construction proceeds with the generation of events in a successive manner until the events do not need to be developed any further.

FTA offers the distinct advantage of an event-oriented methodology for evaluating the likelihood of occurrence of a system or component failure. As an extremely flexible analysis methodology, FTA allows for the incorporation of a number of different contributing events, including a combination of software or hardware failures, human errors, and environmental influences all within a single Fault Tree. By using a logic tree to graphically represent the contributing events, FTA can employ quantitative or qualitative analysis to determine the criticality of each contributing factor, identify the minimum combination of contributing factors that can lead to the failure, and assist in the development of control measures that would prevent or mitigate the circumstances leading to the top-level failure or event. Additional quantitative techniques available in FTA use failure and repair data about lower-level components to calculate the likelihood of the top-level event. FTA also incorporates importance measures that help the analyst determine which factors need to be improved by identifying the criticality of contributing events, including the probability that the top event is a contributing factor, as well as the maximum risk to the system if the contributing factor fails versus if it is operational.

The conclusion of the FTA is the analysis of the found correlations regarding to the probability of failure occurrence. Like the FMEA, the FTA does not cover complex relationships between sub-systems [65].

3.3.3 Comparing FMEA and FTA

Recall that FMEA is a bottom-up analysis methodology, beginning with the identification of the potential failure modes of component parts and identifying the effects of their failures on sub-assemblies, assemblies, and, ultimately, the system as a whole. In contrast, FTA employs a top-down method: beginning with the undesirable top-level event and identifying the events and factors — down to the failure of lowest-level components or processes — that may contribute to the top-level failure. FMEA and FTA analyses can be used together. When it is easier to identify an end-level failure and work backward to determine what caused it, FTA is ideal.

From those lower-level failures, a FMEA may be generated to determine other effects they could have throughout the system. Similarly, when a FMEA process has identified system-level failures caused by failures in lower levels of the system, a Fault Tree analysis can be incorporated to identify other sources that may also contribute to the failure.

3.4 Fault detection and maintainability

3.4.1 Fault detection and fault tolerance

Once the faults in the system are identified, a reconfiguration/repair can be performed in order to go back to a normal functioning. These operations are time consuming and have associated costs, which requires the system to be as much fault tolerant as possible. The available techniques to achieve fault tolerance in the most critical blocks of the system need to be evaluated, considering the same restrains for the fault detection (namely by means of redundancy which implies more area, extra cost, increase in power consumption and more bulk and heavy systems).

In consequence testing operations, including built-in self-test, can be employed in order to ensure the highest dependability levels. For the design of fault detection circuits several aspects need to be considered, such as fault mechanisms, test methods, fault coverage the extra area added with this feature, the extra cost, increase in power consumption and more bulk and heavy system.

3.4.2 Data fusion

The rate of collected data is high in medical sensor networks and is continuously increasing as new measurements are taken over time. Thus an efficient data cleaning process is necessary in the data collection step to identify and keep relevant data summaries. The second issue is how to generate a reliable context in the information system using data aggregation and data fusion. Different aggregation and fusion techniques may need to be applied depending on the types of sensed data. In addition, reliable and robust communication is necessary in the data fusion step. The goal is to produce high confidence data for medical diagnosis and treatment. This leads to a high belief level in the generated context.

Generally, data fusion is the process of putting together information obtained from many heterogeneous sensors, on many platforms, into a single composite picture of the environment. Also, fusion of data from multiple sensors is useful for obtaining more reliable information than individual measurements obtained from a single type of sensor.

In a pervasive healthcare system, three levels of data fusion are employed. Raw sensor data fusion provides better information at raw level. Feature level fusion finds relevant features among various features coming from different methods. Decision level fusion combines decisions or confidence levels coming from several experts.

In addition, there are some challenges such as sensor or information normalization, estimation of parameters, dynamic optimization, data pre-processing for extraction, and optimal algorithms. The main issue in data fusion is to provide higher accuracy and improved robustness against uncertainty and unreliable integration. Lee *et al.* [66] suggest a hierarchical decomposing method to minimize the probability of an unacceptable error (figure 3.5). A context is defined as a pattern of behaviour or relations among variables data that potentially affect user behaviour and system performance. It is derived from fused data in combination with a decision making policy. Several

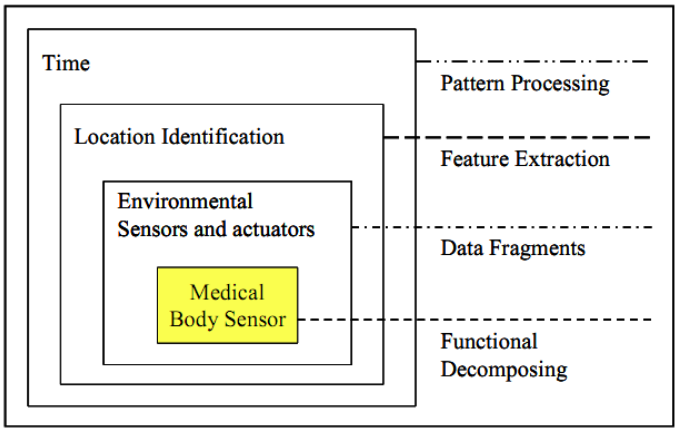

Figure 3.5: Data fusion model for pervasive healthcare [66].

types of decision-making techniques are used in health-care systems. For instance, probabilistic model (Bayesian reasoning, Belief network and Markov Decision Process), least squares model (Kalman filtering) and intelligent fusion model (fuzzy logic, neural network, genetic algorithm and reinforcement learning) are used.

Data fusion techniques have been applied by several authors after a combined analysis of several physiological signals that can potentially provide additional information on the patient's condition. In [67] the fusion of ECG, blood pressure, saturated oxygen content and respiratory data for achieving improved clinical diagnosis of patients in cardiac care units is performed. In [68] the recorded signals from the ECG, the blood pressure and the skin temperature are treated, knowing data from a 3D-acceleration sensor to determine movements occurred during recording, using a data fusion system to deal with motion artifacts in order to reject or correct distorted vital sign signals. Alemzadeh *et al.* [69] stated that "a robust medical monitoring device should be able to provide intelligent diagnosis based on accurate analysis of physiological parameters in real-time" and "such device must be able to adapt to the characteristics of a specific patient and desired diagnostic needs, and continue to operate even in presence of unexpected artifacts and accidental errors". In order to accomplish that, a system capable of a real-time assessment of individual's health status based on development of a patient-specific health index and online analysis and fusion of multi-parameter physiological signals (blood pressure, heart rate, and ECG) was developed.

In [70] the challenge of the telemonitoring context is characterised: different sensors use different physical principles, cover different information space, and generate data in different formats at different sampling rates. The obtained data have different resolution, accuracy, and reliability properties. Based on those characteristics, the key to produce the required detection is to use the right method that properly fuses the provided data from various sources. This is what multimodal data fusion stands for. The authors analysed typical multisensors data fusion methods in seeking for the most generalizable and adaptable method to use in their multimodal system called EMUTEM (Environnement Multimodal pour la Télévigilance Médicale).

The classical inference method quantitatively compares the probability that an observation can be attributed to a given assumed hypothesis. But it shows as major disadvantages: difficulty in obtaining the density functions that describe observations used to classify the object; complexities that arise when multivariate data are encountered; its capability to assess only two hypotheses at a time; and its inability to take direct advantage of a priori likelihood probabilities.

The Bayesian inference method also has some weaknesses that prevent it from being used in our multimodal data fusion module. The key limits are: difficulty in defining a priori probabilities, complexities when there are multiple potential hypotheses and multiple conditionally dependent events, mutual exclusivity required for competing hypotheses; and inability to account for general uncertainty and to represent imprecision. Even if Dempster-Shafer methods use a general level of uncertainty, they cannot be the main data fusion method for two reasons: the difficulty to estimate mass function and their restrict domain of application.

The neural networks method is not very well adapted to EMUTEM's data fusion module because of three main drawbacks. First, the mapping mechanism is not well understood even if the network can provide the desired behaviour. Second, the neural network method is, generally speaking, not suitable to work in a dynamic sensor configuration environment, because each sensor needs a unique input node and each possible sensor-set configuration needs to be specifically trained. Third, the complex architecture of neural networks prevents experts adding their knowledge easily.

Support vector machine (SVM) methods, despite their transit in the characteristics space which is disconnected from any physical reality, could fulfil the requirement of intelligibility because only support vectors are important in identifying margins between classes. However, it is necessary that boundaries between classes are rendered intelligible by a graphical way in the space of inputs. This vision must take into account an input space of any size even if greater than 3. In this case, the SVM identifies a large majority of learning examples as support examples. It means that an analyst should remember too many relevant individuals for the construction of boundaries between classes and this is impossible.

The fuzzy logic method is the proposed way to meet these challenges of this multimodal data fusion application. According to the nature of data to process in EMUTEM platform, fuzzy logic is the well adapted approach for the telemonitoring decision. It deals with inaccuracy and uncertainty. It allows a great flexibility to combine several sensors. The main advantages of using fuzzy logic are the simplicity of the approach and the capacity of dealing with the complex data acquired from the subsystems described previously in the second section. Fuzzy set theory offers a convenient way to do all possible combinations with these data. Fuzzy set theory is used in this system to determine the most likely distress situations that might occur for elderly persons in their home.

The multimodal data fusion method based on fuzzy logic proposed by Medjahed et. al represents a fast and easy tool for the interpretation of the fuzzy decision process even for very high dimensional input spaces and allows fast detection of errors. The impact of the input features plays an important role on the final decision process [70].

3.5 Examples for achieving dependability in medical devices

A dependability analysis can be conducted at a system level or at different levels, such as analogue circuits, software and/or network levels, each one requiring a specific approach in order to increase dependability.

3.5.1 Analogue circuits

Reliability simulations are usually used in analogue and mixed-signal circuits in order to estimate the effect of degradation mechanisms like NBTI, PBTI, HCI, and TDDB. The simulations are normally performed in two phases. First fresh circuit simulations are carried out using fresh and original device models. Based on these simulations, circuits activity and their impact on circuit lifetime are evaluated. These are further used to generate degraded device models. In the second simulation phase fresh and original device models are replaced with these degraded models to evaluate circuit performance after a certain amount of operational time. This shows that the accuracy of reliability simulations is very much dependent on the accuracy of the circuits degradation models generated based on circuit activities and their impact on the circuit's lifetime. The results of these simulations can then be used to reconsider the designed circuit for better reliability or lifetime performance.

Another technique based upon reusable intellectual property blocks (IP) has been proposed in which different analogue and mixed-signal IPs, that are already designed to be reliable under different applications and lifetime conditions, are stored in an IP library. The designer makes use of this information to choose the best combination of components to meet the dependability requirements of the designed circuit/system. Most efforts have been made in manipulating circuits at the design stage to tackle dependability, especially reliability, issues. Like in the case of reliability simulations, degraded models are extracted and simulated for lifetime behaviour of analogue and mixed-signal circuits. This information is then further used to redesign or incorporating circuit strategies for reliability or dependability improvements. It will result in a number of IPs having the same functionality, but belonging to different reliability or dependability levels. This can be further used to select the best combination of IPs for desired reliability or dependability levels of the designed system. Both these techniques are used at design levels but they lack in dealing with lifetime dependability aspects related to complete IP failures, and system availability and maintainability issues. These issues require further considerations that will deal with lifetime dependability concerns [60].

To address these issues an improved hardware platform for dependability enhancement, combined with an early selection of IPs to find the best possible combination in terms of dependability, is proposed in [71]. The suggested strategy is based upon the same concept of digitally assisted analogue and mixed-signal circuits where some on-chip measurement infrastructure is added to calibrate the performance of each analogue and mixed-signal IP. While dependability issues have been resolved at the design stage by selecting suitable IPs for better dependability performance

and for the lifetime of the product, some built-in tuning/trimming and switching techniques are also added [72].

3.5.2 Software

Despite the contemporary research has not focused on assessing dependability in the software domain, the use of quantitative and qualitative dependability analysis techniques enables the production of Ambient Assisted Living (AAL) solutions with high levels of accuracy. This approach allows to seamlessly integrate the analysis during subsequent software life cycle stages in critical scenarios and helps to identify the components which have the highest impact on software system dependability, and therefore, be able to address software architecture and individual software component problems before they are implemented and critical errors occur.

Since the design of AAL systems is in its early stages, it is not completely clear how to address dependability of such systems. Hence, the importance of conducting a dependability analysis in the early stages of the software development cycle becomes even more evident. Such analysis would provide early identification of system problems which would avoid unforeseen expenditures of cost, time, and effort. It is still difficult to do verification and validation of AAL systems in real scenarios due to their complexity and the unavailability of reference implementations. Therefore the need to find ways to quantitatively assess the architecture of AAL systems for dependability. To accomplish that, dependability needs to be expressed in terms of relevant domain properties and critical components that may require special design attention and project resource allocation need to be identified [73].

3.5.3 Network

Regarding the dependability of sensor networks, the authors of [74] proposed a new architecture to increase dependability levels by means of using a generic divided system model (intra-BAN and extra-BAN) to identify potential areas of failure. The intra-BAN network comprises a set of physiological sensors and a local aggregator that serves as a gateway and local processing unit (data fusion, compression, security) for the network due to its higher computational and power capabilities. The extra-BAN network consists of the communication infrastructure used for communicating between the aggregator and destination database, computer or smartphone. By dividing up the BAN into this split architecture, the analysis of the possible faults and solutions becomes simpler. Dependable models for generic sensor networks can be adopted for the intra-BAN network subject to a few changes and likewise for the extra-BAN network for respective communication media.

Wu *et al.* [75] employed a decision fusion method in Wireless Sensor Networks (WSN) in order to increase the dependability and reliability of the network. This technique uses additional components in the system to execute mutually or parallel in order to reduce the probability of error. Therefore, an important problem towards such scenarios is to determine the decision fusion rules under those uncertain environments, so that this WSN is able to perform ideally. For the definition

of the fusion rules, first the authors defined models and measurements: placement model, sensing model, coverage measure (the coverage density represents redundancy level of sensor deployment for a certain point in the detection area) and performance measures. A fusion rule that efficiently and accurately identifies false through additional information is introduced. By means of this analysis the authors concluded that global optimization is possible through tuning the fusion policy and in order to reach a high performance of WSN fusion policy should be allowed to be self-adaptive.

3.5.4 Dependability as risk management

A research team at LIRMM (France) faced the same challenges while developing implants for Functional Electrical Stimulation (FES). A strategy for risk management at system level is proposed after a methodological study of the problem [76]. The researchers developed an algorithm for the risk management which gives a guideline to follow in order to obtain an exhaustive list of potential failures (figure 3.6). After the list is constituted Built-In-Self-Test (BIST) and Built-In-Self-Repair (BISR) solutions can be employed. This approach is iterative and needs to be updated during the entire life of the implant [77]. Thanks to the experiment feedback on the old implant generations and the developed algorithm, these successive approaches procedure will provide a complete list of failures. It is a top-down approach covering the system from a macro overview to a micro decomposition, and a bottom-up approach where the experience feedback is used to repair known defects. This merge will bring us a highly safe and reliable medical implant to the patient advantage [12].

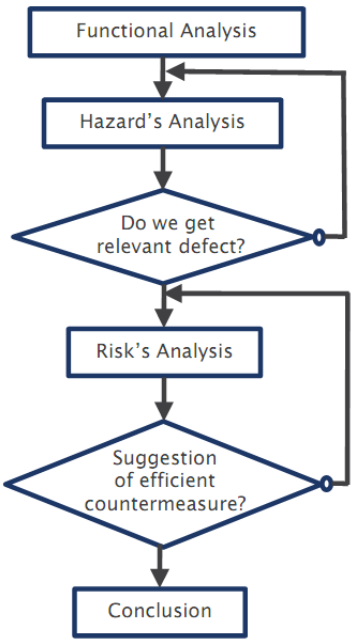

Figure 3.6: Algorithm of the dependability management[76].

This algorithm provides a uniform framework for risk management in implantable medical devices, and works as a guideline for the people responsible for the dependability analysis. No mathematical model is included in this algorithm for the estimation of the dependability attributes (reliability, availability, etc).

3.5.4.1 The *iFEM* method

To improve the risk management process the iFEM method (innovative Function Effect Modeling) was developed, which is a new approach to identify and assess risks. First of all, critical risk areas are identified by the creation of a tree that visualizes the actual state of a complete technological system. After that, these critical risk areas are analysed by an object model and a function-effect model. The result is a comprehensive risk inventory in which the cause and assessment for each of the risks have been defined. These results can be directly addressed through an effective risk mitigation. The validation of iFEM was carried out in an enterprise from the medical engineering industries. The results were structured and documented so that the information could be used to improve the method. iFEM is a suitable method to model an overall system for the multidisciplinary analysis of a complex product. It permits a common understanding of a system and combines manufacturing and operational processes with system functions and inherent risks. The benefits of iFEM are the systematic risk identification of inconsistencies and expansion of employee's system understanding.

3.5.5 Dependability and quality of service in medical devices

Abkai and Hesser [78] developed a dependability strategy for medical devices based on the difference between real time physiological simulations and real data.

The dependability is defined as a dynamic region/boundary of the system operation. Figure 3.7 shows a system theoretic way of view for the given problem, namely to monitor patients physiological system by the meaning of patient vital parameters. The upper part of the diagram shows the real patient block represented as a black box model and including some observable and non-observable internal states. This block describes the physiology (behaviour) of the patient, in other words the patient's health states, which could be multi parametric. According to system dynamics — subsequent patient states are correlated to earlier ones — a dynamic feedback loop is necessary. As mentioned before, we are unable to observe and measure all patient internal parameters, which is depicted by a patient observer block. The lower part of the diagram represents the virtual physiological model, which can be realized by simulation. The result is a simulated patient block. Also, here the model is a dynamic model, thus a dynamic feedback is needed and additionally results of the simulation can be observed by an observer block.

The patient model may be any mixture of time-invariant dynamic models, even containing non-stationary probabilistic temporal models. As proposed by this work a mixture of deterministic and probabilistic modelling approaches by the meaning of system of ordinary differential equations (ODE) and Bayesian Networks (BN)/Dynamic BN mixture can be used. If the virtual model is

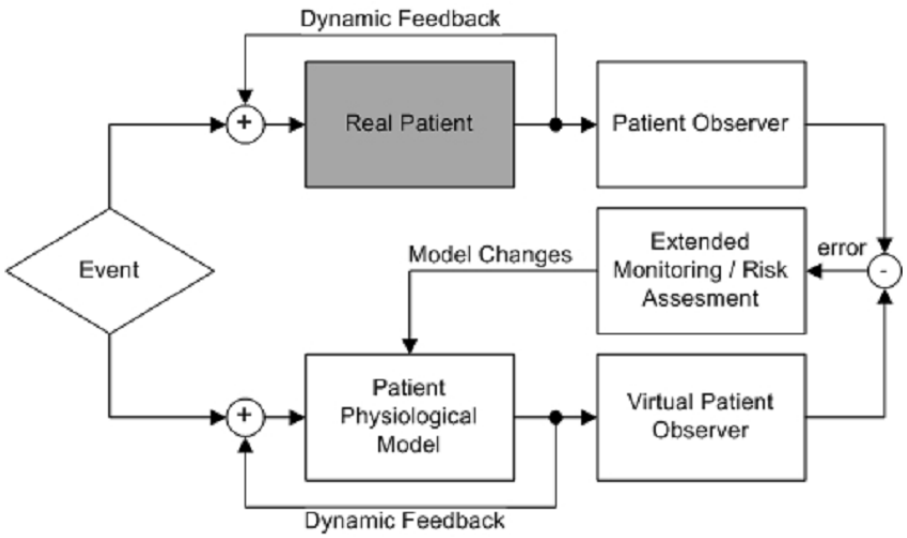

Figure 3.7: Vital signal observation and comparison between real and simulated physiological reactions to an induced event. A system theoretical view for patient monitoring is depicted. Upper part: real patient loop and observation. Lower part: simulated patient loop and observation. Intermediate part: comparator and extended dependability and monitoring analysis [78].

mimicking/simulating the real world perfectly, there will be no difference in both observations. A difference, however, is interpreted as error given by the simulation, which — as depicted in the intermediate layer — allows extending the monitoring by providing more knowledge about patient states and even extend to patient dependability and risk analysis. Normally, if the virtual patient model is accurate and well suited, the error is a significant sign for a deviation between real patient states and virtual patient states. Such a deviation may be interpreted as a deviation from safety boundaries and hints towards possible safety critical situations.

The authors created a general framework to estimate the system dependability without a fault tree or risk analysis. The dependability measure for future risk and past model differences is a new view on patient's critical situations and the quality of service is a measure for the applicability of the virtual physiological models.

Although this approach has well defined mathematical models and outputs values for the dependability and quality of service, the lack of a risk analysis requires a very precise physiological simulator. Also in wearable medical devices the measured vital signal is significantly affected by the quality of the interface (garment/electrodes), and its properties can vary during time. Another issue is that a difference between the simulated and measured signal does not indicate what part of the system is causing this fault.

3.6 Conclusions

The increase in complexity of wearable medical monitoring systems demands an integrated strategy in order to assure that each and every block of the system shows the required levels of dependability. A wearable monitoring system consists of several components such as: sensors, acquisition circuits, controlling and processing units, network, and software. Each block will have dependability attributes (reliability, security, safety, availability and maintainability) with different weights (for instance in case of implanted sensors the safety of the patient will be the most important attribute), and due to their characteristics the risks (defects/faults, failures and errors) that can affect the systems performance will also differ.

Based on the study of dependability in wearable medical system, fault detection and fusion techniques for the SIVIC system (case study for this thesis) will be presented in the next chapters.

Due to the heterogeneity in wearable medical devices, the SIVIC system will also be characterized and modelled in the next chapter, with the aim of improving its levels of dependability. The system's model will be used to generate a fault dictionary, where the inputs of the system (biosignals) are affected by the main components of the system, namely the sensing elements (pressure sensor and ECG electrodes) and signal conditioning block (amplifiers and filters). The fault dictionary will enable the evaluation of data fusion algorithms to correlate data obtained from different sensors and detect faults in the system or a health condition in the patient.

Chapter 4

Modelling of the SIVIC System and Fault Detection

The use of the wearable monitoring systems developed in the SIVIC for medical purposes (continuous monitoring, diagnosis, etc.), requires that the reliability and safety of the system be perfectly controlled. From a systemic perspective these wearable systems comprise a module to capture the biosignals, including the electrodes and the analogue front-end, a microcontroller, and a radiofrequency emitter to transmit the signal to the smartphone or a personal computer. In order to achieve the desired levels of dependability the SIVIC system was moduled based on the signal path from the biosignals to the smartphone. Based on this model a fault dictionary could be establish by taking into account the expected faults in the system, namely the sensors. Since the pressure sensors and the textile electrodes were developed for the SIVIC project there was no data available regarding the electrical characteristics and expected behaviour for the usage of such sensors in an hospital or ambulatory. Therefore sensors employed in the SIVIC project were characterized in order to improved the system modeling and the fault dictionary. Also a fault detection technique was proposed for the pressure sensors.

4.1 Fault Dictionary

4.1.1 System Modeling

A diagram of the main SIVIC blocks is presented in Fig. 4.1. This model includes the vital signs being measured, the sensor model (for the pressure sensors) and the electrode-skin interface model (for the ECG and respiration electrodes), the amplifiers, the ADC, the microcontroller, the BLE communication, and the smartphone. Associated to these are the anomalies that can occur: faults in the system (electrodes, analogue front-end, microcontroller, communication link) and extreme change of the physical activity or pathology in the wearer.

To ensure that the evaluation of the test and diagnosis approaches under analysis is carried out with a large number of real cases, the inputs of this model (ECG and ABP signals) are obtained from the MIT Multiparameter database (MGH/MF) [79, 80]. This database includes ECG signals

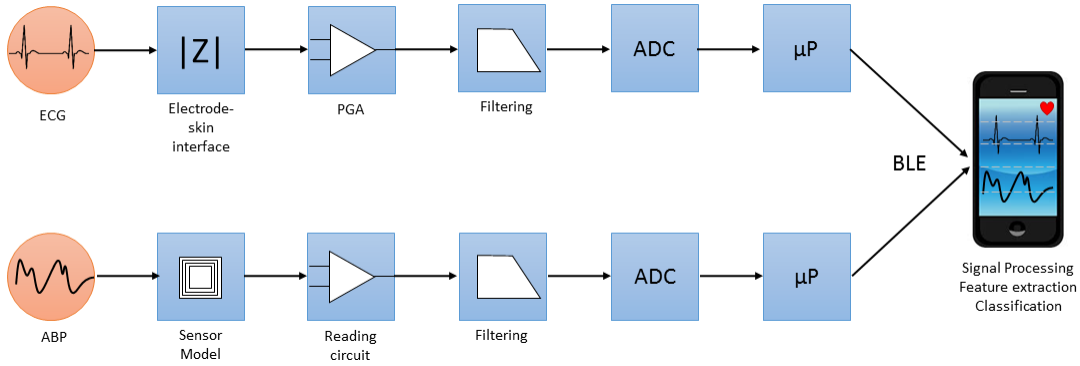

Figure 4.1: Block diagram of the SIVIC system describing the signal path from the sensors to the smartphone.

(leads I, II and V), the arterial blood pressure, and respiratory rate. Since this database includes annotations of the patients' conditions made by doctors and presents also a broad diversity of cases, information is available to validate the diagnosis performed in the smartphone.

4.1.2 Vital Signs Database

As the SIVIC system is still under development not enough data from measurements performed in patients is yet available. To overcome this a database with all possible hardware faults, a fault dictionary, and clinical data of patients being monitored was created. Data from the MIT Multi-parameter database (MGH/MF) was used to test the classification algorithms presented in the next section [79, 80]. The features from ECG signals (leads I, II and V) and the arterial blood pressure (ART) were extracted and feed to the model of the SIVIC system. The ECG provides the HR information and the ART waveform is used to know the systolic and diastolic pressures.

4.2 Pressure Sensor Fault Detection

An important aspect to be considered within the abdominal aorta pressure monitoring system being proposed, concerns the frequency shift due to the sensor's inductor bending after placement in the stent. Consequently the corresponding inductance can change [81] due to bending. This deformation may have a direct impact on variations of the sensor's oscillation frequency, leading to an uncertainty in the detected pressure. Furthermore, interpreting the captured oscillation frequency cannot be made in a simple single observation. The pressure in the stent-graft varies periodically with the arterial blood pressure. In consequence, what one actually captures is a distribution of resonant frequencies, modulated, on one hand, by the cardiac beating (60 to 100 beats per minute for a healthy heart) and the range of pressures it generates. On the other hand, the frequency is also affected by the operating condition status of the pressure sensor. Therefore, in case an abnormal resonant frequency distribution is observed, how can one distinguish a defective stent-graft from a defective sensor? The following section addresses this issue in order to improve the reliability of the proposed endoleakage monitor.

4.2.1 Sensor defects and fault modelling

As this detection process provides an indirect pressure measurement, the occurrence of defects in the pressure sensor may mask the detection of anomalies in the stent-graft. The extreme cases in the *LC* network are an open-circuit due to a connection break or a short-circuit. Since the pressure is being sensed by the two plates capacitor, this is the most sensitive element of the *LC* network and the most likely to cause faults in the pressure measurements. Possible capacitor defects are listed in table 4.1. The work presented herein addresses the implementation of additional measurements and operations which allow diagnosing the occurrence of defects in the *LC* sensor.

Table 4.1: List of possible sensor defects and their influence on the pressure measurements.

Capacitor Defects	**Effects on Measurements**
Stuck capacitor	Leads to a constant resonant frequency measurement
Reduction of capacitor's nominal measurement range	Allows detecting pressure deviations but in a narrower range, these measurements could still be taken as admissible
Large deviation of capacitor's nominal value	Could lead to a false defective stent-graft detection (e.g. a leaking stent-graft)
Collapsed capacitor	Shows no oscillation frequency
Bending of the structure	Deviation of the inductance and capacitor values
Ageing of the structure	Increase of inductor resistance

The aortic blood pressure (ABP) waveform (figure 4.2) conveys information about the cardiovascular system such as heart rate, systolic, diastolic and mean arterial pressures. Moreover, it provides information on possible complications in the endovascular stent-graft. Reading the stent-graft pressure (i. e., *LC* resonant frequency) at a 100-200 Hz sampling frequency allows reconstructing the ABP signal for future features extraction.

When the sensor is calibrated and ready to be placed around the stent-graft all the circuit elements (Ls, Rs and Cs) values are known. However, these components' performance may change overtime due to bending, wear and friction. In cases where the measured ABP is outside the nominal range, distinguishing that these values are caused by the pressure applied on the stent and not due to changes in the sensor components' values are of utmost importance.

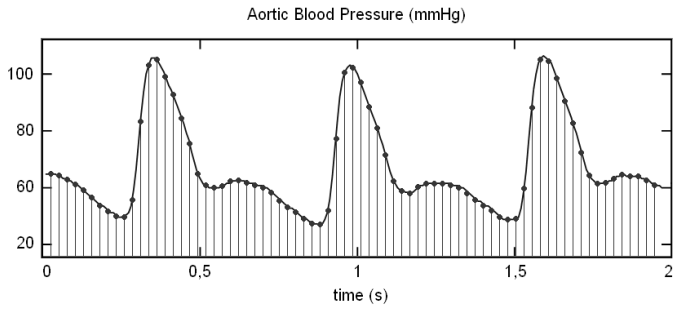

Figure 4.2: Typical aortic blood pressure waveform.

The set of resonant frequencies captured during a number of ABP cycles allows building an histogram of the captured values distribution. The shape of this histogram provides a preliminary indicator of the occurrence of anomalies.

4.2.2 System Description

To distinguish between each possible situation, one can resort to the measure of the power transmission from the sensor to the reader circuit, as well as from the impedance seen at node $v_o(\omega)$ (figure 4.3). These additional measurements combined with the measured oscillating frequency enable determining the circuit components values. The circuit is similar to the network analyser, where sine waves with different frequencies are sent to the network to transmit power. Since each sensor has a unique impedance at the oscillation frequency, this is reflected in the power transmitted when the sine wave frequency matches the sensors' oscillation frequency. The transformer captures the current i(ω) that is being drawn and converts the current to a proportional voltage vi(ω).

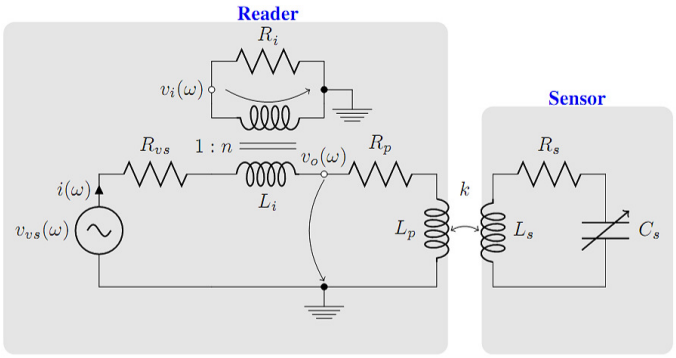

Figure 4.3: Circuit used to measure coupling power and impedance.

Using the circuit presented in figure 4.3 one can perform a frequency sweep to obtain the characteristics of input impedance (Z_L) and power (P) as functions of frequency — power is proportional to the product of $v_o(\omega)$ and $v_i(\omega)$ and $Z_L = \frac{v_o}{v_i} nR_i$. With m frequency sweeps one can obtain the inductive coupling power spectrum (figure 4.4) which allow us to obtain the quality factor ($Q = \frac{1}{R_s}\sqrt{\frac{L_s}{C_s}}$) of the resonant circuit.

$$\overline{P} = \frac{1}{m}\sum_{j=0}^{m} v_o(\omega)i(\omega) \equiv \frac{1}{m}\sum_{j=0}^{m} \frac{v_o(\omega)v_i(\omega)}{nR_i} \tag{4.1}$$

The real and imaginary parts of the impedance obtained from the frequency sweep (figure 4.4) are given by equations 4.2.

$$\mathscr{R}(Z_L) = R_p + \frac{\omega^4 R_s L_m^2 C_s^2}{1+\omega^2(R_s^2C_s^2 - 2L_sC_s) + \omega^4 L_s^2 C_s^2}$$
$$\mathscr{I}(Z_L) = \omega(L_p - L_m) + \frac{\omega L_m + \omega^3(R_s^2 L_m C_s^2 + L_m^2 C_s - 2L_s L_m C_s) + \omega^5 C_s^2(L_s^2 L_m - L_m^2 L_s)}{1+\omega^2(R_s^2C_s^2 - 2L_sC_s) + \omega^4 L_s^2 C_s^2} \quad (4.2)$$

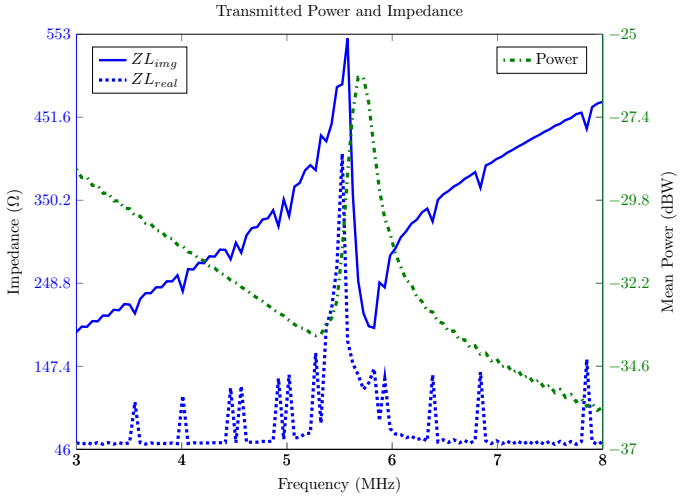

Figure 4.4: Transmitted power and impedance (simulation results).

Once power and impedance measurements have been performed, the preliminary values for the coupling factor k and R_s, using f_o and Q equations and the nominal L_s and C_s values as a first guess ("seed") values, can be estimated. The L_s and C_s values are then estimated by means of a fitting process of the measured impedance real and imaginary parts to equations 4.2. This process is then iterated until a specified estimation error (difference between measured and estimated resonant frequencies) is verified. The following pseudo-code summarizes this approach.

```
Introduce the estimated values
start_points =
=[k=1, Rs=50, Cs=10e-12, Ls=10e-6]

  WHILE (abs(fo_meas-fo_calc))>100
    Rs_iter = 1/Q_meas*sqrt(Ls/Cs)
    Rs = Rs_iter
    FUNCTION curvefitting(ZL_real, ZL_imag)
        estimate Ls_iter
        estimate Cs_iter
    Ls=Ls_iter
    Cs=Cs_iter
    fo_calc=1/2*pi*sqrt(Ls*Cs*(1-k^2))
  END
```

This data assumes capacitor's value *Cs* remains constant during the measurements but in a real time measurement it varies with the pressure inside the aneurysm sac. A sequence of operations must be performed in order to acquire the needed data (transmitted power and impedance) during a time interval corresponding to a known pressure when the capacitor has a low variability (figure 4.5).

The fault detection process takes advantage of the SIVIC ECG data capture module to provide a real time ECG and of the auxiliary circuits to measure the transmitted power and impedance. The ECG acquisition has two purposes, the assessment of the patient's cardiac condition and to provide the fault detection trigger signal. The ECG is a widely used exam in patients with diseases associated to cardiac function, and is an important factor in the determination of risk of open surgery and EVAR [82].

To ensure that the transmitted power and impedance measurements are carried out during a period when the sensor capacitance is almost constant, the measurements must start in the onset of the systolic pressure and stop when the blood pressure drops again. The systole occurs around 0.2 seconds after the contraction of the ventricles (QRS complex), so if the ECG is recorded in real time it is possible to determine the QRS occurrence and start the fault detection measurements during the systole. Then, the recorded transmitted power and impedance are used for the data modelling to extract the nominal values of the sensor's components. With this approach the small variability of the capacitor sensor is assured and the signal acquisition is carried-out during the most critical situation when the pressure is maximum. The fault detection system enables the assessment of sensor's components values and, depending on the fault severity, it could help recalibrating the reading system so the sensor's readings are used instead of its dismissal.

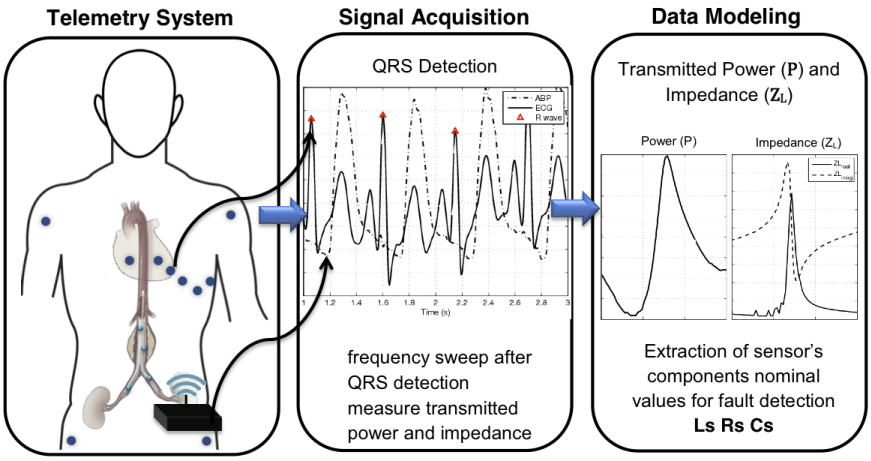

Figure 4.5: Fault detection procedure block diagram.

4.2.3 Results

Simulations were performed in order to estimate the power transmission and the reflected impedance of the sensors using the antenna model in figure 2.13 and the fault detection circuit described in 4.3. Figure 4.4 displays the curves for power and impedance of sensor S4. This model predicts well the small resonances around the main frequency of the sensor due to its design, and the measurement curves are very similar to the simulation predictions. However, the simple *LC* sensor model will still be used to extract the values for L_{stotal} and C_{stotal}, since there are only 2 measurements (power and impedance) to estimate the two parameters. These extracted values are related with the antenna model from Figure 2.13 in the following way: $L_{stotal} = 4L_s$, $R_{total} = 2R_s$ and $C_{stotal} = C_{layer} + C_{sensor}$.

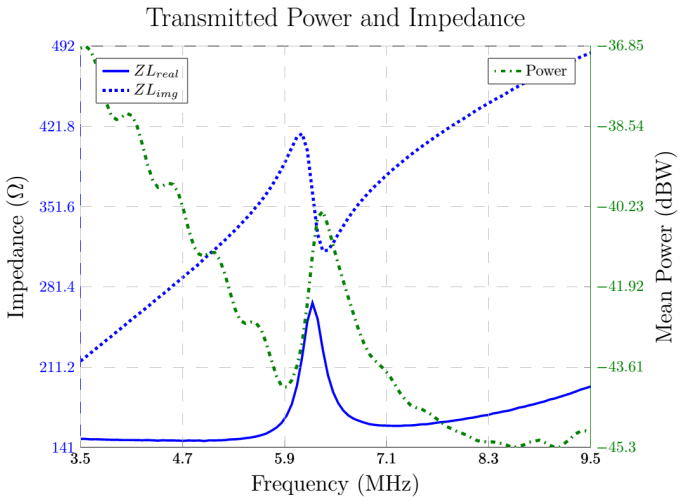

Figure 4.6: Measurements of the mean transmitted power and impedance (real and imaginary parts) for sensor C1.

Measurements were performed in order to estimate the power transmission and the reflected impedance of the sensor under test. Fig. 4.6 displays the power and impedance curves obtained for sensor C1. Table 4.2 depicts the calculated and extracted values for all the sensors using the fault detection algorithm to measure power and impedance. Extraction is performed after fitting the measured power and impedance curves with those obtained with the sensor's parameter values. As expected the extracted resistance and capacitance are higher than calculations, due to the fact that during the assembly of the A–CNTs onto the flex PCB using a special conductive glue extra parasitic capacitance and resistance are inserted, which cannot be calculated. The antenna's inductance was measured with a network analyser prior to the assembly of the A–CNTs. The measured inductance is lower than the extracted value. However, as mentioned before, the antenna is not purely inductive since the overlap of the top and bottom coils introduces a significant series capacitance, which causes the difference in the inductance value.

The fault detection circuit was also tested on a sensor with the top A–CNTs membrane detached from the sensor. As a consequence power is not transmitted back to the test circuit, and the reflected impedance is floating, as displayed in Figure 4.7.

Table 4.2: Results from the fitting algorithm and parameter extraction based on the impedance measurements.

Sensor	R_s [Ω]	L_s [μH]	C_s+C_l [pF]
C4	9.70	4.50	31.69
C6	9.12	4.17	34.38
S4	9.75	4.90	43.89
S6	9.34	4.70	47.10

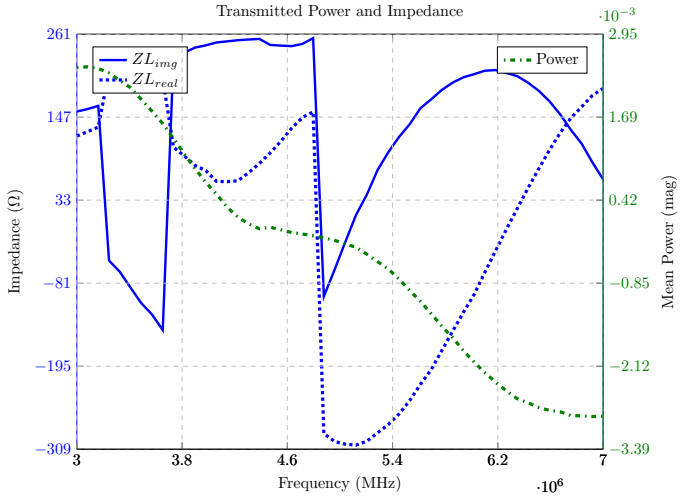

Figure 4.7: Transmitted power and impedance measurements for a faulty sensor.

This testing procedure can also be used to characterize the sensors after the fabrication process, once the deposition of the PDMS layer to protect the sensor and make it biocompatible can change some parameters, like the resistance and capacitance, and prevents electrical access to probing points once it is totally coated.

4.3 Fault Detection in the ECG Electrodes

Most electrode based medical equipment perform a verification of the contact impedance prior to a measurement. Portable verifiers are available which physicians use for that purpose. The fast pace evolution of personal monitoring technology is affecting the traditional approach towards electrode utilization, in particular when considering extended monitoring periods. Careful skin preparation, electrode positioning and continuous verification, which most healthcare personnel are accustomed to, are not readily applicable to certain subjects, such as elderly, allergenic and paediatric [83], and for the case of personal monitoring technology, might not even represent an alternative; moreover, variations of the electrode-skin interface impedance are to be expected. When considering athlete's performance, daily activities monitoring, and other scenarios where the individuals will have to position the electrodes themselves or the electrodes are integrated within a garment (as in the case of textile electrodes), careful positioning and skin preparation cannot be considered a part of the procedure.

Textile electrodes present several advantages compared with the conventional silver/silver chloride (Ag/AgCl) type electrodes. They are flexible, unobtrusive, do not cause skin irritation due to the gel, and are a good candidate for chronic applications. Moreover, unlike Ag/AgCl electrodes, do not need to be changed in long-term applications. However, the textile electrodes come in different shapes, materials and formats. The biopotentials recorded with these new electrodes might not be comparable in terms of signal quality with the gold standard of gel electrodes, but it has been shown that still good results can be obtained. However, their behaviour has not been fully studied to properly understand how they affect the captured signal quality.

For example, experiments performed on human skin are difficult to analyse since the conductivity properties of human skin differ for each person and can change within hours. Also, since no adhesive forcing the contact with the skin is used, textile electrodes are subject to higher levels of noise and artefacts caused by motion and loosening contact.

Beckmann et al. [84] developed setups to characterize textile electrodes focusing on the contact impedance between the electrode and skin, and to characterize the textile conductors. The objective of their work was to measure the complex impedance of textile fabrics and to explore the influence of pressure, humidity, anatomical shapes and stretch.

The electrode-skin impedance is often modelled with the equivalent circuit shown in Fig. 4.8 [85]. The voltage source E_{hc} models the half cell potential, capacitance C_d is related with the electrical charge accumulated between the electrode and the skin, R_d is the resistance between the electrode and the skin during the charge transfer, and R_s is related with the electrolyte gel, sweat and the underlying skin tissue.

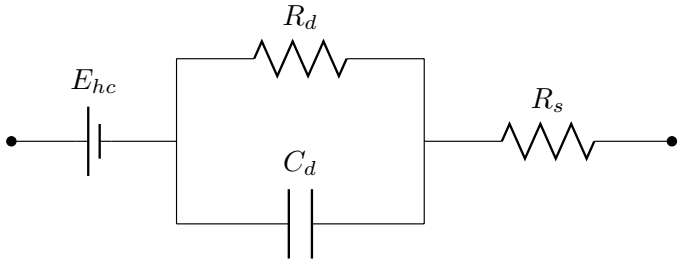

Figure 4.8: Electrical model of the electrode-skin impedance.

$$Z(j\omega) = R_s + \frac{R_d}{1 + j\omega R_d C_d} \tag{4.3}$$

Besides the electrode-skin contact impedance dependency with the signal frequency, it also depends on the exerted pressure which can be considered in the impedance equation 4.3 after the use of pressure dependent R_d and C_d elements. Albulbul et al. [86] studied the effect of an externally applied pressure on Ag/AgCl electrodes. It was concluded that a light to moderate applied pressure can decrease the electrode-skin impedance, but a large one may result in an impedance increase. According to the authors, this increase may be caused by a redistribution of the electrolyte used with non-polarizable electrodes. Mihajlovic et al. [87] also studied the pressure effect in the electrode-skin interface of Ag/AgCl and gold plated flat dry electrodes for

electroencephalographic (EEG) monitoring. It was concluded that after applying a force, both the Ag/AgCl and gold-plated electrodes present lower resistances and higher capacitances. Taji et al. [88] studied the effect of applied pressure in electrode-ski impedance for conductive textile electrodes. By increasing the pressure, the impedance magnitude decreased, as well as modelled resistors R_d and R_s, and the capacitance C_d increased. These studies obtained different impedance values for different electrodes, and even observed distinct behaviour for the same electrodes.

The electrode-skin impedance is known to affect the measured biopotentials, namely the noise level. Puurtinen et al. [89] measured the impedance and noise of surface electromyographic (EMG) signals captured with dry textile electrodes, textile electrodes moistened with water, and textile electrodes covered with hydrogel, for five different electrode sizes. The authors noted that the noise level increases as the electrode size decreases. The noise level obtained with dry textile electrodes was high, but that obtained with wet textile electrodes was low and similar to the noise level obtained with textile electrodes covered with hydrogel. The authors also found that hydrogel did not seem to improve noise properties, however it may have effects on movement artifacts. In this study they concluded that it is feasible to use textile embedded sensors in physiological monitoring applications when moistening or hydrogel is applied.

Taji et al. [88] developed a hardware-based configuration for acquiring electrocardiographic (ECG) signals with conductive textile, using various types of electrodes from different locations on the body. This was done to evaluate the overall quality of the acquired ECG based on the electrode-skin impedance measurements. The authors showed that the electrode-skin interface influences the quality and shape of the ECG signal registered at the electrode, and used the measured impedance to reconstruct the ECG signal.

The objective of this study is to identify the influence of the pressure applied to the electrode-skin interface of embroidered textile electrodes with no hydrogel or moistened water on a long-term basis, i. e., after observing the variation of the electrode-skin impedance components over time. Measurements of EMG were also performed simultaneously with the purpose of studying the influence of the impedance in the recorded biopotentials. The electrode-skin interface impedance is known to be related with the quality of the biopotential recordings. A mismatch between the electrode-skin impedances causes a degradation in the common mode rejection ratio (CMRR) and an increase in the power line frequency interference [90]. Some commercial ECG monitors include a test named lead-off to check the connectivity of an electrode to a patient. This test allows to verify if electrode is completely disconnected or when the connection is weak. However it is limited to the measurement of the impedance magnitude in just one frequency, and the lead-off threshold as to be defined by the system developer, and might differ for different electrodes [91]. There is a need to perform a test, based on the electrode-skin impedance, that is able to check the biosignal quality, and if possible correct the distorted signal. The relation between the impedance and the biosignal is not clear and needs to be further studied for textile electrodes.

4.3.1 Methods

An elastic and adjustable forearm sleeve made of neoprene was realized at UBI for measurements of bio impedance and electromyography under controlled applied pressure on the region of the electrodes (see Fig. 4.9). The sleeve integrated two snap fasteners spaced apart by 4 cm, for attachment of gel or dry electrodes and a textile pressure sensor. Textile electrodes having a circular a shape and 16 mm of diameter and integrating snap fasteners for attachment were realized using a 6-needle digital embroidery machine and electrically conductive threads Silverpam 250 from Tibtech having a resistivity of 200 Ωm^{-1} [92]. The textile pressure sensor was realized with embroidery processes and a plain weave fabric of bamboo with 30% silver from Less EMF Inc., Velostat and polyester foam. The sleeve allows the adjustment with Velcro of four tightening positions being the corresponding applied pressure on the electrodes region monitored with the pressure sensor.

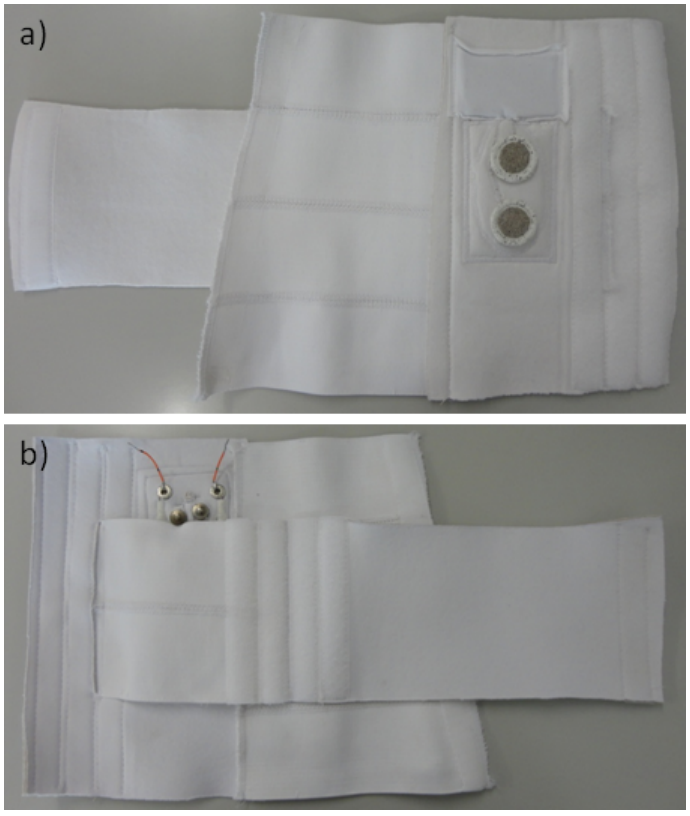

Figure 4.9: Partial views of the forearm sleeve: a) inner part with textile electrodes b) outer part with a pair of snap fasteners to connected the data acquisition terminals and a pair of wires connected to the pressure sensor.

The skin impedance is affected by temperature and total body water content [88]. In order to avoid detecting changes in the measured impedance that were not related to the electrode-skin impedance variations over time, all the measurements were performed in a room kept at a constant temperature. During the impedance measurements the test subject did not ingest any food or

beverage. Prior to the measurements, the volunteer also went through skin preparation (skin was cleaned with alcohol).

The textile electrodes pair was placed on the surface of the *flexor carpi radialis* muscle to acquire the EMG signal, and a standard Ag/AgCl electrode with 1 cm diameter (Dormo, Telic S.A., Spain) was placed on the elbow to establish the reference.

4.3.1.1 Electrode-Skin Impedance Measurements

The impedance was measured for all the levels of tightening of the sleeve, in order to know which value of pressure ensures the best results, i. e., the lower levels of contact impedance.

The electrode-skin impedance was measured right after placing the sleeve, followed by the measurement of the EMG. This protocol was repeated after 15 minutes, after 30 minutes, and then every half an hour for two hours.

The impedance measurement was performed with the circuit described in [93]. A two-electrode configuration was used, with which a 10 Hz to 100 kHz current sinewave (100 frequency steps in a logarithmic scale) signal was injected into one electrode and the voltage drop between the two electrodes was measured. This method allows the measurement of the impedance of the electrode pair plus the skin and body impedance. Since we want to study the electrode-skin interface of a single electrode, the measured impedance was divided by two, considering the two electrodes are identical. The measured impedance curves (magnitude and phase) were fitted to equation 4.3 using the least squares method.

A PCB (printed circuit board) with discrete components, creating the circuit in Fig. 4.8 with values in the range expected for the electrode-skin impedance, was utilized to perform the initial impedance measurements in order to test the accuracy of the impedance acquisition circuit and the fitting algorithm for the extraction of the circuit model parameters for the electrode-skin interface.

Table E.1 presents the values of the PCB components, the extracted values from the fitting of the impedance measurements, and the relative error. The error is within the components tolerance. This measurement allowed to validate the impedance measurement circuit and the fitting algorithm.

Table 4.3: Circuit parameters extraction using the impedance measurement.

Parameters	R_s (Ω)	R_d (kΩ)	C_d (nF)
Nominal	1000	100.0	47
Fitted	1049	114.8	41.07
Error (%)	4.88	14.78	12.61

4.3.1.2 Electromyographic measurements

The EMG signal was acquired with a Biopac MP35 (Biopac Systems Inc, USA) with a sampling frequency of 2 kHz, and a bandpass filter between 5 Hz to 200 Hz. During the first measurement the volunteer was asked to hold a hand dynamometer connected to the Biopac (SS25LA, BIOPAC

Systems Inc., CA, USA) and clench it with the maximum force during maximum of 5 seconds. This was done three times, with 1 minute rest interval. The maximum value of force recorded was registered as the maximum voluntary contraction (MVC). During the next measurements the volunteer was asked to hold the hand dynamometer until 25% of the MVC for 5 seconds. This ensured that the EMG signal was acquired in the same circumstances and the SNR calculations are valid.

After the measurements of the EMG and clench force the SNR was estimated. For that purpose the recorded EMG signal was processed using Matlab R2013b (MathWorks Inc, MA, USA). First the DC component of the EMG signal was removed by subtracting its mean value. The signal was then rectified and smoothed with an envelope filter (cut-off frequency of 6 Hz). The measured force was normalized by the MVC. The processed EMG and force signals are displayed in Fig. 4.10

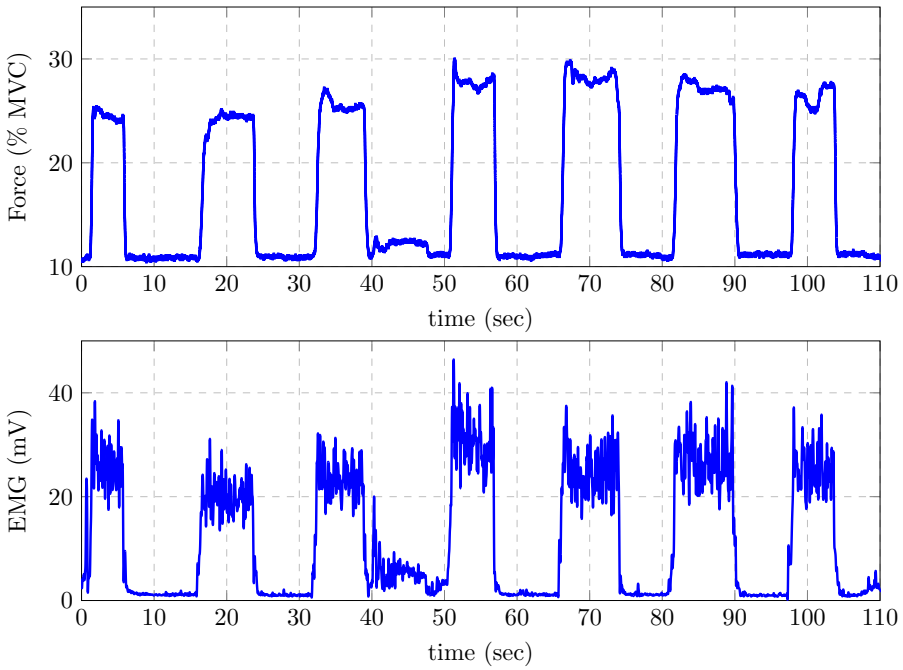

Figure 4.10: Top: Force (normalized to the MVC) made by the volunteer when holding the hand dynamometer; Bottom: amplitude of the acquired EMG signal.

$$SNR = 20log_{10}\left(\frac{A_{signal}}{A_{noise}}\right) \tag{4.4}$$

The EMG segments with activity that corresponded to a force of 25% of the MVC were chosen as the signal component, picking a length of 3 seconds.

The *rms* value of that signal was registered and the same procedure was used for the noise during a period of no activation of the muscles. The SNR is a ratio between the signal (A_{signal}) and noise (A_{noise}) amplitudes (see equation 4.4).

4.3.2 Results

4.3.2.1 Effect of pressure on electrode-skin impedance

The electrode-skin impedance was measured with four different values of pressure applied to the electrodes. The highest value of pressure produced the lowest interface impedance. Fig. 4.11 displays the variation of the impedance magnitude with the frequency.

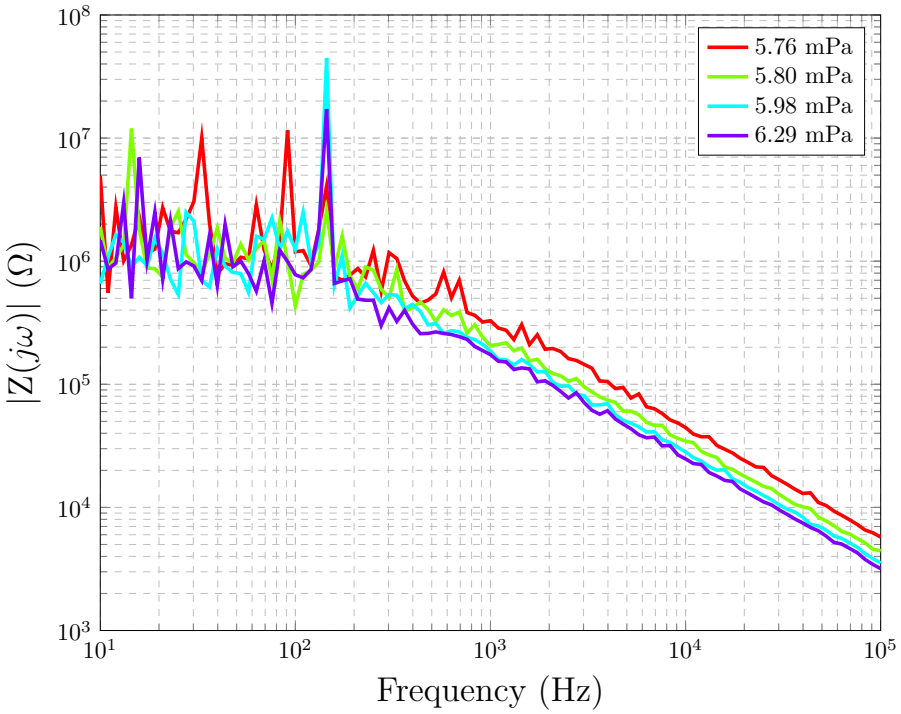

Figure 4.11: Variation of the measured impedance magnitude with pressure and frequency.

The measured impedance curves (magnitude and phase) were fitted to equation 4.3 using the least squares method for each applied pressure. The values obtained for the model components are presented in table 4.4. The C_d capacitance is given by $C_d = \varepsilon \frac{A}{d}$, with ε being the dielectric constant of the material between the electrode and the skin, A is the area of the parallel plates that comprise the electrode, and d is the distance between the plates, in this case the electrode and the skin. As the applied pressure increases, the effective contact area of the electrode increases (notice that the surface of the textile electrode is irregular) and the distance between the electrode and the skin decreases, which leads to a higher capacitance. The resistances R_d and R_s are given by $R = \rho \frac{L}{A}$, where ρ is the resistivity of the material and L the length. If were consider that the main varying factor is the contact area, a decrease in the resistances values is expected with an increase of the applied pressure. However, our observations show that this behaviour is not linear, most likely because the sweat that is naturally produced and the humidity formed in the arm sleeve change the resistivity in the media between the electrode and the skin.

The following measurements were performed with the sleeve tightened with the highest level, in order to accomplish a lower electrode-skin impedance, and therefore a better signal quality.

Table 4.4: Equivalent circuit model parameters for the electrode-skin impedance for different applied pressures.

Pressure (mPa)	R_s (kΩ)	R_d (MΩ)	C_d (nF)
5.76	6.75	2.11	0.30
5.80	5.22	3.41	1.99
5.98	3.94	1.12	2.96
6.29	3.89	1.37	17.19

4.3.2.2 Variation of electrode-skin impedance and SNR during long-term monitoring

To evaluate long-term effects, impedance as well as EMG measurements were performed over time in four volunteers. Due to hardware restrictions the impedance and the EMG were not measured simultaneously, but both measurements were taken within less than 1 minute interval. All the volunteers performed their daily activities in the along the measurement period. The measurements for volunteer#1 were taken 3 month before the measurements performed with the remaining volunteers. The impedances (magnitude and phase) obtained over time for all the volunteers are illustrated in Fig. 4.12- 4.15.

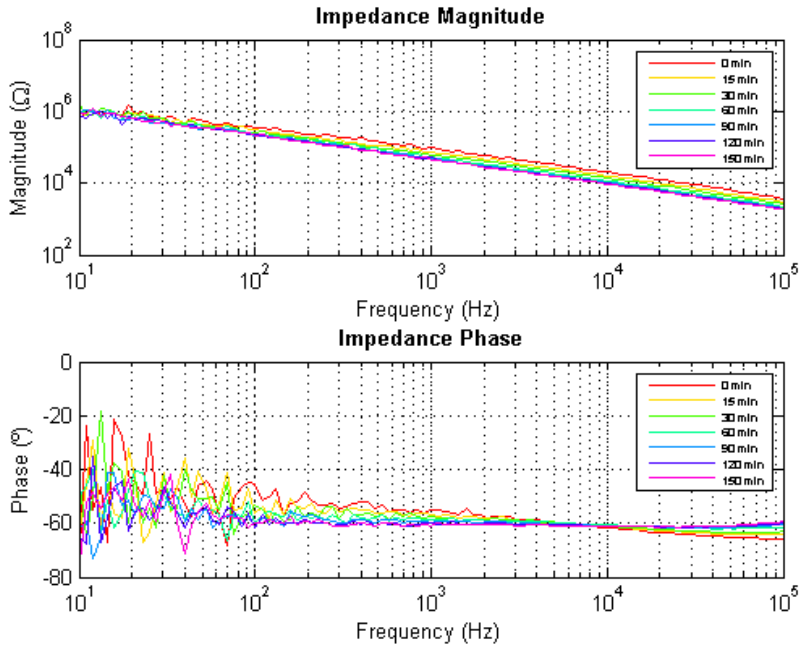

Figure 4.12: Measured impedance for volunteer#1.

The parameters for the electrode-skin impedance equivalent circuit (see Fig. 4.8) were extracted, and the SNR was calculated for each measurement. The variation of the impedance parameters R_s, R_d and C_d are plotted for all the measurement sessions with the volunteers (Fig.4.16 to 4.19). The evolution of the SNR is also included in the plots to provide a better insight of the parameters evolution and their influence on the signal quality.

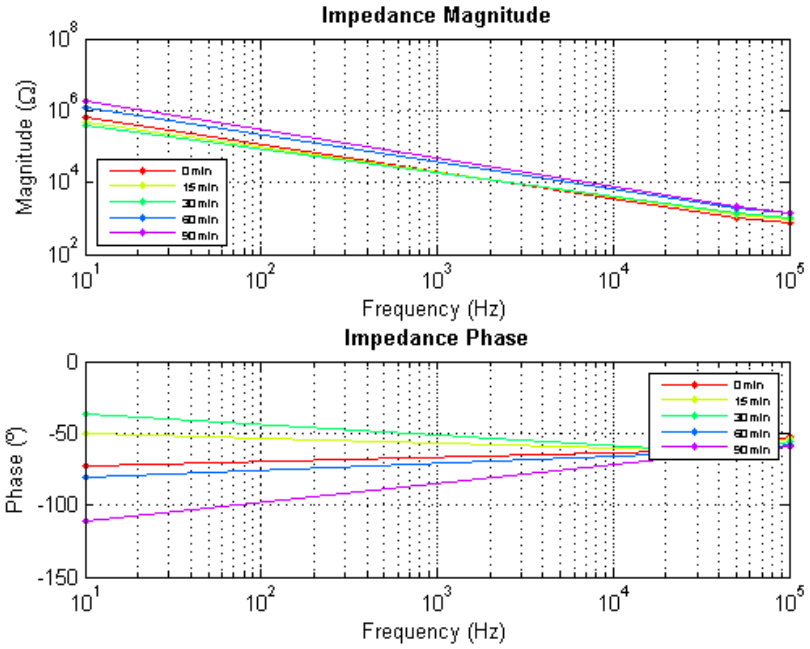

Figure 4.13: Measured impedance for volunteer#2.

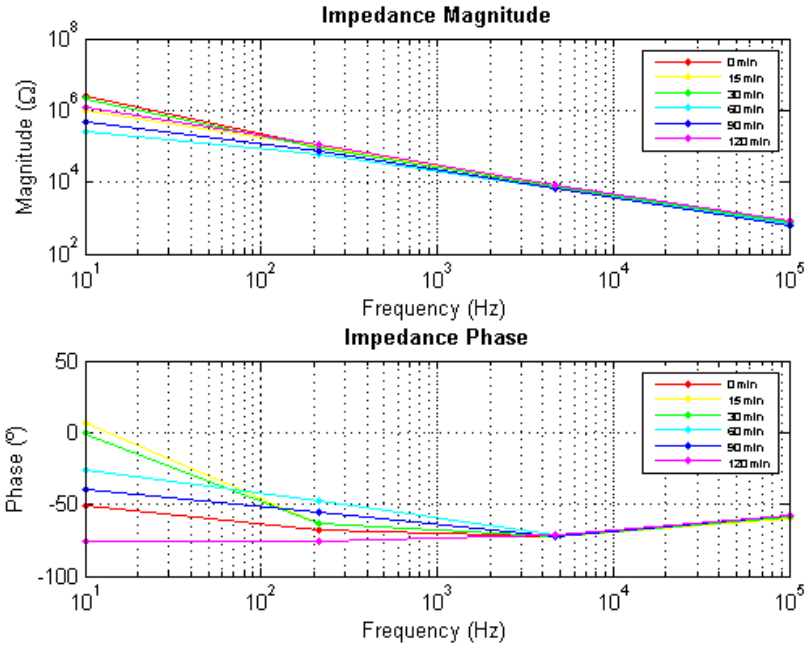

Figure 4.14: Measured impedance for volunteer#3.

4.3.3 Discussion

Electrode-skin impedance measurements were carried out during long-term monitoring and evaluated considering EMG measurements performed at the same time, with the same electrodes. These measurements allow to study the variations of the electrode-skin interface impedance and

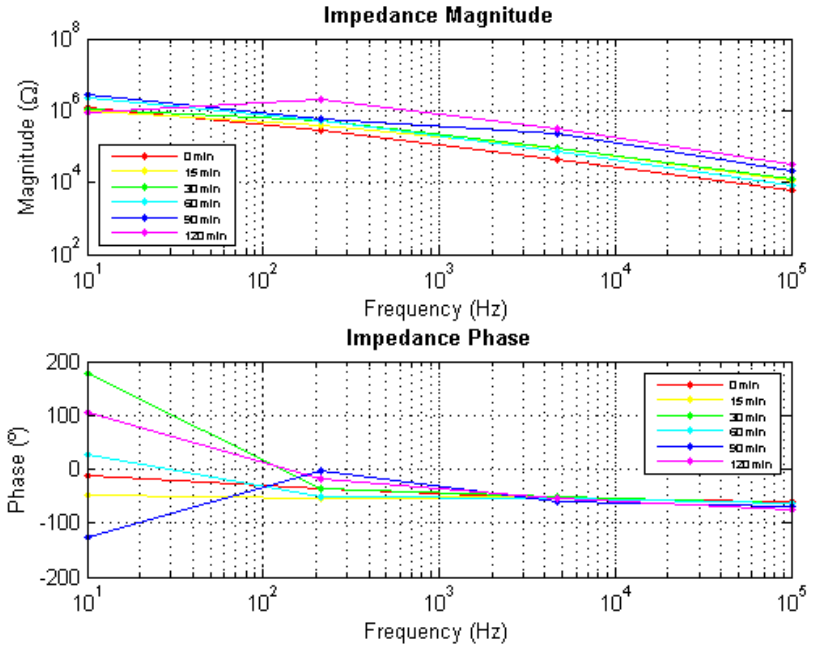

Figure 4.15: Measured impedance for volunteer#4.

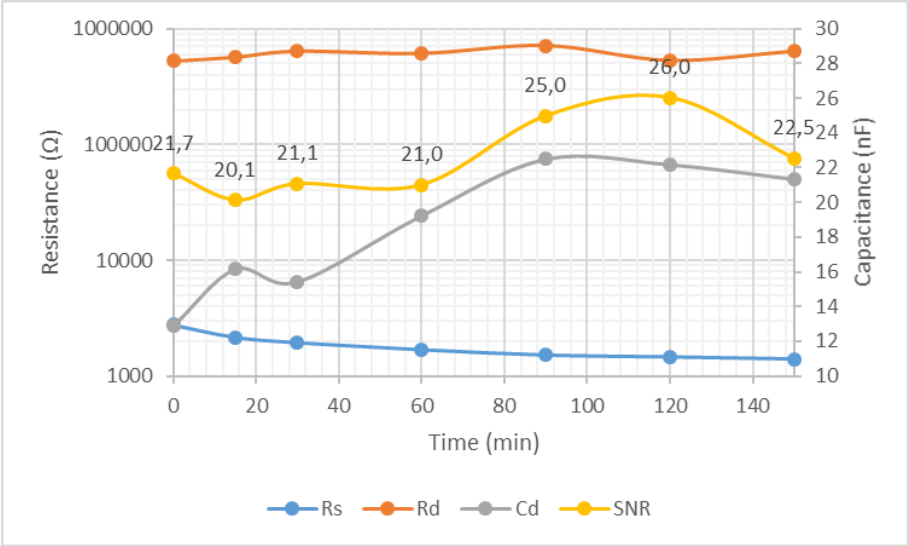

Figure 4.16: Variation of R_s, R_d, C_d and SNR for volunteer#1.

its influence on the acquired signal, namely the SNR.

After observing the values of the electrode-skin impedance over time one can notice that its variation is very different among the volunteers. Although all of them were asked not to drink or eat anything during the measurements, they were free to perform their daily activities in the measurement period. During that time the hand sleeve and the electrodes might suffer small displacements, that could cause a shift in the impedance of the electrode-skin interface. From the observation of the impedance plots we could not see a relation with the SNR of the EMG signal.

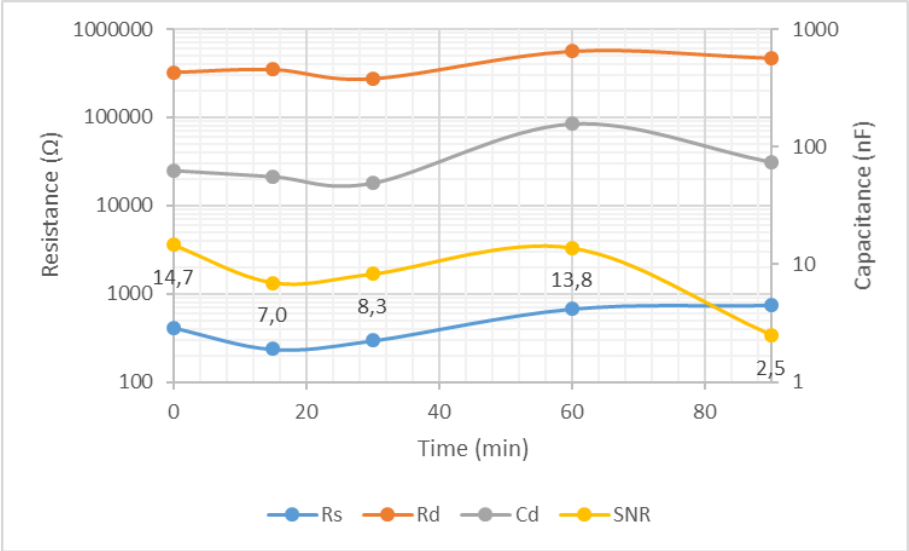

Figure 4.17: Variation of R_s, R_d, C_d and SNR for volunteer#2.

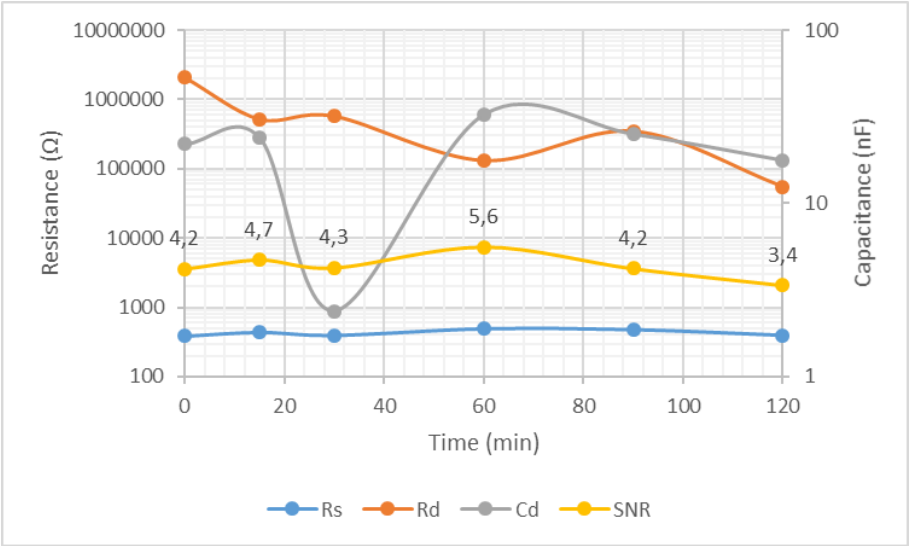

Figure 4.18: Variation of R_s, R_d, C_d and SNR for volunteer#3.

As the impedance measurements are influenced by the properties of the electrode/electrolyte and skin, we extracted the values of R_s, R_d and C_d to study their relation with the SNR individually.

If we hypothesize that the main factor for the SNR variation is the contact between the electrodes and the skin, the contact area would define how the impedance parameters would relate with the SNR. When the contact is better (higher effective area) the SNR and the C_d should increase and the resistances R_d and R_s should decrease. Conversely, if the contact between the electrodes and the skin is loose the SNR and the C_d decreases, and the R_d and R_s values increase. From the measurements of the impedance as a function of applied pressure (see Table 4.4) we observed that the impedance parameters are indeed related with the electrode-skin contact and their values changed as expected, i.e., as the pressure increased the C_d decreased and both R_d and R_s decreased.

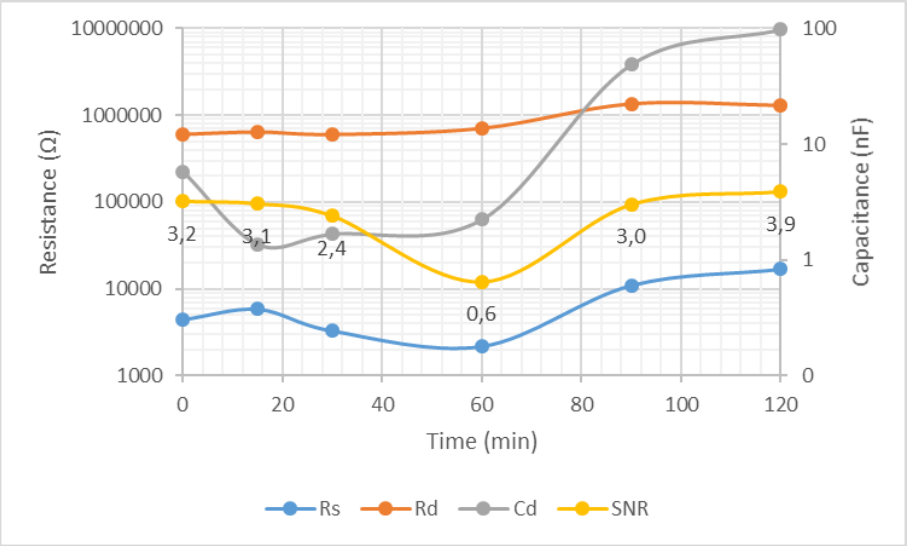

Figure 4.19: Variation of R_s, R_d, C_d and SNR for volunteer#4.

From Fig. 4.16 to Fig. 4.19 we notice the SNR is related with C_d and R_s. When the SNR increases both C_d and R_s also increase, likewise for the reverse behaviour. From our observations the R_d has no relation with the SNR. Since these measurements were performed during an average of 2 hours, the electrode-skin interface changes (e. g., due to humidity in the sleeve), skin might produce sweet and the electrode surface adapts to the skin. Also, the human body impedance of each person varies differently during the day. The R_d could be more influenced by these parameters than the contact area itself. This study shows that an impedance magnitude measurement is not enough to monitor the quality of biosignals, since the resistance if affected by the person's own impedance variation. The extraction of the parameters of the electrode-skin impedance electrical model, after performing phase and magnitude measurements, is more reliable for the purpose of the signal quality monitoring.

A significant reduction of the SNR is observed comparing the measurements with the volunteer#1 and the remaining measurements. As mentioned before these measurements were performed with an interval of 3 months. During this period the electrodes suffered ageing, which is a known characteristic of textile electrodes.

In wearable devices the comfort is an important factor. In future measurements the volunteers should be given a questionnaire to assess the comfort of the sleeve and textile electrodes. Also, the optimum pressure applied to the garment should not be chosen solemnly based on the impedance values, but also on the feedback from the volunteers. If possible the values of applied pressure on the skin should be checked in the literature and/or with a physician to make sure the applied force does no affect the circulatory system.

To the best of our knowledge, this is the first study that relates the electrode-skin impedance and a biopotential (EMG) using textile electrodes without any hydrogel or water moistening. From our point of view the main advantages of textile electrodes are the no need for skin and electrode preparation, easy of use, and no need for using hydrogel. If the electrode-skin impedance is one

of the factors that degrades the quality of the signal in textile electrodes, this parameter should be studied and compensated directly in the circuit and/or by means of post-processing.

4.4 Conclusions

The last decade has witnessed an explosion on the number of personal monitoring systems for different applications such as medical, rehabilitation, sports, and leisure. Electrical biosignals are commonly utilized within such systems and are traditionally captured with electrodes in their many forms.

The electrode-skin interface is constantly changing, thus affecting the signal integrity and degrading at times the quality of the signal captured. To address this issue the textile electrodes in the SIVIC system were characterized. The work presented in this chapter relates the electrode-skin impedance and the EMG signal quality (SNR) in textile electrodes with no hydrogel or water moistening. It was observed that over time the impedance decreased and the SNR improved. This situation is more noticeable in the first hour, and after that time the impedance and signal quality tend to stabilize

Also a methodology to diagnose deviations in the pressure sensors of the developed telemetry system for wireless monitoring of aortic stent-grafts was developed. Deviations in the sensor's *LC* values were detected after measurements of the power and impedance seen from the reader circuit. This verification is an essential step to distinguish whether deviations observed in the captured vital signs are due to pathologies in the patient or to defects of the monitoring system. With this aim data fusion techniques are explored in the next chapter to improve the cardiac and aortic surveillance system in order to achieve a highly reliable system.

Chapter 5

Data Fusion

5.1 Background

To overcome the lack of a dependability model that can be used for the development of complex pervasive medical monitoring devices, a fault tree analysis approach has been developed to identify the main risk of failure (see Fig. 5.1). A typical wearable device (hereafter the system) comprises a module to capture the biosignals, including the electrodes and the analogue front-end, a microcontroller, and a radio-frequency module to transmit data to a smartphone or personal computer. In our approach the captured biosignals are received and analysed within a smartphone. A classification algorithm decides whether these are normal or not. If not, it is diagnosed if the wearer shows an abnormal situation or instead the system is faulty. That is, a data abnormality can be due to a wearer irregular state (pathological condition or intense physical activity) or due to a degradation of the system operation. On the other hand, cases can occur where measured data is taken as correct when actually the system is faulty or the measurement procedure is not performed correctly. A flatline ECG is obtained when either the person is dead or the ECG meter is faulty. A correct heart beat rate could be fooled by an oscillating circuit.

Methodologies have been proposed to increase the reliability of medical wearable systems, which address faults detection in sensors, electronic modules, and communication links [69, 71, 72, 74, 94, 95]. Data fusion techniques have also been applied as a means for a combined analysis of several physiological signals to extract additional information on a patient's condition. Kenneth et. al performed the fusion of ECG, blood pressure, saturated oxygen content and respiratory data for achieving improved clinical diagnosis of patients in cardiac care units [67].

The main goal is to achieve the fastest and most efficient way to detect and diagnose deviations occurring in the captured data, having in mind the concern of correctly differentiating errors due to faults in the system, from those due to a change of the person health status. This procedure should be done in ambulatory and able to run in the microcontroller of the data capture module and/or in a smartphone. That is, the overall procedure is divided in different operations, being the data aggregation device (typically a smartphone) the main information processing device, due to the need of high computation capabilities and to minimize power consumption in the wearable

devices. These are involved in the dependability process when specific local test operations need to be executed.

A data fusion model for wearable medical systems based on fuzzy logic was presented in [96]. It was shown how fuzzy logic can be explored to correlate data obtained from different sensors in order to obtain status indicators that characterize the operation correctness of a monitoring system or a pathological condition of the wearer. Ideally there should be a database with all possible hardware faults (a fault dictionary) and a database with the clinical data of each wearer (patient being monitored). If clinical data records are not available, or the database of a new patient does not have enough information to build a reliable classifier, the diagnosis could be run based on fuzzy logic, until enough data is gathered to create a robust classifier.

In this chapter a database with information regarding the hardware (fault dictionary) and clinical data is introduced and utilized to explore possible data fusion algorithms capable of both system and patient diagnosis. The data fusion algorithms evaluated here are all supervised learning algorithms. Their inputs (features from the monitoring system and the patient vital signs) and outputs (system and patient status) are labelled and this information is used in the training process. There are several supervised learning algorithms available, with different processing speeds, memory usage needs and interpretability. Four data processing approaches to fuse data extracted from features, based on Fuzzy Logic (FL), Artificial Neural Networks (ANN), Classification Trees (CT), and Naive Bayes Classifiers (NBC), were evaluated for anomaly detection and classification purposes.

Fuzzy Logic can be used to solve problems of different types and domains, including medicine, as it resembles human reasoning and decision making. It looks into the not precisely formulated relationships and solves uncertainties and ambiguities created by human language where everything cannot be described in precise and discrete terms. ANN offer a number of advantages, such as requiring less formal statistical training, ability to implicitly detect complex nonlinear relationships between dependent and independent variables, ability to detect all possible interactions between predictor variables, and the availability of multiple training algorithms. However, its "black box" nature does not allow to see the relations between inputs and outputs. CT have a fast prediction speed, small memory usage and the results are easy to interpret. NBC prediction speed and memory usage vary according to the distribution size, but usually perform better than CT and the results are also easy to interpret.

The on-line methodology being proposed is based on a top-down evaluation process that starts with the detection of anomalies in the captured data. This detection triggers an analysis to check if actually the wearer shows a degradation of his health condition or if the system is reporting erroneous values. If it is found that the system is faulty, specific test operations can be executed to find the origin of the fault. To the best of our knowledge, no previous work was published where fusing data from both the data acquisition system and patient vital signs, is explored for simultaneous diagnosis of the patient health condition and the system status.

Next sections describe the dependability strategy being proposed and introduces the mode how data fusion algorithms are being explored.

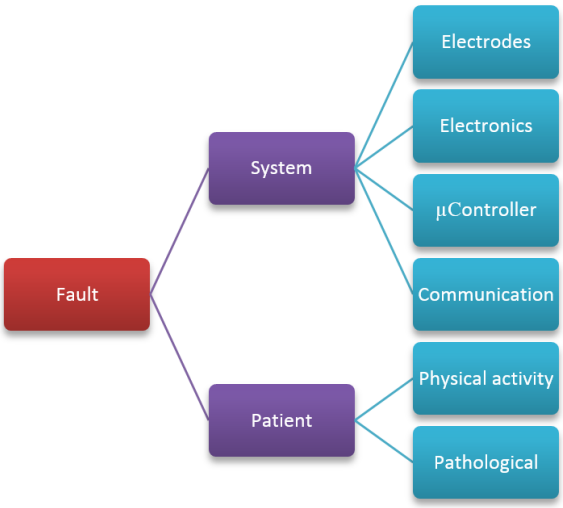

Figure 5.1: Fault tree analysis of the wearable monitoring system.

5.2 Feature Selection

5.2.1 Failure mode and effects analysis

A FMEA based on the approach made in [97] was carried out during the system's design. This analysis is very important to identify the most problematic components and functions of the system and determine, at the system design phase, which components or blocks should include built-in self-test (BIST) or other type of testing. From this analysis it was concluded that the wearable system blocks with higher severity and probability classification, i.e., those whose failure is more dangerous and probable, are located in the sensing hardware, power supply and microcontroller. Therefore it is necessary to be able to detect faults in the sensors (ECG electrodes and implantable pressure sensors), the sensors conditioning circuits, the battery and the microcontroller.

Concerning testing and BIST for these parts the following features are available. The ADS1298 IC provides an electrodes impedance measurement circuit, as well as internally-generated test stimuli for subsystem verification, which allows testing the entire analogue front-end chain. The electrode-skin impedance measurement circuit enables detecting if the electrodes are connected to the patient or are loose/disconnected.

The signal-to-noise ratio (SNR) of bioelectrical signals is known to be related to the electrode-skin impedance [11]. Since the impedance varies for each person and is affected by other factors like temperature and applied pressure, the electrode-skin impedance is measured when the system is switched on and afterwards it is monitored periodically to establish a normal region for the impedance values, for which the acquired ECG quality is considered acceptable. These values are then used for comparison with the impedance measured during normal operation of the system.

The Programmable Gain Amplifier (PGA) can be tested for high gain variations, e. g. due to components aging and for catastrophic faults, by using an internal square wave stimulus with an amplitude of +/- 2 mV and a frequency of 4 Hz. Class B safety software library routines, which comply with IEC 60730 Class B certification process standard, allow detecting faults in the

microcontroller. A power supply monitoring circuit, such as an watchdog circuit, allows detecting battery failures.

A methodology to test and measure the L and C values of the pressure sensors, after measurements of the power and impedance seen from the reader circuit, was developed using a simple data fusion approach [98] . The processing of the implantable pressure sensor signals with other physiological signals like the electrocardiogram (ECG) and arterial blood pressure (ABP) allows obtaining better resolution and decision trust with the acquired information in terms of diagnosability of faults eventually occurring in the stent-graft and the pressure sensors.

An alternative BIST approach that could be used to test the front-end of data acquisition unit was proposed in [93]. The targeted tests are electrode-skin impedance measurement and detection of functional deviations of the signal conditioning circuit.

5.2.2 Medical Diagnosis

The ECG conveys important hemodynamic information, such has the heart rate (HR). During an ECG cycle three main events take place: the P wave (contraction of the atria), the QRS complex (corresponding to the contraction of left ventricle) and the T wave (relaxation of the ventricles) (see Fig. 5.2). Their morphologies (amplitude and interval/segment length) will vary according to the person's physiological condition.

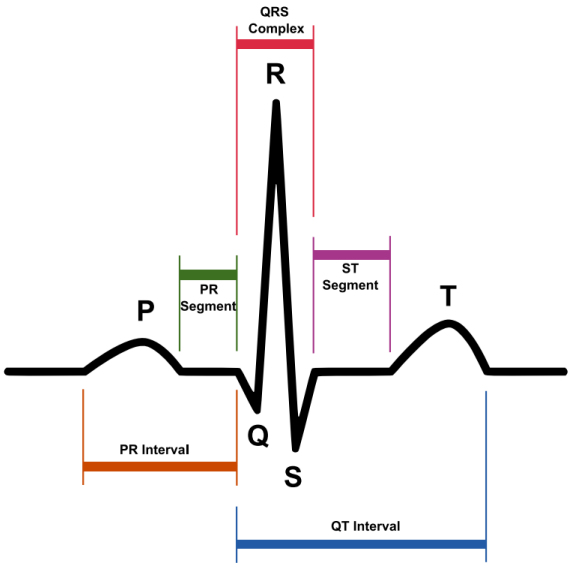

Figure 5.2: Typical ECG signal and its main characterizing waves [99].

The HR is given by the counting in beats per minute (bpm) of consecutive R-waves. However, noise contamination such as baseline wander, power line interference and muscle activities can corrupt the signal and reduce the clinical value of an ECG recording. Since wearable devices are more prone to perturbations by noise, filtering of the ECG is a necessary pre-processing step to ensure a reduction of the noise components while preserving the QRS complex shape. The Pan-Tompkins algorithm is used for ECG filtering and the HR calculation [100]. Other biosignals, such

as the blood pressure (BP) can provide important information about the patient condition. BP is defined by the mean arterial pressure (MAP) and is measured in millimetres of mercury (mmHg). BP is affected by the physical activity of the patient or associated diseases.

The combined analysis of other physiological signals provides relevant information regarding the patient's condition [101, 102, 103]. E.g., heartbeat variability and the cardiac output can be extracted from the ECG and the arterial blood pressure (ABP). The low heart rate variability is associated with pathologies like heart failure, and the cardiac output is one of the most important hemodynamic signals that are measured on patients with deficient compromised cardiac function. Combining this additional information (in the external data processing unit) allows diagnosing the origin of an eventual defective value. Different data fusion and anomaly detection algorithms, such as fuzzy logic, Artificial Neural Networks, Decision Trees and Naive Bayes classification will be evaluated, due to the good results they have provided on reasoning uncertainty in different application areas. Fig.5.3 describes the necessary steps in the system's development in order to achieve a reliable diagnosis. In the case of the AAA a literature survey was conducted in order to access what conditions (co-morbidities) are often associated with the pathologies, and what biosignals are more suitable for this monitoring.

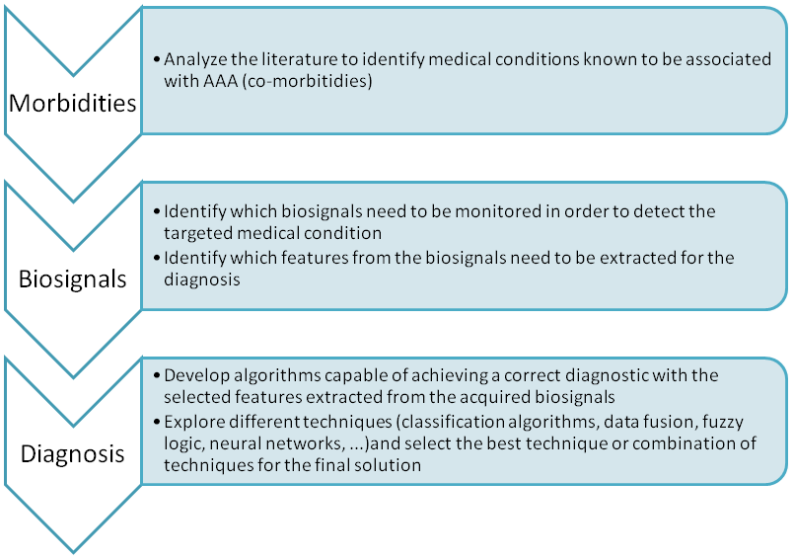

Figure 5.3: Diagnosis of comorbidities in case of AAA.

Several authors have noted an increased incidence of AAA in patients with peripheral artery disease (PAD) and coronary artery disease (CAD). Kanagasabay et al. conducted a study to see whether patients with AAA had a higher than average rate of vascular and pulmonary co-morbidity in a group of 5392 people screened for AAA [104]. The only conditions which were significantly associated with AAA in both sexes were myocardial infarction with an odds ratio (OR) of 1.66 (95% confidence interval (CI) 1.06 to 2.60) and claudication (cramping in the lower leg while walking or exercising caused by blocked arteries in the leg) with an OR of 1.68 (95% CI 1.17 to 2.42). Several reports have shown the high incidence (between 40% and 60%) of coronary artery disease in patients with abdominal aortic aneurysm, which could be explained by common risk

factors (e.g., tobacco smoking and hypertension). Complications related to coronary artery disease are the main cause of the operative mortality of aneurysm surgery [105]. Moreover, because this disorder is invariably associated with severe atherosclerotic damage of the aortic wall, it has been traditionally regarded as a consequence of atherosclerosis. The development of abdominal aortic aneurysms is clearly associated with alterations of the connective tissue in the aortic wall. Patients with poor medical condition have a significantly higher mortality after EVAR compared with patients fit for open surgery. But none of the investigated co-existing diseases affected mortality in patients unfit for surgery or anesthesia. Patients with good medical condition and diabetes or pulmonary disease at entry had higher mortality rate. In consequence, EVAR seems to have a limited benefit in patients ineligible for open surgery [106].

The main features of each signal eventually measured by the SIVIC system and the classification of the patient or system condition are presented in table 5.1.

Table 5.1: Data fusion model for the measured signals.

Signals	**Features**	**Classifier**
ECG	HR I HR II HR III ⋮	Normal/Abnormal
Blood Pressure	MAP	Hypotensive/Normal/Hypertensive
AAA Pressure	Mean Pressure	Normal/Endoleak
Electrode-Skin Impedance	Resistance	Electrodes Connected/ Disconnected
Square-wave Stimulus	Amplitude and Frequency	PGA Stuck-at/ High Gain / High Frequency variation

5.3 Classification Algorithms

The proposed anomaly detection algorithms yields two outputs (Patient Status and System Status) that constitute a critical and extremely useful step of the diagnosis process.

The dataset for training, testing and validating the algorithms contains 161 data cases collected during experiments and/or from simulations (in the case of the hardware). The dataset was normalized so that all the input values range from 0 to 1 and randomly divided in two sets: training (70%) and testing (30%).

The goal is to compare all the supervised learning classification algorithms presented in this section in terms of performance, complexity and computation load (time and memory requirements), so that the classification can be implemented in the wearable system and achieved in real time.

The inputs for the classifiers are:

- HR: Mean heart rate of the 5 last beats;

- BP: Mean MAP of samples with the same length as the HR;
- ABP: Pressure measured by the sensors implanted inside the aneurysm sac;
- Z: electrode-skin impedance;
- Amp_{Min}: Minimum amplitude of the test square wave;
- Amp_{Max}: Maximum amplitude of the test square wave;
- Freq: Frequency of the test square wave.

The outputs of the classification algorithms that provide binary classifiers (Fuzzy Logic and ANN) are:

- Patient Status: 1 if ok, 0 if there is a health problem;
- System Status: 1 if ok, 0 in case a fault is detected.

while for the categorical classification algorithms (Decision Trees and Naive Bayes Classifier) the provided output classes are:

- *ok* - both the patient and the system are good;
- *pf* - the patient shows a health problem;
- *sf* - the system is failing;
- and *pf-sf* - the patient shows a health problem and the system is failing.

5.3.1 Fuzzy Logic

Fuzzy Logic enables the creation of a decision making process based on logic and straightforward principles. Its implementation is relatively easy and thus suitable for implementation in a smartphone. The extensive literature in the medical field provides a solid knowledge base for the implementation of a medical decision support system. This technique can be applied to monitoring a patient's vital signs during an invasive surgery [107], support medical decisions in a intensive care unit [108], or cancer diagnosis based on image processing [109, 110].

In our case, FL is used in the data fusion process taking adavantage of its probability assignment based on rules. Since the values of the features extracted from the biosignals can be sorted in ranges well defined in the medical literature, the creation of rules is relatively straightforward. Table 5.2 shows common normal values for the HR and BP, and some pathological cases.

The FL decision process comprises 4 main components: fuzzy rules (knowledge base), fuzzy sets, fuzzy inference engine and defuzzification (Fig. 5.4) [111]. The inputs of the FL algorithm are the features previously extracted from the measured signals (Table 5.1). The outputs are the diagnostic results inferred from the observed quantities values and their correlations, i. e, *Patient Status* and the *System Status*, which can be normal or anomalous. The outputs are determined

Table 5.2: Fusion rules for patient condition diagnosis.

Features	**Condition**	**Rule**
HR (ms)	Normal	HR between 60 and 100 bpm
	Asystole	No QRS for at least 4 seconds
	Extreme Bradycardia	HR lower than 40 bpm for 5 consecutive beats
	Extreme Tachycardia	HR higher than 140 bpm for 17 consecutive beats
MAP (mmHg)	Normal Hypotension Hypertension	70-105 < 70 < 105
ABP (mmHg)	Normal Endoleak	Low pressure ($\sim$40) Sistemic Pressure ($\geq$ MAP)
Z (Ω)	Normal Disconnected	$< 1e^6$ $> 1e^6$
$Amp_{Min,Max}$ (mV)	Normal Fault	$\pm$ 2mV * PGA Gain DC or dif $>$ 25 % from expected
Freq (Hz)	Normal Fault	4 0 or dif $>$ 25 % from expected

based on the input values of the fuzzy sets and the rules assigned for each output. The rules to define the *Patient Status* are based on information found in the literature or provided by a physician, the rules for the *System Status* are defined from the system specifications and the previously performed FMEA analysis.

The fuzzy sets include the HR for each channel, the blood pressure (MAP), and can also include the ABP pressure, the acceleration of the patient's activity, and the electrode-skin contact resistance if these data are available.

In case the impedance values are higher than expected, signalling a potential loose connected electrodes situation, the fuzzy logic system updates the *System Status*.

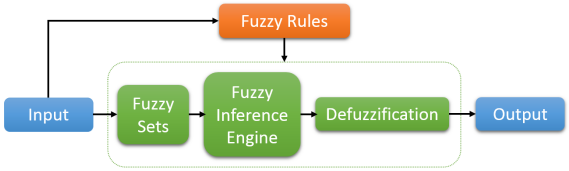

Figure 5.4: Block diagram of the FL algorithm.

The trapezoidal curve was chosen for the membership function. This is a function of a vector, x, and depends on four scalar parameters a, b, c, and d (equation 5.1). The parameters a and d

locate the "feet" of the trapezoid and the parameters b and c locate the "shoulders".

$$\mu_{trapezoidal}(x) = \begin{cases} 0, & x < a \text{ or } x > d \\ \dfrac{x-a}{b-a}, & a \leq x \leq b \\ 1, & b \leq x \leq c \\ \dfrac{d-x}{d-c}, & c \leq x \leq d \end{cases} \tag{5.1}$$

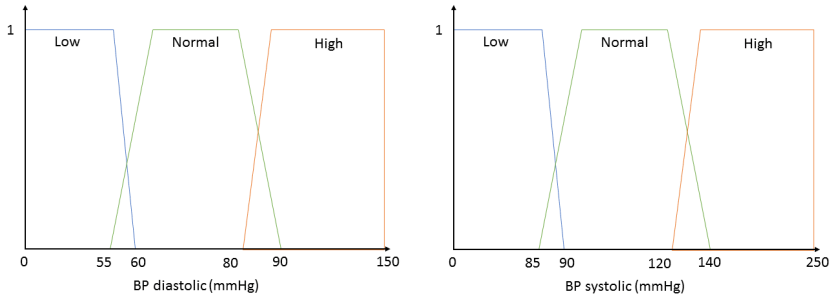

Figure 5.5: Fuzzy sets for the a) diastolic BP; b) systolic BP.

The BP is divided in three sets: low (hypotension), normal and high (hypertension). Figure 5.5 displays the membership functions for diastolic (a) and systolic (b) BP sets, respectively.

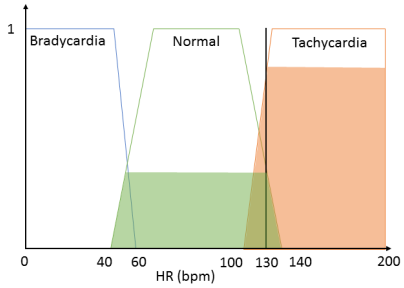

Figure 5.6: Fuzzy sets for the HR.

The HR includes the following sets: bradycardia, normal and tachycardia. The vertical black line in Fig. 5.6 represents a HR measurement of 130 bpm, which has a membership level of 0.3 in the normal set and a level of 0.8 in the tachycardia set.

The output variables *Patient Status*, *System Status*, and *Global Status* have 2 sets: abnormal (from 0 to 0.5) and normal (from 0.5 to 1). The normal sets from the inputs are assigned to the normal set of the outputs, and the remaining input sets are assigned to the abnormal output set.

5.3.2 Artificial Neural Networks

Artificial Neural Networks (ANN) are learning algorithms inspired by biological neural networks. These are typically organized in layers, which are made up of a number of interconnected *nodes* containing an *activation function*. Patterns are presented to the network via the *input layer*, which

communicates to one or more *hidden layers* where the actual processing is done after a combination of weighted *connections*. The hidden layers then link to an *output layer* where the answer is collected. Most ANN contain some form of learning rule which modifies the weights of the connections according to the patterns presented to the input.

For anomaly diagnosis purposes, the backpropagation neural network algorithm was used. The backpropagation is a supervised process that occurs with each cycle or 'epoch' (i.e., each time the network is presented with a new input pattern) through a forward activation flow of outputs, and the backwards error propagation of weight adjustments.

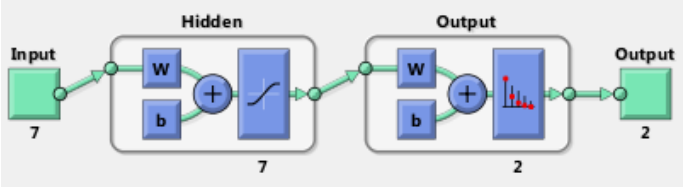

Figure 5.7: ANN architecture.

The ANN (see Fig. 5.7) was trained using the scaled conjugate gradient backpropagation algorithm [112]. The ANN has 7 hidden neurons (the same as the number of inputs) and the training is stopped after 27 epochs. The training dataset was used for building the ANN and the testing dataset was divided in two sub sets: half for validation of the ANN and half for testing.

Figure 5.8 displays the receiver operating characteristics (ROC) of the ANN for training, validation and test. The ROC is a metric used to check the quality of the classifiers. For each class of a classifier (Class 1: patient status, Class 2: system status) the true positive rate against the false positive rate of the different possible cut-points are calculated. These plots show the trade-off between sensitivity and specificity. The area under the ROC curve (AUC) is a measure of a test accuracy, and also a common metric that can be used to compare different tests.

5.3.3 Decision Trees

Decision trees (DT) are a non-parametric supervised learning method used for classification and regression. The goal is to create a model that predicts the value of a target variable by learning simple decision rules inferred from the data features. A DT important feature is their capability to break down a complex decision-making process into a collection of simpler decisions that are easier to interpret. This algorithm consists of several test nodes and class (or decision) leaves. It classifies an input by executing the tests in the tree beginning at the root, and going down the branches until a leaf is reached which gives the class of the input (or the decision to be taken).

The mathematical formulation is based on [113]. To each leaf a class or even a class probability is assigned. Each of the non-leave nodes represents a split regarding the input space. Such split is represented by a decision Q. Given training vectors of features (vital signs and system signals) $x_i \in R^n$, $i = 1, ..., n$ and an output label vector (patient status and system status) $C \in R^k$, the decision tree recursively partitions the space in such a way that the samples with the same labels are grouped

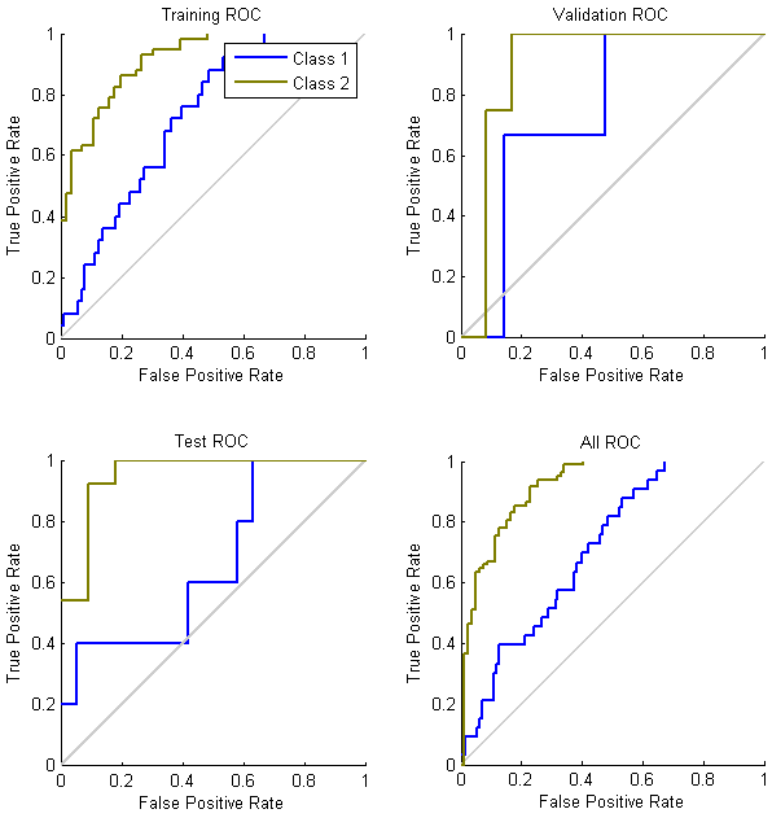

Figure 5.8: Receiver operating characteristic for the ANN.

together. For each candidate split $\theta = (j, t_m)$ consisting of a feature j and threshold t_m, partition the data into branches left ($Q_{left}(\theta)$) or right ($Q_{right}(\theta)$).

$$Q_{left}(\theta) = (x,y)|x_j <= t_m Q_{right}(\theta) = Q \setminus Q_{left}(\theta) \tag{5.2}$$

A decision tree is built top-down from a root node and involves partitioning the data into subsets that contain instances with similar values (homogeneous). Most DT algorithms use cross entropy to calculate the homogeneity of a sample m. If the sample is completely homogeneous the entropy is zero and if the sample is equally divided it has entropy of one.

Using the Matlab decision tree code available in the Statistical Toolbox, a classification decision tree can be generated using the cross-entropy for pruning. The model is constructed using t = classregtree(Inputs,Outputs,'States','HR' 'BP' 'ABP' 'Z' 'Amp_{Min}' 'Amp_{Max}' 'Freq') and the tree is optimized using [c,s,n,best] = test(t,'cross',Inputs,C) and tmin = prune(t,'level',best). Figure 5.9 displays the classification tree for anomaly diagnosis.

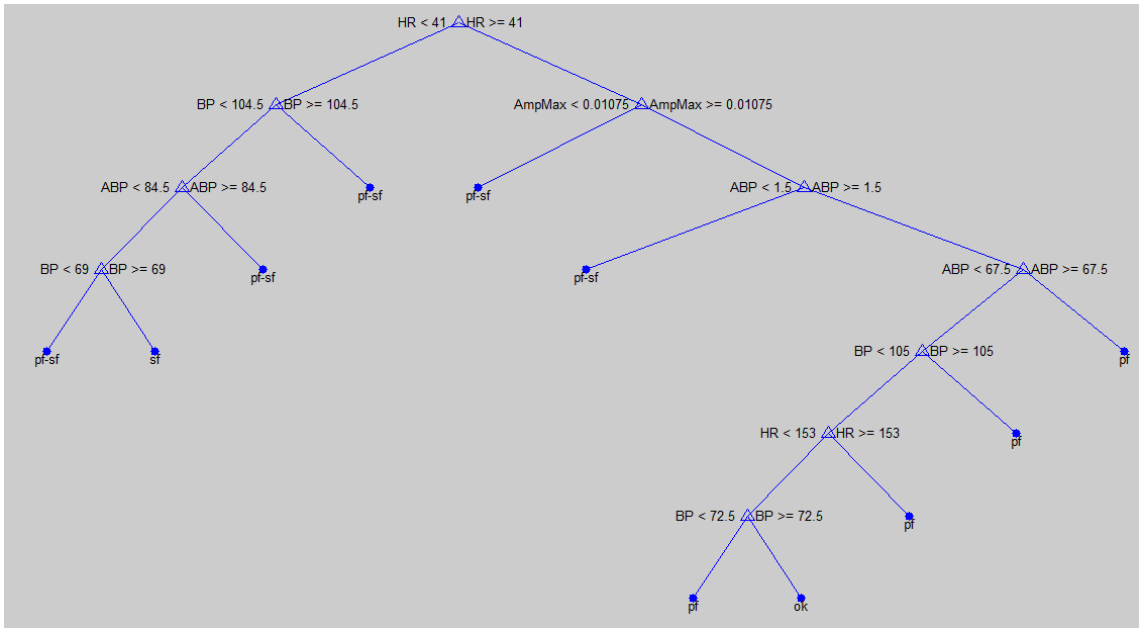

Figure 5.9: Classification decision tree.

5.3.4 Naive Bayes Classifier

The Naive Bayesian Classifier (NBC) is based on Bayes' theorem with independence assumptions between features. An NBC model is easy to build, with no complicated iterative parameter estimation, making it particularly useful for very large datasets. The NBC relies on a strong hypothesis — the value of any feature is independent of the existence of any other feature. In most of the real life examples the Naive Bayes hypothesis is never satisfied, but the algorithm predicts the classes with good enough accuracy. Despite its simplicity the NBC often does surprisingly well and is widely used because it often outperforms more sophisticated classification methods.

Bayes theorem provides a way of calculating the posterior probability, $P(C_k|x)$, from the prior probability of possible classes (system and patient status) C_k ($P(C_k)$), the evidence of the features (vital signs and system signals) $x = (x_1, x_2, ..., x_n)$ to be classified ($P(x)$), and the class conditional probability $P(x|C_k)$ (equation 5.3).

$$P(C_k|x) = \frac{P(x|C_k)P(C_k)}{P(x)} \tag{5.3}$$

NBC assumes that the effect of the value of a feature x_n on a given class C_k is independent of the values of other features. This assumption is called class conditional independence. Based on this, the likelihood can be decomposed to a product of terms:

$$P(C_k|x) = P(C_k)\Pi_{i=1}^{n} P(x_i|C_k) \tag{5.4}$$

Using Bayes' rule above it is possible to classify a new set of features (classifier inputs) x_n into a class (classifier outputs) C_k that achieves the highest posterior probability. Naive Bayes can be modelled in several different ways including normal, lognormal, gamma and Poisson density functions. For this work the normal (Gaussian) distribution was assumed:

$$P(x_i|C_k) = \frac{1}{\sqrt{2\pi\sigma_{ik}^2}} e^{-\frac{(x-\mu_{ik})^2}{2\sigma_{ik}^2}} \tag{5.5}$$

To train this classifier the mean (μ) and variance (σ^2) of each feature in the training set was calculated. These values are then used in the testing set.

5.3.5 Algorithms comparison

The training set of the database was used to compute the classification models of all four classification algorithms. The test set of the database was used to predict the output values and compare them to the actual outputs. In order to evaluate the performance of the algorithms a confusion matrix was calculated for all the predicted outputs.

A confusion matrix is a table whose rows provide the predicted values for each class (Hypothesized classes) and the columns the true values for each class (True classes). These values allow to calculate the sensibility, specificity and accuracy of the Hypothesized classes. Table 5.3 shows an example of a confusion matrix containing the values of True Positives(TP), True Negatives (TN), False Positives (FP) and False Negatives (FN) for two classes.

Table 5.3: Confusion Matrix.

		True Class	
		P	N
Hypothesized class	P	TP	FP
	N	FN	TN

The sensibility, specificity and accuracy can then be calculated after the following equations:

$$Specificity = \frac{TN}{TN+FP} \tag{5.6}$$

$$Sensibility = \frac{TP}{TP+FN} \tag{5.7}$$

$$Accuracy = \frac{TP+TN}{TP+FP+TN+FN} \tag{5.8}$$

Table 5.4 presents the accuracy values for all the tested algorithms. The NBC presents the best accuracy and the DT provides the lowest score. The accuracy might not be a reliable metric for the real performance of a classifier, because it will yield misleading results if the data set is unbalanced (that is, when the number of samples in different classes vary greatly). For this work the dataset used had balanced inputs, i.e. half the input values correspond to a fault in the patient/system and half the values are ok. However, since the combined inputs will affect the outputs (Patient and System Status) differently, the output classes are unbalanced (there are more faults than non faults situations).

Table 5.4: Accuracy values for all the classification algorithms.

Algorithm	FL	ANN	DT	NBC
Accuracy	85.7%	87.5%	77.6%	95.0%

In order to better evaluate the ability of the classifiers to correctly predict the Patient and System Status, the sensitivity and specificity of each output class was calculated for all the algorithms. The results are presented in Tables 5.5 for FL and ANN, and 5.6 for DT and NBC, respectively.

Table 5.5: Results for the FL and ANN classifications.

FL		
Class	'Patient Status'	'System Status'
Sensitivity	32.6%	85.3%
Specificity	93.3%	79.1%
ANN		
Class	'Patient Status'	'System Status'
Sensitivity	33.3%	80%
Specificity	100%	100%

The FL is better at predicting the 'System Status', with high values of sensitivity and specificity. As for the 'Patient Status' the algorithm is able to avoid the false positives (specificity) but sensitivity (true positive rate) is very low, making this algorithm unfit for patient diagnosis. A possible way to improve the algorithm would be to add more features from the ECG or other vital signs in order to correctly detect a health condition.

The data fuzzy model is flexible, in the sense that further inputs can be added to the system with extra information regarding the patient and the system. For instance, behaviour identification

sensors like accelerometers can be added to monitor the patient activity. If motion is detected at the same time the ECG signal is degraded, the system can determine the degradation of the biosignal as temporary and not related with any fault from the electronics or the electrodes. A body temperature sensor allows verifying if a moderately accelerated HR is due to a fever situation (the heart rate increases on average 8.5 beats per minute for a 1 degree C increase in body temperature [114]).

The ANN exhibits slightly better results than the FL, but also fails to deliver an acceptable 'Patient Status' prediction.

For the classification algorithms with categorical outputs the sensitivity and specificity are displayed for all the possible status: both the patient and the system are normal (ok), patient anomaly (pa), system anomaly (sa), and both the patient and the system are anomalous (psa).

Table 5.6: Results for the DT and NBC classifications.

DT				
Class	'ok'	'pa'	'sa'	'psa'
Sensitivity	62.5%	78.5%	84.6%	77.1%
Specificity	38.5%	88.6%	52.4%	82.5%
NBC				
Class	'ok'	'pa'	'sa'	'psa'
Sensitivity	100%	92.1%	100%	96.6%
Specificity	76.9%	100%	81.0%	98.3%

The DT algorithm presents good scores for detection of a patient health problem (pa) and simultaneous patient health problem and system anomaly (psa) cases. The DT performs poorly predicting when detecting the 'ok' case. For the system anomaly (sa) situation the specificity value is not good enough for our application, because almost half of the anomalous system cases are not being classified as such. Also the DT contains some decision branches that don't make sense in terms of the system features and patient's vital signs. These results might be improved by adding more data to the training set and increasing the number of input variables.

The NBC has acceptable sensitivity and specificity values for all the output cases. This algorithm is able to correctly predict and distinguish a patient health problem and/or a system fault/failure.

The next step of this work is to implement this algorithm in the smartphone connected to the wearable monitoring system to make the diagnosis in real time.

The results presented in this paper could be improved by adding more input features (signals from the hardware and the patient) and/or by a combination of classifiers. Also, since a high level of dependability is required for wearable devices, the system could be improved by guard-banding the predictions and let the classifiers indicate whenever they are not able to diagnose with confidence. This error moderation approach has been proposed in the field of circuit testing using classifiers [115].

5.4 Conclusion

Diverse wearable medical monitoring systems are being made available, all with different architectures, components, characteristics, and designs. It is common sense and well accepted that high levels of reliability, security, safety, availability and maintainability are required. Such high levels of dependability are difficult to achieve due to the complexity of these monitoring systems, which have different blocks and functional layers (sensors, data acquisition front-end, software, networks, etc) and the fact that the performance of the captured data actually convey information on both the system behaviour and the wearer physical activity and health condition, making it mandatory to correctly interpret the detected anomalies. Four algorithms based on data fusion, for patient and system diagnosis applied to a wearable medical system case, were presented. It is shown how the algorithms perform and can be explored to correlate data obtained from different sensors, in order to obtain status indicators that characterize the operation correctness of the monitoring system and the health condition of the wearer. The Naive Bayes Classifier algorithm presented the best performance in terms of accuracy, sensitivity and specificity. To overcome memory and processing time issues in the smartphone, the training or change (for example, to include more inputs or update the database) of this classifier can be done in a PC, being the probabilities uploaded afterwords to the smartphone for the on-line classification and diagnosis.

Chapter 6

Conclusions and Future Work

6.1 Conclusions

The advances on sensors, wireless communications and information technologies have promoted the rapid development of various wellness or disease monitoring systems, which enable extended independent living at home and improve the quality of life of patients with chronic disorders or who require a permanent vigilance.

That can be accomplished after the continuous monitoring of vital signals with wearable medical systems. These provide a faster and eventually more correct intervention of medical care professionals, as well as, information about the health status related to lifestyle and overall quality of life.

Wearable medical systems comprise one or more hard-wired or wireless interconnected sensors, strategically placed on the human body, which allow to obtain prompt information on the wearer's condition and provide a real-time feedback to medical personnel, issuing alert messages when life threatening changes occur.

However, the availability of reliable wearable medical systems and data communication infrastructures is an issue that has prevented a faster and more wider adoption of these systems. It is also one of the key factors required for the success of eHealth strategies.

Several wearable medical surveillance systems have been proposed, all with different architectures, components, characteristics, and designs. Nevertheless, all authors state that high levels of reliability, security, safety, availability and maintainability are required. Such high levels of dependability are difficult to achieve due to the complexity of these surveillance systems, which have different blocks and layers (sensors, acquisition system, software, networks, etc). Moreover, a dependability model to evaluate these systems as a whole has not been made available.

The lack of widely accepted methodologies for the development of complex pervasive medical monitoring devices, motivated the need for developing an approach for carrying out their analysis and evaluation based on a dependability framework. The proposed dependability framework comprised four main sets: dependability attributes, risks, means to achieve dependability and fault detection and maintainability. After determining the required levels of dependability (reliability,

availability, maintainability) and security/safety for medical wearable devices, the SIVIC system's risks of not achieving acceptable levels of dependability were identified using a fault tree analysis. Fault detection techniques were employed to detect system malfunctions and correct them in order to achieve high levels of dependability, namely for the pressure sensor and the electrode-skin interface.

Many of these procedures and techniques are already known and have been used in different applications fields, but, to the best of my knowledge, it is the first time they are systematically organized in a single framework addressing particularly wearable medical systems.

Central to the dependability framework being proposed and one of the main contribution of this thesis, is the exploring of sensor data fusion as a means to perform a more reliable detection and diagnosis of anomalous captured data. Besides the detection of anomalies in the electronic system operation, data fusion is explored to distinguish anomalous signals due to system's faults from those caused by pathologies of the wearer subject. Concerning, particularly, the case of the cardiovascular surveillance system that was developed, data fusion is used to increase the trust levels of the read biosignals after rejecting or correcting distorted vital sign signals, and to provide additional information on the patient's condition by classifying the set of signals into normal or abnormal condition (e.g. arrhythmia, chest angina, stroke, etc).

Data fusion techniques, namely fuzzy logic, artificial neural networks, decision trees and naive Bayes classifiers were employed to process the captured data to increase the trust levels with which diagnostics are made. The algorithms performance were evaluated based on their sensitivity, specificity and accuracy. It is demonstrated that all algorithms were able to correctly diagnose the system and patient status. The Naive Bayes classifier showed the best performance.

In conclusion, the proposed framework can be used for both the design, development and usage of wearable medical systems. The first step is identify what are the likely pathologies of the patients being monitored. This information is crucial for selecting the necessary sensors as well as the bio signals main features required for patient and monitoring system diagnosis. For this assessment a revision of medical literature needs to be performed, in order to evaluate what are the most likely clinical conditions associated for the typical user of the designed monitoring system. Once the required sensors and system architecture is established a FMEA analysis should be performed, if possible involving both engineers and health care practitioners. This analysis will be the basis for defining necessary test circuits in critical points of the system, as well as deciding if there is a need of sensor's redundancy. After the monitoring system is designed and implemented, a classification algorithm is necessary for the patient diagnosis. The classification algorithm receives as inputs information from sensors that monitor the patient as well as information regarding the monitoring system like self-test results. The fusion of the information from both sensors and system enables a diagnosis with a high level of reliability and indicates if there is a problem in the monitoring system or if the patient's health is degrading. For achieving a correct diagnostic, the classification algorithm design, training and testing requires a large database with the clinical status of the patient. Creating such a database requires a considerable amount of volunteers to performed measurements, that ideally present the same pathologies that the monitoring system is

expected to register and diagnose, as well as annotations with the patient status by doctors. This process can take years, and can only take place when the monitoring system is fully developed and satisfies all the required safety norms to be used in a hospital. To mitigate this issue a fault dictionary with the model of the monitoring system is created. The input for the model are signals from well established databases with medical annotations. The monitoring system main block that are more likely to cause distortions or corrupt the bio signals are included in the fault dictionary. In this way the classification algorithm can be designed and improved during the development phase of the monitoring system.

Other contributions of this thesis concern a technique to remotely monitor the condition of the abdominal aorta after an endovascular aortic aneurysm repair with the insertion of a graft, as well as a method to test the pressure sensor attached to the graft. A telemetry system was developed which allows detecting endoleaks, increased aneurysm diameter, and possible device migration, avoiding the need to subject the patient to periodic CT and MRI imaging.

Concerning the test of the abdominal aorta pressure sensor after insertion in the aorta sac, the test method being proposed allows evaluating the status of sensor, including detecting catastrophic faults as well as parametric deviations, providing thus the capability of diagnosing whether an abnormal detected pressure is due to a patient at risk case or actually to a defective sensor.

Still regarding the test and evaluation of the system, besides the above mentioned test and the implementation of different hardware and software self-tests that are already known, contributions are provided regarding the evaluation of the impedance established between electrodes and the skin, namely in the context of the capture of electrocardiographic and electromyographic data. It is shown that an impedance magnitude measurement is not enough to monitor the quality of biosignals, since the resistance if affected by the person's own impedance variation. The extraction of the parameters of the electrode-skin impedance electrical model, after performing phase and magnitude measurements, is more reliable for the purpose of the signal quality monitoring.

6.2 Future Work

The circuits and sensors that comprise the SIVIC system were successfully developed and tested, namely the pressure sensor, the T-shirt with embedded textile electrodes for the ECG monitoring, the external reading circuit to measure the pressure inside the AAA and a module that amplifies the ECG signals, makes the A/D conversion and sends the data to a smartphone via Bluetooth LE. Currently only the module that reads the ECG signal is integrated in the T-shirt, but it would be a matter of scaling down the reading circuit or using the new semi-passive pressure sensor and reading systems developed in the supervised MSc dissertations and incorporate a textile antenna for a full integration.

Also the presented classification algorithms for the system and patient diagnosis were implemented and tested in a PC, but after the comparison of all the tested algorithms the one with best

performance will be implemented in the smartphone that receives the ECG data for making a diagnosis in real time and possibly send an alert to the nearest hospital in case the patient condition deteriorates.

The classification algorithms could also be improved by adjusting the parameters for each patient. Right now the classification algorithms were trained and tested using medical vital signs databases that include data from different types of patients, with different pathologies, age, gender, ethnicity, etc. If this data was categorized and divided in subsets, for instance by gender, age or associated pathologies, the classification algorithms could be designed to best fit each subgroup. By assigning a category to the patient, the parameters of the classification algorithm for this subgroup would be loaded and a more precise diagnosis could be achieved.

Publications

The work carried out in the framework of this thesis was presented and discussed in the following international journals and conferences:

Journals

1. Cristina C. Oliveira and José Machado da Silva, “Fault diagnosis methods for highly dependable medical wearable systems”, Journal of Electronic Testing: Theory and Applications, August 2016.

2. Cristina C. Oliveira, Alexandra T. Sepúlveda, Nuno Almeida, Brian L. Wardle, José Machado da Silva and Luís A. Rocha, "Implantable Flexible Pressure Measurement System Based on Inductive Coupling", IEEE Transactions on Biomedical Engineering, February 2015.

International Conferences

1. Cristina C. Oliveira, Ruben Dias and José Machado da Silva, “A Fuzzy Logic Approach for a Wearable Cardiovascular and Aortic Monitoring System”, International Workshop on Connected Health Technologies, COHEAT-2015 in conjunction with ICT Innovations Conference, Ohrid, 3rd October, 2015.

2. Isabel Trindade, Frederico Martins, Rúben Dias, Cristina Oliveira and José Machado da Silva, “Novel Textile Systems for the Continuous Monitoring of Vital Signals: Design and Characterization”, 37th Annual International Conference of the IEEE Engineering in Medicine and Biology Society, Milan, 25-29 August, 2015.

3. José Machado da Silva, Cristina Oliveira, Bruno Mendes, Rúben Dias and Tiago Marques, “Design for Dependability and Autonomy of a Wearable Cardiac and Coronary Monitor”, EuroMicro Conference on Digital Systems Design, Funchal, 26-28 August, 2015.

4. Cristina C. Oliveira and José Machado da Silva, "A fuzzy logic approach for highly dependable medical wearable systems", 20th International Mixed-Signal Testing Workshop (IMSTW 2015), Paris, 24-26 June, 2015.

5. Cristina Oliveira, José Machado da Silva, Isabel Trindade and Frederico Martins, "Characterization of the Electrode-Skin Impedance of Textile Electrodes", XXIX Conference on Design of Circuits and Integrated Systems (DCIS 2014), Madrid, 26-28 November, 2014.

6. Cristina C. Oliveira and José Machado da Silva, "Towards a Dependable Cardiovascular Surveillance System", IFMBE International Conference on Health Informatics (ICHI 2013), Vilamoura, 7-9 November, 2013. (**3rd Prize on the IFMBE Young Investigator Competition**).

7. C. Oliveira, N. Almeida, and J. Machado da Silva, "A stent-graft endoleakage monitor: Telemetry system based on inductive-coupling transmission for implantable pressure sensors", in IEEE 3rd Portuguese Meeting in Bioengineering (ENBENG), 20-23 February 2013.

8. Cristina Oliveira, Nuno Almeida, and José Machado da Silva, "Inductive Coupling System for Endovascular Aneurysm Repair Monitoring", 9th International Conference on Wearable Micro and Nano Technologies for Personalized Health (pHealth 2012), Volume 177 - Studies in Health Technology and Informatics, Porto, June 2012. (**Best Poster Award**).

9. Cristina Oliveira and José Machado da Silva, "Fault Detection System for a Stent-Graft Endoleakage Monitor, 18th IEEE International Mixed Signals, Sensors and Systems Test Workshop, Taiwan, May, 2012.

10. Cristina Oliveira, José Machado da Silva and Luís Rocha: "A Methodology to Test a Stent-Graft Endoleakage Monitor": Proceedings of DCIS 2011, 26th Conference on Design of Circuits and Integrated Systems (DCIS), Albufeira, 2011.

Other Oral and Poster Presentations

1. Cristina C. Oliveira and José Machado da Silva, “A fuzzy logic approach for highly dependable medical wearable systems” DCE 2015 - 1st Doctoral Congress in Engineering, 11-13 June, 2015, FEUP, Porto.

2. C. Oliveira and J. Machado da Silva, "Towards a dependable wearable medical device", *2nd PhD Students Conference in Electrical and Computer Engineering (StudECE)*, Porto, Portugal, June 2012.

3. C. Oliveira and J. Machado da Silva, "Towards a Dependable Cardiovascular Surveillance System", *PhD Forum of the 1st Biannual European - Latin American Summer School on Design, Test and Reliability (BELAS)*, Tallinn, Estonia, June 2013. (**Honorable Mention Award**).

4. C. Oliveira, N. Almeida, and J. Machado da Silva, "RF-based Stent–Graft Endoleakage Monitoring System", *6^{o} Congresso do Comité Português da URSI. Aplicações das ondas eletromagnéticas: da eficiência energética à bioengenharia*, Lisbon, November 2012.

5. Cristina da Cunha Oliveira, Nuno Almeida, José Machado da Silva, "RF-based Stent-Graft Endoleakage Monitoring System", 6^{o} Congresso do Comité Português da URSI, 16 November, 2012, Lisboa.

6. C. Oliveira, N. Almeida, and J. Machado da Silva, "Wireless Stent–Graft Endoleakage Monitor", *1st PhD Students Conference in Electrical and Computer Engineering (StudECE)*, Porto, Portugal, June 2012. (**Best oral presentation award**).

7. Cristina Oliveira and José Machado da Silva, "Inductive-Coupling Based Stent-Graft EndoleakageMonitor", Workshop of the IEEE CE/CAS/BT Chapter on Power Harvesting Circuits, Lisbon, June 11th 2012.

Prizes and distinctions

1. 3rd Prize on the IFMBE Young Investigator Competition International Conference on Health Informatics (ICHI 2013), Vilamoura, Portugal, November 2013

2. Honorable Mention Award of the PhD Forum of the 1st Biannual European - Latin American Summer School on Design, Test and Reliability (BELAS), Tallinn, Estonia, June 2013.

3. Best poster award of the 9th International Conference on Wearable Micro and Nano Technologies for Personalized Health (pHealth), Porto, Portugal, June 2012.

4. Best oral presentation award of the 1st PhD Students Conference in Electrical and Computer Engineering (StudECE), Porto, Portugal, June 2012.

Appendix A

Schematic of the reader circuit

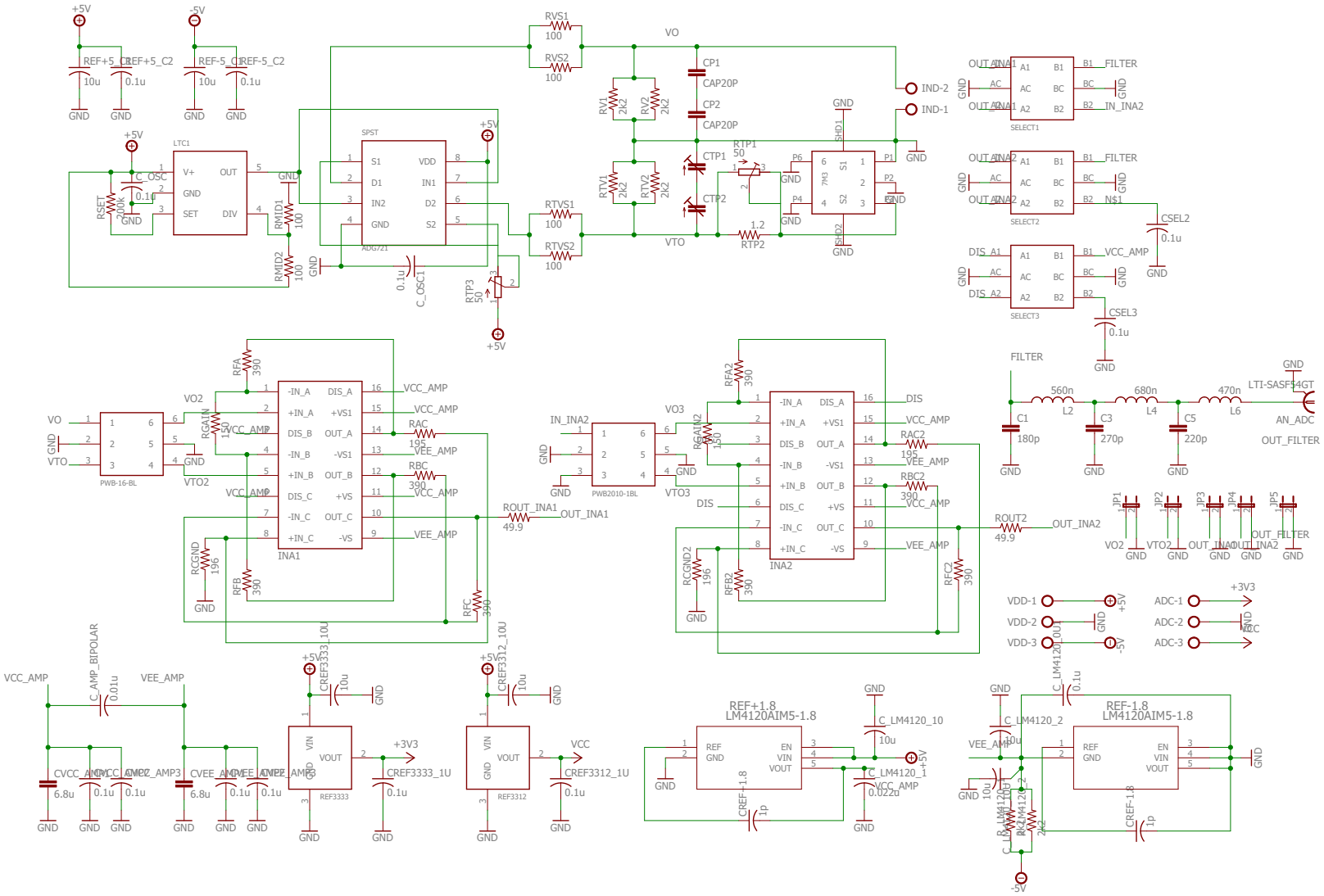

Figure A.1: Schematic of the reader circuit.

Appendix B

Alternative frequency variation detection systems

B.1 Heterodyne based receiver

The previously presented reader system allowed to experiment with and validate the different pressure sensors that were developed. However, it is not feasible to be used in a portable and wearable platform since a very high frequency (higher than 100 MHz) data acquisition board has to be used to capture and digitize the oscillating signal.

To avoid the need for such a high sampling frequency system, a frequency down-converting circuit is being developed by master's student Joana Maciel. With this circuit the captured differential resonant frequency signal (vdif) is converted to a lower frequency suitable to be captured by the μC available in the wearable platform.

This detection system is based in a heterodyne receiver topology implemented with the SA612A double-balanced mixer and oscillator integrated circuit. The output signal of the mixer is filtered and amplified in order to obtain a square wave whose frequency conveys the information on the sensor's capacitance. A digitally controlled variable capacitor, the MAX1474, is used to shift the frequency of the local oscillator of the mixer. A pair of inductors, controlled with a switch, allows extending the combination of *LC* values that determine the local oscillation frequency. This way a scan in frequency can be performed, after which the frequency of the sensor's signal can be detected and down converted to an easier to capture lower frequency. This process is performed under the control of a microcontroller, with which the frequency of the square wave obtained after the down conversion process is measured using a counter.

As this master dissertation is still under conclusion no more details are presented. Preliminary experiments allowed to conclude that the *LC* oscillation could be detected in the 10.2 MHz – 20.2 MHz frequency range with a resolution of approximately 32 kHz.

B.2 Semi-passive pressure sensor

The LC pressure sensor described in chapter2 shows the advantage of not requiring the use of a power supply, but on the other hand the level of the captured signal is very small, making the pressure detection process prone to measurement errors. To circumvent this, a semi-passive pressure sensor was developed, not with the objective of replacing the fully passive solution, but to evaluate alternative solutions. This work was developed in the context of an MSc dissertation carried out by Filipe Alves [116].

A semi-passive tag sensor operates by first accumulating energy received through the inductive link, which then allows a backscattering process to transmit back the required information. Figure B.1 shows the schematic of the circuit specifically responsible for detecting the variation of capacitance of the pressure sensor (C_{sens}), given by the expression $C_{sens} = C_{s2} \times \frac{t_{Csens}}{t_{Cs2}}$.

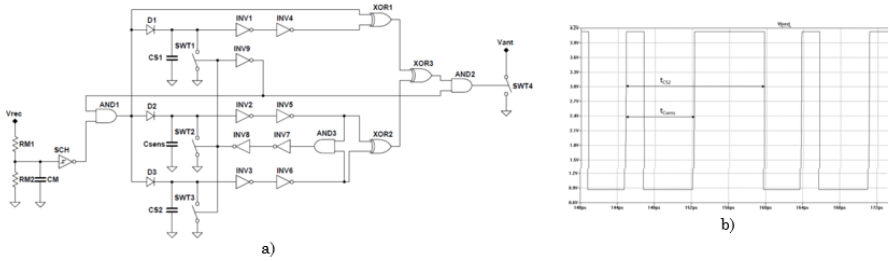

Figure B.1: a) Schematic of the semi-passive pressure sensor and b) Waveform of its output signal which controls the backscattering switch connected to the tag antenna.

The backscattering is detected in the external reader as an amplitude modulation of the current in the primary antenna. This envelope (Figure B.2.b) is extracted with the circuit shown in Figure B.2.a) and processed to reconstruct the backscattering controlling signal (figure B.1b) at its output (Vsec in Figure B.2a).

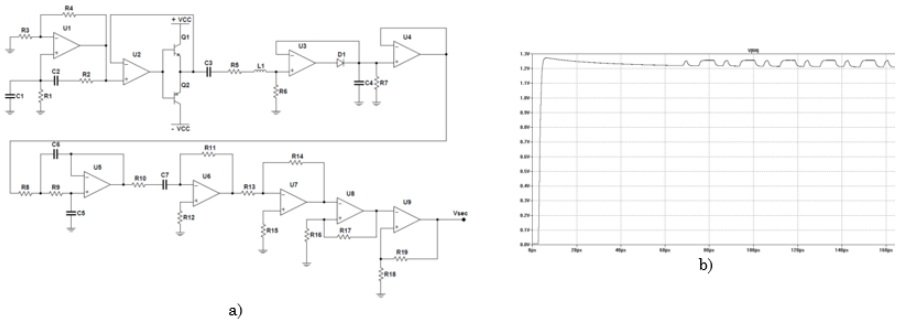

Figure B.2: a) Schematic of the external reader, comprising the driver of the primary antenna (L1) and envelope detector b) Waveform of the envelope of the primary antenna current obtained after the peak detector.

Appendix C

Recipes for tissue simulating fluid

The recipes developed by Hartsgrove et al. [46] are for materials at room temperature that simulate the permittivity and conductivity of muscle, brain, lung and bone tissues at temperature (37°C) in the frequency range of 100-1000 MHz. These materials are all easy to prepare, inexpensive, and retain their properties for an extended period of time.

Table C.1: Materials and quantities for the tissue simulating fluid.

Ingredients (% by weight)	**Head/Brain**	**Body/Muscle**
Water	40.4	52.5
Salt (NaCl)	2.5	1.4
Sugar	56.0	45.0
Hydroxyethyl cellulose (HEC)	1.0	1.0
Bactericide	0.1	0.1
Dielectric constant @ 900 MHz	41.2	54.7
Conductivity @ 900 MHz (S/m)	1.22	1.38

Preparation Methods

The following procedure is used to prepare muscle, brain and lung tissue equivalent material:

1. Weigh all materials accurately;
2. Heat water to 40°C;
3. Add salt and bactericide with stirring;
4. Add sugar (and microspheres in case of lung);
5. Continue to stir at low speed to minimize the amount of air bubbles in the solution;
6. Add the hydroxyethyl cellulose (HEC);
7. Remove from heat;
8. Continue to stir until mixture thickens;

9. Let cool to room temperature.

When not used the materials should be stored in a covered container to prevent evaporation of water. If, however, the material does lose some water the original properties can usual be restored by the addition of a small amount of water that is simply stirred into the existing material.

Appendix D

SEMCAD Simulations

D.1 Motivation

An important issue when building a system that resorts to inductive coupling to communicate with an implantable sensor is the level of energy absorbed by the body that causes the tissues to heat and ultimately damage the living cells and tissues. This issue is going to be studied in the next section and the obtained values of energy absorbed by the living tissue using this system are going to be compared with the legislation. Since the sensor is going to be placed inside the human body, more realistic measurements were performed using a slice of pork meat between the reader and the sensor. As can be observed in Fig. D.1, the presence of the tissue caused a large shifting in the received signal frequency as well as decrease in the signal's amplitude. This can be due to the change in the medium permittivity to magnetic induction, also affected by the quality factor, as has been reported in [47, 48].

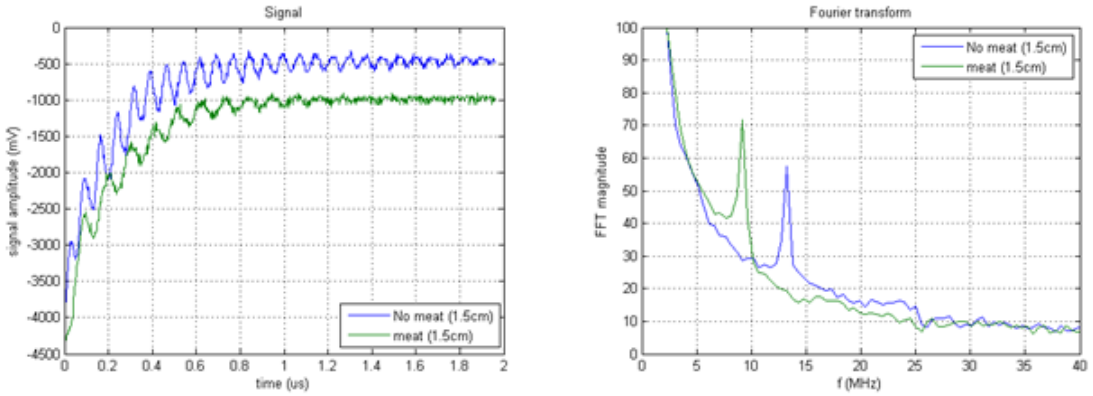

Figure D.1: Effect of biological tissue on the signal capture.

This can be regarded has the bottleneck of the system and further study needs to be conducted in order to quantify exactly how the biological tissue changes the captured oscillating frequency and how this effect can be compensated to acquire acceptable pressure readings. The communications' performance in a biological medium is very different from that in classic communications

systems. Since the electromagnetic wave is passing through different media that have vastly different electrical properties, the wave propagation speed is significantly reduced in some organs and may induce significant time dispersion that varies with each organ and body tissue. The existing literature on the influence of biological tissue in implantable sensors communications only approaches the ultra-wide band (UWB) with frequencies between 3.1 GHz and 10.6 GHz, but for frequencies between 12.5-20MHz, which correspond to the system's working frequencies, this issue was not studied. The electrical characteristics of human tissue at the frequencies of interest are going to be checked in the literature in order to build a phantom capable of emulating the human tissues' properties. This phantom will be used to quantify the effect of biological tissue in the inductive coupling link and study the shift of the detect oscillating frequency over a distance range in opposition with the frequencies obtained when the dielectric between the reading circuit and the sensor is the air.

D.2 Simulations

The use of electromagnetic fields (EMFs) in the radiofrequency (RF) and microwave (MW) regions of the spectrum is fundamental in many medical diagnostic and therapeutic techniques such as magnetic resonance imaging (MRI), hyperthermia/thermal ablation and implantable sensors. The proliferation these systems has leaden the concern of ensuring national and international guidelines and legislation have been established to determine exposure limits and safe practices. These guidelines rely heavily on studies that describe the internal electric fields, currents and the deposition of energy within the human body that are caused by the exposure to such EMFs. Since the internal electric fields and currents are difficult to determine directly, it is important to understand how they relate to the external electric and magnetic fields that can be measured relatively easily. Numerical methods that describe the interactions of EMFs with the body provide a means of obtaining this information, as well as the spatial, and in some applications the temporal, variations of internal electric fields, currents and energy deposition that are prerequisites when assessing the safety of exposure to EMFs or when assessing or optimizing therapeutic or diagnostic medical applications. Several techniques that provide a numerical solution to Maxwell's equations, subject to boundary conditions, and can be implemented on powerful PCs and other computing platforms are available. In general, these may be classified broadly into two categories—those based on a differential equation (DE) model and those based on an integral equation (IE) model. Further classification can be made according to whether the computation is made in the time domain or frequency domain. One of the most promising techniques for the study and optimization of antennas' parameters is the Finite-Difference Time-Domain (FDTD). The specific absorption rate (*SAR*) is also computed by most part of the available commercial solvers since this parameters is used as a standard to quantify the heat generated by magnetic and electrical fields in biological tissue and is included in the legislation for electronic devices such has cell phones and MRI equipment.

$$SAR[W/Kg] = \frac{\sigma E^2}{\rho} \tag{D.1}$$

The SAR is mainly dependent on the incident electrical field (E) and is also related with the tissue electrical conductivity (σ) and density (ρ). According to the European directive 1999/519/CE the SAR should be calculated over a period of 6 minutes and the maximum average *SAR* for the whole body for frequencies between 10 MHz and 10 GHz is 0.08 W/Kg [117].

D.3 SEMCAD

The SEMCAD program, by Shmid & Partner AG is used to construct a model for the sensor and estimate the sensor's oscillating frequency and the SAR. This program implements an FDTD algorithm that uses non-uniform grids in order to reduce the memory requirements [118].

D.3.1 Finite Difference Time Domain (FDTD)

The Finite-Difference Time-Domain (FDTD) method is based on a spatial and temporal discretization of Maxwell's curl equations, commonly within a rectilinear Cartesian grid originally proposed by Yee in 1966. Within the last two decades FDTD gained rapidly increasing interest, mainly in electromagnetics (EM), for the simulation of complex and largely inhomogeneous structures due to its straightforward and explicit approach. The electric and magnetic field components are allocated in space on a staggered mesh of a Cartesian coordinate system (Fig. D.2). The electrical (E) field and magnetic (H) field components are updated in a leap-frog scheme using the finite-difference form of the curl which surrounds the component. The transient fields can be calculated when the initial field, boundary and source conditions are known.

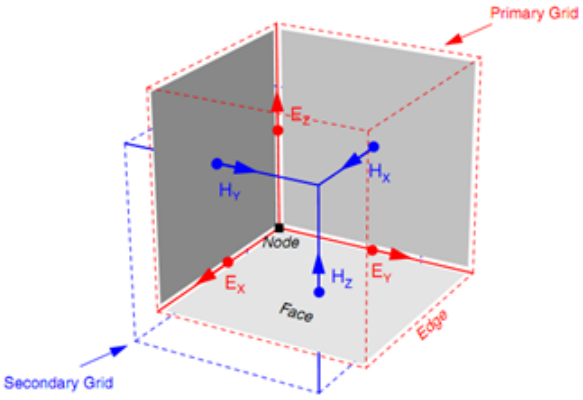

Figure D.2: 3D Yee cell showing the E- and H-field components in the staggered grid.

The main advantage of the FDTD algorithm is its ability to solve Maxwell's equations directly in the time domain, thus providing accurate broadband solutions to electromagnetic wave propagation and scattering problems.

The Maxwell equations used for the FDTD algorithm are the Faraday's law for the magnetic field calculation (equation 10) and the Ampere's law for the electric field calculation (Fig. D.3).

Faraday's Law	Ampere's Law
$\nabla \times \vec{E} = -\frac{\partial \vec{B}}{\partial t} - \vec{M}$ (9)	$\nabla \times \vec{H} = -\frac{\partial \vec{D}}{\partial t} - \vec{J_f}$ (11)
$\frac{\partial \vec{H}}{\partial t} = -\frac{1}{\mu}\nabla \times \vec{E} - \frac{\rho'}{\mu}\vec{H}$ (10)	$\frac{\partial \vec{E}}{\partial t} = \frac{1}{\epsilon}\nabla \times \vec{H} - \frac{\sigma}{\epsilon}\vec{E}$ (12)
E – electrical field H – magnetic field M – magnetization D - electric flux density ε- permittivity of free space μ -permeability of free space, ρ - total charge density J_f - free current density	

Figure D.3: Maxwell's equations.

D.3.2 Simulation Results

The SEMCAD simulator was used for modeling the sensor (Fig. D.4) and predict some parameters such has the antenna resonating frequency and SAR. The sensor has been made by a PCB with a square planar inductor with L=9μH, a discrete resistor =12 Ω and a discrete capacitor C=10pF. The materials used for the model correspond to those of the real sensor characteristics, since SEMCAD has a material database where the cupper and the FR4 (PCB dielectric) are available.

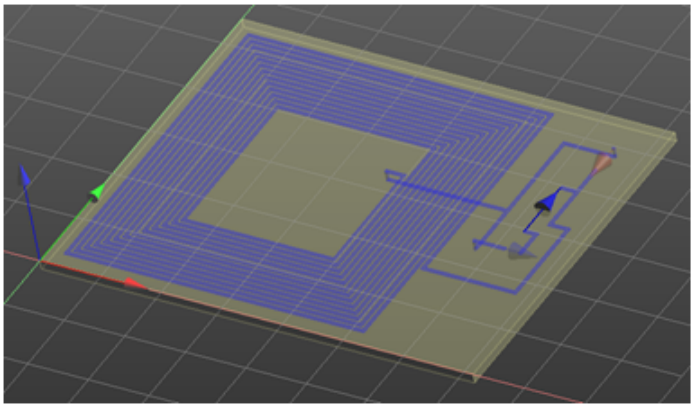

Figure D.4: Sensor antenna model on SEMCAD.

A broadband simulation with a center frequency of 16 MHz and a bandwidth of 12 MHz was performed using the FDTD solver. This simulation allows the calculation of the magnetic and the electrical fields over time has well has the voltages and currents on the resistor, capacitor and the source components. However the needed computation time is high requiring 36h to run this simulation. Since this solver makes the calculations in the time domain when running simulations for higher frequencies, for instance in the microwave domain, the simulation times decrease rapidly. Resorting to equation $f = \frac{1}{2\pi L_s C_s}$ the sensor's oscillating frequency was expected to be 16.8 MHz for the inductance and capacitance values inserted in the model. The reflection coefficient S11 obtained after the FDTD simulation is in accordance with the calculations (Fig. D.5) . This fact recalls that this simulator can be used to optimize an antenna's geometry and study its behavior.

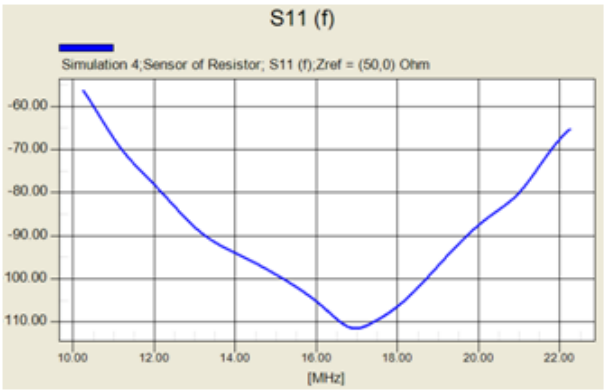

Figure D.5: Sensor's reflection coefficient S11.

Since the aim of this work is to understand the effect of biological tissue in the inductive coupling link a more realistic model was designed. The previous model was inserted in a box with dimensions 200x200x75mm with the electrical properties of tissue simulant. The reader antenna was added on the wall of the box to stimulate the sensor (Fig. D.6).

A low frequency simulation with the electric static solver was performed in order to calculate the magnetic and electrical fields, as well as the SAR (Fig. D.7). The SEMCAD postprocessor tool enables the SAR estimation for a solid and also computes the average SAR for a volume. The reader antenna placed on the wall of the simulant tissue box caused a heating mainly close to the antenna's windings and the remaining of the tissue was slight affected by the antenna. The sensor model used for this simulation is the sensor prototype made in a PCB board, which has totally different properties from the sensor that is being developed by the partners in the SenseCardioHealth project. Also the copper windings are in direct contact with the tissue without any protective layer, unlike a final solution where the sensor and reader coils would be covered in a protective layer to prevent any damage in the human tissue. The average SAR for the tissue was 0.0136 W/kg, which is significantly lower than the legislation limit (maximum SARaverage = 0.08 W/Kg).

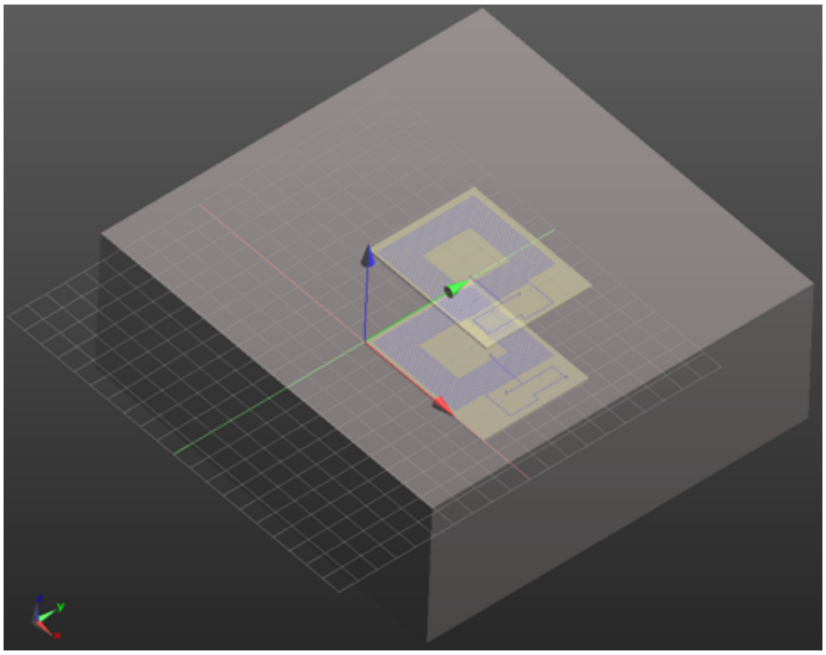

Figure D.6: Model of the sensor antenna inserted on simulant fluid.

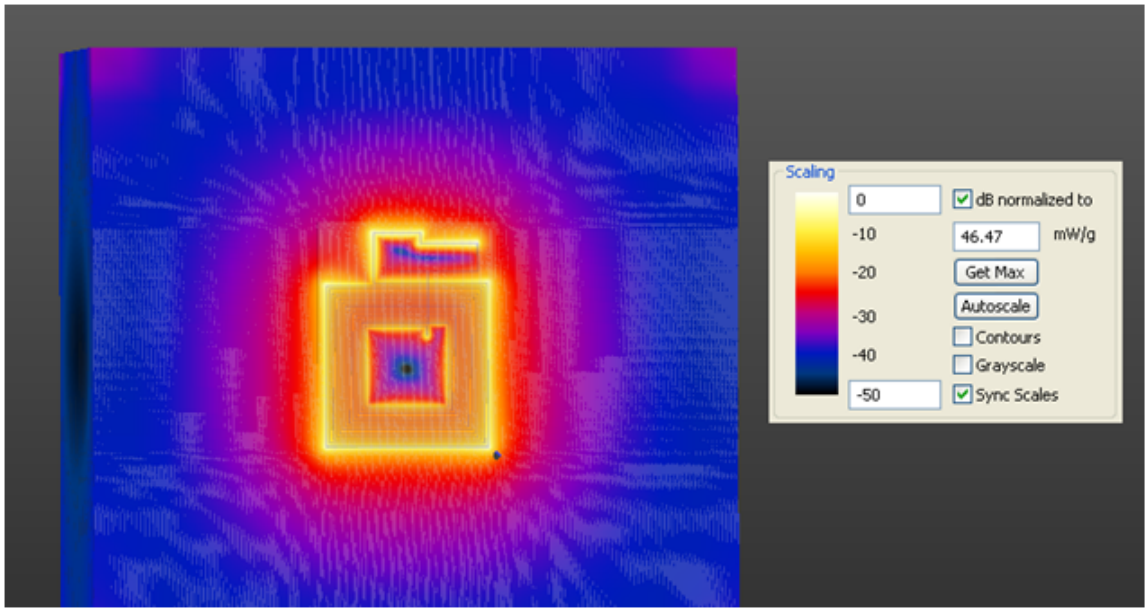

Figure D.7: SAR field on the simulant tissue box.

D.4 Conclusions

The effect of the biological tissue dielectric properties on inductive coupling based communications was studied in the 12.5-20 MHz bandwidth using the implantable sensor and the reader circuit developed in the scope of the SenseCardioHealth. The sensor CAD model was built and simulated in the SEMCAD program having been verified that the sensor's simulated resonant frequency is in accordance with the frequency obtained from the analytical calculations. When inserting the sensor model in a more complex simulation with a box emulating the body tissue the specific absorption rate (SAR) was computed in order to estimate the effect of the electromagnetic waves in human tissue. The average SAR for the simulating tissue was lower than the legislation indicating that the projected system is not harmful to possible patients.

Appendix E

Textile Antennas

The wire which is used for the antennas, electrodes and electrical connections is composed essentially of polyamide and silver, the latter in very small quantities but which confers electrical conductivity to the wire. The antenna in structure A uses 7 embroidery crossings while the antenna in structure C uses only 3 crossings. The structures A and C were characterized (See Fig. E.3).

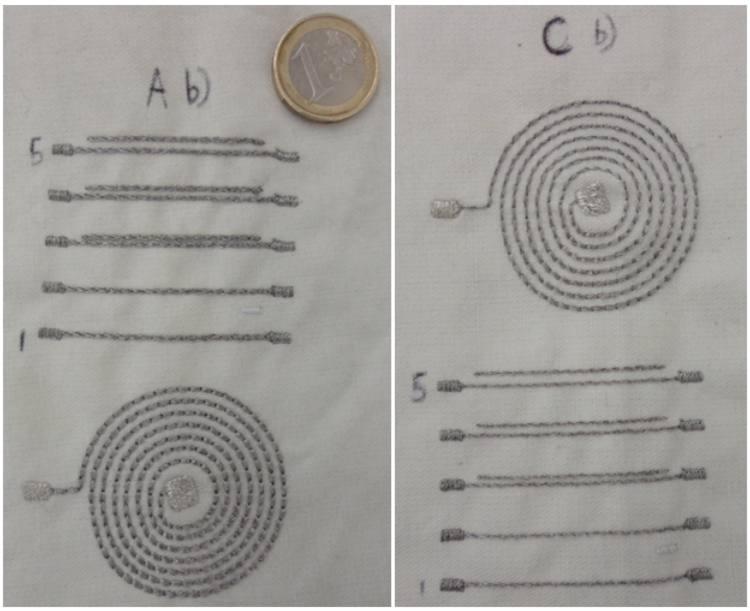

Figure E.1: Test Structures.

E.1 Calculation of spiral planar inductances

It is possible to achieve a simple and accurate expression for calculating the inductance of a flat spiral by approximating the sides of the sheets of symmetrical current loops of equivalent current densities. For example, in the case of a square inductance obtained four identical power leafs. The streams of sheets on opposite sides are parallel to each other, while adjacent are orthogonal. Using the symmetry and the fact that the leaves with the orthogonal currents have zero mutual

inductance, calculation of inductance is now reduced to evaluate the self-induction of a leaf and the mutual inductance between the currents of opposite sheets.

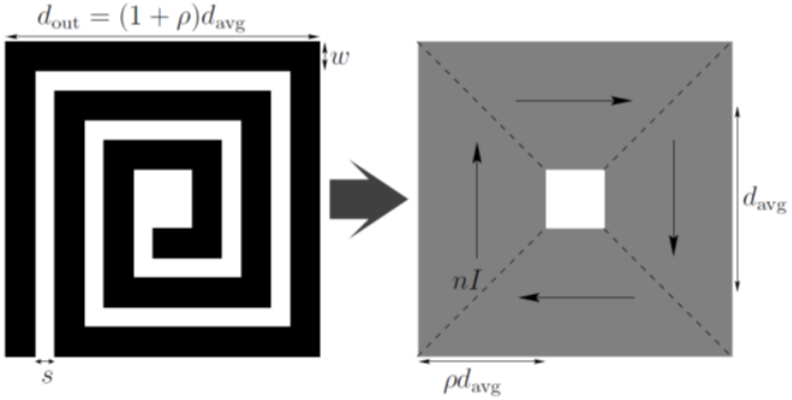

Figure E.2: Approximation to a square spiral[45].

For a given shape, an inductor is completely specified by the number of turns N, the width w of the loops, the space between coils s, the average diameter D_{Avg} and filling ratio ρ. The thickness of the inductor has a small effect on inductance. Although the accuracy of this expression worsens as the relationship $s = w$ becomes large, it exhibits a maximum error of 8% for $s = w$. Note that the typical integrated spiral inductors are built with $s \leq w$. The reason is that a smaller spacing improves the magnetic coupling inter-coils and reduces the area occupied by spiral. A large spacing is only desired to reduce inter-turns parasites capabilities. In practice, this is not a concern, since this capability is covered by the capacity formed by the lower bound of the inductor [45].

Expressions based on approximation of current sheets (Mohan)

$$L = \frac{\mu_0 N^2 d_{avg} C_1}{2}\left(ln\frac{C_2}{\rho} + C_3\rho + C_4\rho\right) \tag{E.1}$$

$$d_{avg} = \frac{d_{out} + d_{in}}{2} \tag{E.2}$$

$$\rho = \frac{d_{out} - d_{in}}{d_{out} + d_{in}} \tag{E.3}$$

Table E.1: Coefficients for the expression of current sheets.

Geometry	C1	C2	C3	C4
Square	1.27	2.07	0.18	0.13
Hexagonal	1.09	2.23	0.00	0.17
Octogonal	1.07	2.29	0.00	0.19
Circular	1.00	2.46	0.00	0.20

Wheeler expressions to calculate inductances

Wheeler formula is suitable for inductors with a thicker winding area than the average diameter of the inductor. The equation is defined by the average radius, the thickness of the coils c, the magnetic permeability of vacuum ρ_0 (4π x 10^{-7} H / m), the number of turns N and the filling ratio ρ [119].

$$L_{circular} = 31.33\mu_0 N^2 \frac{a^2}{8a+11c} = 31.33\mu_0 \frac{N^2 a}{8+22\rho} \tag{E.4}$$

$$L_{square} = 2.34\mu_0 N^2 \frac{a^2}{a+1.875c} = 2.34\mu_0 \frac{N^2 a}{1+1.875\rho} \tag{E.5}$$

Inductance Calculation

Table E.2: Antenna characteristics.

Antenna	D_{in}	D_{out}	s	w
A	1.1 cm	4.4 cm	0.1 mm	1.5 mm
C	1.2 cm	4.4 cm	1.5 mm	1 mm

Table E.3: Calculated Inductances.

Inductance (μH)	Mohan	Wheeler
A	1.256	1.251
C	1.315	1.313

The C structure has a slightly higher inductance due to its bigger internal diameter. An increase of the width w of the coils does not affect the inductance of the antenna, however decreases the resistance of the inductance which causes an increase in the quality factor (Q).

Calculation of the inductance in parallel lines

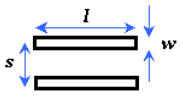

Figure E.3: Inductance in parallel lines.

The inductance is influenced by the line's lenght l, the width w and the distance between the center of each line s.

$$L \approx \frac{\mu_0 \mu_r s}{l} (l \gg s, s > w) \tag{E.6}$$

Series resistance

To determine the total parasitic resistance of the inductor, it is necessary to know the length of the conductor track l_c, the conductivity of the conductive material σ, and its thickness t_c.

$$R_s(DC) = \frac{1}{\sigma}\frac{l_c}{Area} = \frac{l_c}{\sigma w t_c} \tag{E.7}$$

The skin effect will increase the AC resistance of the inductor at higher frequencies, and must be taken into account, of which δ is the depth foil, and μ is the absolute permeability of the conductor.

$$\delta = \sqrt{\frac{1}{\sigma \mu f}} \tag{E.8}$$

$$R_s = R:DC\frac{t_c}{\delta(1-e^{\frac{-t_c}{\delta}})} \tag{E.9}$$

Parasitic capacitance

The calculations of the parasitic capacitances are based on the parallel plate capacitor, and ε_r is the dielectric constant of the material, ε_0 is the vacuum permittivity, A_p is the area of the capacitor and d_p the distance between the plates.

$$C = \varepsilon_r \varepsilon_0 \frac{A_p}{d_p} \tag{E.10}$$

E.2 Materials and methods

The antennas and thread segments were characterized in terms of electrical properties using a network analyzer. This equipment allows to measure the S-parameters. Since there are 2 terminals only the $S11$ parameter was measured, and from this measurements the inductance and AC resistance of the structures were calculated . The network analyzer was configured to make a sweep between 300 kHz and 100 MHz so as to comprise the frequencies of interest. Copper adhesive tape was used with a soldering drop in the center, to establish contact with the pads without damaging them. A multimeter was used to verify that this method introduces a negligible resistance.

E.3 Results

Through the $S11$ parameter, also called reflection coefficient Γ , the load impedance ZL of the device under test (DUT) can be extracted, knowing that the line impedance $Z0$ is 50 Ω.

$$S11 = \Gamma = \frac{Z_L - Z_0}{Z_L + Z_0} \tag{E.11}$$

$$Z_L = \frac{1+S11}{1-S11} \tag{E.12}$$

(E.13)

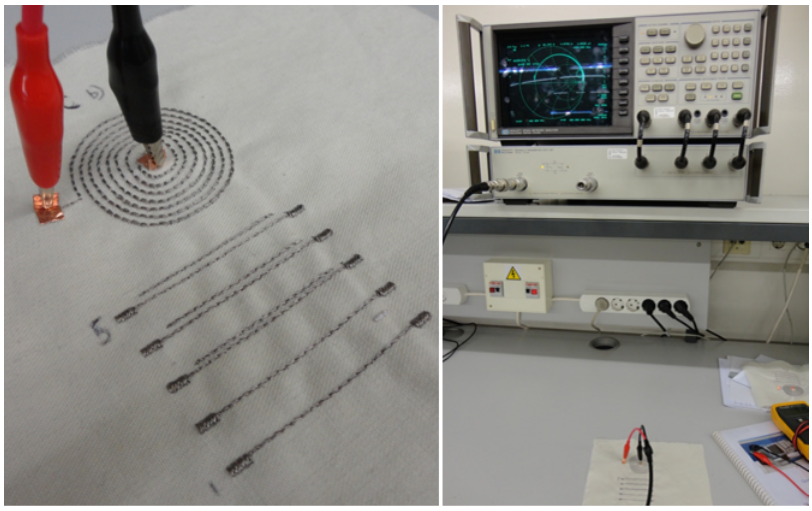

Figure E.4: Measurements setup.

From Z_L the values of inductance L (H), the AC resistance R (Ω) and quality factor (Q) are extracted.

$$L = \frac{imag(Z_L)}{\omega} = \frac{imag(Z_L)}{2\pi f} \tag{E.14}$$

$$R = real(Z_L) \tag{E.15}$$

$$Q = \frac{2\pi f L}{R} \tag{E.16}$$

Table E.4: Spiral antennas' inductance.

Inductance (μH)	300 kHz	1 MHz	10 MHz	20 MHz
A	0.956	0.938	0.464	0.293
C	1.214	1.215	1.215	1.241

Table E.5: Spiral antennas' resistance.

AC Resistance (Ω)	300 kHz	1 MHz	10 MHz	20 MHz
A	6.375	7.061	29.177	40.833
C	16.171	16.249	15.240	11.187

Table E.6: Spiral antennas' quality factor.

Q	300 kHz	1 MHz	10 MHz	20 MHz
A	0.283	0.875	1.002	0.903
C	0.142	0.492	5.020	13.977

E.4 Discussion

The antenna of structure A has a lower inductance, even though the geometry is similar to structure C. The antenna has more yarn passages, hence the parasitic capacitance formed between the yarns of the top and bottom layers is increased, which also explains the low quality factor. In addition there may be contact between the coils, due to the spacing between them being smaller. Another issue relates to possible leaks due to the characteristics of the fabric and environmental (e.g. humidity) and the manufacturing process of the yarn itself (the wire is coated with silver).

Bibliographic References

[1] S. Park and S. Jayaraman, "Enhancing the quality of life through wearable technology," *Engineering in Medicine and Biology Magazine, IEEE*, vol. 22, no. 3, pp. 41–48, 2003.

[2] R. Paradiso, "Wearable health care system for vital signs monitoring," in *Information Technology Applications in Biomedicine, 2003. 4th International IEEE EMBS Special Topic Conference on*. IEEE, 2003, pp. 283–286.

[3] E. McAdams, A. Krupaviciute, C. Gehin, A. Dittmar, G. Delhomme, P. Rubel, J. Fayn, and J. McLaughlin, "Wearable electronic systems: Applications to medical Diagnostics/Monitoring," in *Wearable Monitoring Systems*, A. Bonfiglio and D. D. Rossi, Eds. Springer US, Jan. 2011, pp. 179–203.

[4] C. Otto, A. Milenkovic, C. Sanders, and E. Jovanov, "System architecture of a wireless body area sensor network for ubiquitous health monitoring," *Journal of Mobile Multimedia*, vol. 1, no. 4, pp. 307–326, 2006.

[5] R. Paradiso, G. Loriga, and N. Taccini, "A wearable health care system based on knitted integrated sensors," *Information Technology in Biomedicine, IEEE Transactions on*, vol. 9, no. 3, pp. 337–344, 2005.

[6] S. Lawless, "Crying wolf: false alarms in a pediatric intensive care unit," *Crit Care Med*, vol. 6, no. 22, pp. 981–985, Jun 1994.

[7] C. Tsien and J. Fackler, "Poor prognosis for existing monitors in the intensive care unit," *Crit Care Med*, vol. 4, no. 25, pp. 614–619, Apr 1997.

[8] C. MC., "Review: Alarms in the intensive care unit: how can the number of false alarms be reduced?" *Critical Care.*, vol. 4, no. 5, pp. 184–8, Aug 2001.

[9] "Council directive 93/42/EEC of 14 june 1993 concerning medical devices," 1993.

[10] A. T. Sepúlveda, R. Guzman de Villoria, J. C. Viana, A. J. Pontes, B. L. Wardle, and L. A. Rocha, "Full elastic constitutive relation of non-isotropic aligned-CNT/PDMS flexible nanocomposites," *Nanoscale*, vol. 5, no. 11, pp. 4847–4854, Jun. 2013, PMID: 23616092.

[11] C. Oliveira, J. Machado da Silva, I. Trindade, and F. Martins, "Characterization of the electrode-skin impedance of textile electrodes," in *2014 Conference on Design of Circuits and Integrated Circuits (DCIS)*, Nov. 2014, pp. 1–6.

[12] F. Le Floch, S. Bernard, G. Bontorin, F. Soulier, and G. Cathebras, "Global strategy to guaranty dependability of electrical medical implanted devices," in *2011 5th International IEEE/EMBS Conference on Neural Engineering (NER)*, 2011, pp. 515–518.

[13] N. Hunn, "The market for smart wearable technology," WiFore Consulting, Report, Feb. 2015.

[14] Qualcomm. (2015) Xprize. [Online]. Available: http://tricorder.xprize.org/

[15] Scanadu. (2015) Scanadu scout tm. [Online]. Available: https://www.scanadu.com/products/vitals

[16] V. Inc. (2015) Devices used for medical applications. [Online]. Available: http://vandrico.com/wearables/device-categories/application/medical

[17] Denise Gershbein (Frog) and Blair Palmer (Unicef Innovation SF). (2015) Innovating for impact: Wearables for good. [Online]. Available: http://wearablesforgood.com/innovating-for-impact-wearables-for-good/

[18] J. Webster, *Medical instrumentation: application and design*. John Wiley & Sons, 2009.

[19] F. Lorussi, W. Rocchia, E. Scilingo, A. Tognetti, and D. De Rossi, "Wearable, redundant fabric-based sensor arrays for reconstruction of body segment posture," *Sensors Journal, IEEE*, vol. 4, no. 6, pp. 807–818, Dec. 2004.

[20] "IEEE standard for signal and test definition - redline," *IEEE Std 1641-2010 (Revision of IEEE Std 1641-2004) - Redline*, pp. 1–336, 2010.

[21] E. P. Scilingo, A. Gemignani, R. Paradiso, N. Taccini, B. Ghelarducci, and D. De Rossi, "Performance evaluation of sensing fabrics for monitoring physiological and biomechanical variables," *Information Technology in Biomedicine, IEEE Transactions on*, vol. 9, no. 3, pp. 345 –352, Sep. 2005.

[22] R. Dobrescu, M. Dobrescu, D. Popescu, and H. Coanda, "Embedded wireless homecare monitoring system," in *eHealth, Telemedicine, and Social Medicine, 2009. eTELEMED '09. International Conference on*, feb. 2009, pp. 66 –71.

[23] V. Srovnal and M. Penhaker, "Health maintenance embedded systems in home care applications," in *Systems, 2007. ICONS '07. Second International Conference on*, april 2007, p. 17.

[24] A. Cheriyan, A. Jarvi, Z. Kalbarczyk, R. Iyer, and K. Watkin, "Pervasive real-time biomedical monitoring system," in *Biomedical and Pharmaceutical Engineering, 2009. ICBPE '09. International Conference on*, dec. 2009, pp. 1 –8.

[25] A. Lymberis and A. Dittmar, "Advanced wearable health systems and applications-research and development efforts in the european union," *Engineering in Medicine and Biology Magazine, IEEE*, vol. 26, no. 3, pp. 29–33, 2007.

[26] N. Noury, A. Dittmar, C. Corroy, R. Baghai, J. Weber, D. Blanc, F. Klefstat, A. Blinovska, S. Vaysse, and B. Comet, "Vtamn-a smart clothe for ambulatory remote monitoring of physiological parameters and activity," in *Engineering in Medicine and Biology Society, 2004. IEMBS'04. 26th Annual International Conference of the IEEE*, vol. 2. IEEE, 2004, pp. 3266–3269.

[27] A. Pantelopoulos and N. Bourbakis, "A survey on wearable sensor-based systems for health monitoring and prognosis," *Systems, Man, and Cybernetics, Part C: Applications and Reviews, IEEE Transactions on*, vol. 40, no. 1, pp. 1–12, 2010.

[28] R. Dias and J. M. d. Silva, "A flexible wearable sensor network for bio-signals and human activity monitoring," *Wearable and Implantable Body Sensor Networks Workshops (BSN Workshops), 11th International Conference on*, pp. 17–22, 2014.

[29] The United Kingdom EVAR Trial Investigators, "Endovascular versus open repair of abdominal aortic aneurysm," *New England Journal of Medicine*, vol. 362, no. 20, pp. 1863–1871, 2010.

[30] C. Oliveira, J. Machado da Silva, I. Trindade, and F. Martins, "Characterization of the electrode-skin impedance of textile electrodes," in *2014 Conference on Design of Circuits and Integrated Circuits (DCIS)*, Nov. 2014, pp. 1–6.

[31] C. Oliveira, N. Almeida, and J. Machado da Silva, "A stent-graft endoleakage monitor: Telemetry system based on inductive-coupling transmission for implantable pressure sensors," in *Bioengineering (ENBENG), 2013 IEEE 3rd Portuguese Meeting in*, 2013, pp. 1–4.

[32] I. Trindade, F. Martins, R. Dias, C. Oliveira, and J. Machado da Silva, "Novel textile systems for the continuous monitoring of vital signals: design and characterization," in *2015 37th Annual International Conference of the IEEE Engineering in Medicine and Biology Society (EMBC)*, Aug. 2015, pp. 3743–3746.

[33] B. Katzen and A. MacLean, "Complications of endovascular repair of abdominal aortic aneurysms: A review," *CardioVascular and Interventional Radiology*, vol. 29, pp. 935–946, 2006.

[34] B. Sonesson, N. Dias, M. Malina, P. Olofsson, D. Griffin, B. Lindblad, and K. Ivancev, "Intra-aneurysm pressure measurements in successfully excluded abdominal aortic aneurysm after endovascular repair," *Journal of Vascular Surgery*, vol. 37, no. 4, pp. 733 – 738, 2003.

[35] T. Ohki, K. Ouriel, P. G. Silveira, B. Katzen, R. White, F. Criado, and E. Diethrich, "Initial results of wireless pressure sensing for endovascular aneurysm repair: The apex trial–acute pressure measurement to confirm aneurysm sac exclusion," *Journal of Vascular Surgery*, vol. 45, no. 2, pp. 236–242, 2007.

[36] C. H. Timaran, T. Ohki, F. J. Veith, E. C. Lipsitz, N. J. G. III, S. J. Rhee, M. B. Malas, W. D. Suggs, and J. P. Pacanowski, "Influence of type II endoleak volume on aneurysm wall pressure and distribution in an experimental model," *Journal of Vascular Surgery*, vol. 41, no. 4, pp. 657–663, 2005.

[37] F. Springer, R. W. Günther, and T. Schmitz-Rode, "Aneurysm Sac Pressure Measurement with Minimally Invasive Implantable Pressure Sensors: An Alternative to Current Surveillance Regimes after EVAR?" *Cardiovasc Intervent Radiol*, vol. 31, no. 3, pp. 460–467, 2008.

[38] C. J. Parsa, M. A. Daneshmand, B. Lima, K. Balsara, R. L. McCann, and G. C. Hughes, "Utility of remote wireless pressure sensing for endovascular leak detection after endovascular thoracic aneurysm repair," *The Annals of Thoracic Surgery*, vol. 89, no. 2, pp. 446 – 452, 2010.

[39] R. Milner, K. Kasirajan, and E. L. Chaikof, "Future of endograft surveillance," *Seminars in Vascular Surgery*, vol. 19, no. 2, pp. 75 – 82, 2006.

[40] K. Finkenzeller, *RFID Handbook: Fundamentals and Applications in Contactless Smart Cards and Identification*, 2nd ed. John Wiley & Sons, Ltd, Jul. 2003.

[41] J. A. Kaufman, S. C. Geller, D. C. Brewster, C. M. Fan, R. P. Cambria, G. M. LaMuraglia, J. P. Gertler, W. M. Abbott, and A. C. Waltman, "Endovascular repair of abdominal aortic aneurysms current status and future directions," *American Journal of Roentgenology*, vol. 175, no. 2, p. 289–302, 2000.

[42] C. Oliveira, N. Almeida, and J. Machado da Silva, *Studies in Health Technology and Informatics; pHealth 2012 - Proceedings of the 9th International Conference on Wearable Micro and Nano Technologies for Personalized Health*. IOS Press, 2012, vol. 177, ch. Inductive coupling system for endovascular aneurysm repair monitoring, pp. 101–6.

[43] "Blood pressure measurement devices (sphygmomanometers)-accuracy," U.S. Department of Health and Human Services, Report CPG 7124.23, 18 Feb. 2005.

[44] J. Potkay, "Long term, implantable blood pressure monitoring systems," *Biomedical Microdevices*, vol. 10, pp. 379–392, 2008.

[45] S. S. Mohan, M. del Mar Hershenson, S. P. Boyd, and T. H. Lee, "Simple accurate expressions for planar spiral inductances," *Solid-State Circuits, IEEE Journal of*, vol. 34, no. 10, p. 1419–1424, 1999.

[46] G. Hartsgrove, A. Kraszewski, and A. Surowiec, "Simulated biological materials for electromagnetic radiation absorption studies," *Bioelectromagnetics*, vol. 8, no. 1, pp. 29–36, 1987.

[47] A. Ingelman-Sundberg and E. Odeblad, "Radio frequency absorption in tissues with special reference to diagnostic applications in gynaecology," *BJOG: An International Journal of Obstetrics & Gynaecology*, vol. 72, no. 6, pp. 940–945, 1965.

[48] M. Yvanoff and J. Venkataraman, "A feasibility study of tissue characterization using lc sensors," *Antennas and Propagation, IEEE Transactions on*, vol. 57, no. 4, pp. 885 –893, april 2009.

[49] M. Narendran and M. S. Baggish, "Mean distance between primary trocar insertion site and major retroperitoneal vessels during routine laparoscopy," *Journal of gynecologic surgery*, vol. 18, no. 4, p. 121–127, 2002.

[50] C. C. Oliveira and J. Machado da Silva, "Towards a dependable cardiovascular surveillance system," in *The International Conference on Health Informatics*, ser. IFMBE Proceedings, Y.-T. Zhang, Ed. Springer International Publishing, Jan. 2014, no. 42, pp. 118–121.

[51] P. Kligfield, L. S. Gettes, J. J. Bailey, R. Childers, B. J. Deal, E. W. Hancock, G. v. Herpen, J. A. Kors, P. Macfarlane, D. M. Mirvis, O. Pahlm, P. Rautaharju, and G. S. Wagner, "Recommendations for the Standardization and Interpretation of the Electrocardiogram Part I: The Electrocardiogram and Its Technology: A Scientific Statement From the American Heart Association Electrocardiography and Arrhythmias Committee, Council on Clinical Cardiology; the American College of Cardiology Foundation; and the Heart Rhythm Society Endorsed by the International Society for Computerized Electrocardiology," *Circulation*, vol. 115, no. 10, pp. 1306–1324, Mar. 2007.

[52] M. K. Delano and C. G. Sodini, "A long-term wearable electrocardiogram measurement system," in *2013 IEEE International Conference on Body Sensor Networks (BSN)*, May 2013, pp. 1–6.

[53] N. Amour, A. Hersi, N. Alajlan, Y. Bazi, and H. AlHichri, "Implementation of a Mobile Health System for Monitoring ECG signals," Academy of Science and Engineering,USA, Working Paper, Jan. 2015.

[54] PTC, "Meeting international standards for medical device reliability and risk management," Quality in Medical Device, PTC, Tech. Rep., 2012.

[55] P. Binkley, "Predicting the potential of wearable technology," *Engineering in Medicine and Biology Magazine, IEEE*, vol. 22, no. 3, pp. 23 – 27, Jun. 2003.

[56] M. Chan, D. Estève, J. Fourniols, C. Escriba, and E. Campo, "Smart wearable systems: Current status and future challenges," *Artificial intelligence in medicine*, Nov. 2012.

[57] ANSI/VITA 51.1-2008, "Reliability Prediction MIL-HDBK 217 Subsidiary Specification," in *American National Standards Institute (ANSI)*, 2008.

[58] R. C. Fries, *Reliable design of medical devices*. Boca Raton: CRC/Taylor & Francis, 2006.

[59] H. Kerkhoff, "New view requirements for Analogue/MS IPs for dependability optimization in heterogeneous SoC design," in *Mixed-Signals, Sensors and Systems Test Workshop (IMS3TW), 2011 IEEE 17th International*, May 2011, pp. 1–6.

[60] M. Khan and H. Kerkhoff, "A system-level platform for dependability enhancement and its analysis for mixed-signal SoCs," in *2011 IEEE 14th International Symposium on Design and Diagnostics of Electronic Circuits Systems (DDECS)*, Apr. 2011, pp. 17–22.

[61] "Council directive 90/385/EEC of 20 june 1990 on the approximation of the laws of the member states relating to active implantable medical devices," 1990.

[62] A. Avizienis, J.-C. Laprie, and B. Randell, "Dependability and its threats: A taxonomy," in *Building the Information Society*, ser. IFIP International Federation for Information Processing, R. Jacquart, Ed. Springer US, Jan. 2004, no. 156, pp. 91–120.

[63] H. Kerkhoff and J. Wan, "Dependable digitally-assisted mixed-signal IPs based on integrated self-test amp; self-calibration," in *Mixed-Signals, Sensors and Systems Test Workshop (IMS3TW), 2010 IEEE 16th International*, Jun. 2010, pp. 1–6.

[64] M. Porter, P. Gerrish, L. Tyler, S. Murray, R. Mauriello, F. Soto, G. Phetteplace, and S. Hareland, "Reliability considerations for implantable medical ICs," in *Reliability Physics Symposium, 2008. IRPS 2008. IEEE International*, 2008, pp. 516–523.

[65] R. Schmitt and T. Zentis, "New approach for risk analysis and management in medical engineering," in *Reliability and Maintainability Symposium (RAMS), 2011 Proceedings - Annual*, 2011, pp. 1–6.

[66] H. Lee, K. Park, B. Lee, J. Choi, and R. Elmasri, "Issues in data fusion for healthcare monitoring," in *Proceedings of the 1st international conference on PErvasive Technologies Related to Assistive Environments*, ser. PETRA '08. New York, NY, USA: ACM, 2008.

[67] E. Kenneth, A. U. Rajendra, N. Kannathal, and C. M. Lim, "Data fusion of multimodal cardiovascular signals," in *Engineering in Medicine and Biology Society, 2005. IEEE-EMBS 2005. 27th Annual International Conference of the*, 2005, pp. 4689 –4692.

[68] T. Klingeberg and M. Schilling, "Mobile wearable device for long term monitoring of vital signs," *Computer Methods and Programs in Biomedicine*, vol. 106, no. 2, pp. 89–96, 2012.

[69] H. Alemzadeh, Z. Jin, Z. Kalbarczyk, and R. Iyer, "An embedded reconfigurable architecture for patient-specific multi-paramater medical monitoring," in *2011 Annual International Conference of the IEEE Engineering in Medicine and Biology Society,EMBC*, 2011, pp. 1896–1900.

[70] H. Medjahed, D. Istrate, J. Boudy, J.-L. Baldinger, and B. Dorizzi, "A pervasive multisensor data fusion for smart home healthcare monitoring," in *2011 IEEE International Conference on Fuzzy Systems (FUZZ)*, 2011, pp. 1466–1473.

[71] M. Khan and H. Kerkhoff, "SoC mixed-signal dependability enhancement: A strategy from design to end-of-life," in *2011 IEEE International Symposium on Defect and Fault Tolerance in VLSI and Nanotechnology Systems (DFT)*, Oct. 2011, pp. 374–381.

[72] J. Wan and H. Kerkhoff, "Boosted gain programmable opamp with embedded gain monitor for dependable SoCs," in *SoC Design Conference (ISOCC), 2011 International*, Nov. 2011, pp. 294–297.

[73] G. Rodrigues, V. Alves, R. Franklin, and L. Laranjeira, "Dependability analysis in the ambient assisted living domain: An exploratory case study," in *2010 Fourth Brazilian Symposium on Software Components, Architectures and Reuse (SBCARS)*, Sep. 2010, pp. 150–159.

[74] Y. Hovakeemian, K. Naik, and A. Nayak, "A survey on dependability in body area networks," in *2011 5th International Symposium on Medical Information Communication Technology (ISMICT)*, Mar. 2011, pp. 10–14.

[75] J. Wu and J. Tong, "An analysis on information dependability measurement of wireless sensor networks," in *The Sixth World Congress on Intelligent Control and Automation, 2006. WCICA 2006*, vol. 1, Jan. 2006, pp. 90–93.

[76] F. Soulier, F. Le Floch, S. Bernard, and G. Cathebras, "New dependability approach for implanted medical devices," in *2009 International Conference on Microelectronics (ICM)*, 2009, pp. 18–21.

[77] G. Cathebras, F. Le Floch, S. Bernard, and F. Soulier, "Dependability: a challenge for electrical medical implants," in *2010 Annual International Conference of the IEEE Engineering in Medicine and Biology Society (EMBC)*, 2010, pp. 5923–5926.

[78] C. Abkai and J. Hesser, "Reasoning and risk assessment based on real-time physiological simulations and dependable vital parameter monitoring," in *World Congress on Medical Physics and Biomedical Engineering, September 7 - 12, 2009, Munich, Germany*, ser. IFMBE Proceedings, O. Dössel and W. C. Schlegel, Eds. Springer Berlin Heidelberg, Jan. 2010, no. 25/4, pp. 1299–1302.

[79] A. L. Goldberger, L. A. N. Amaral, L. Glass, J. M. Hausdorff, P. C. Ivanov, R. G. Mark, J. E. Mietus, G. B. Moody, C.-K. Peng, and H. E. Stanley, "PhysioBank, PhysioToolkit, and PhysioNet Components of a New Research Resource for Complex Physiologic

Signals," *Circulation*, vol. 101, no. 23, pp. e215–e220, Jun. 2000. [Online]. Available: http://circ.ahajournals.org/content/101/23/e215

[80] J. Welch, P. Ford, R. Teplick, and R. Rubsamen, "The massachusetts general hospital-marquette foundation hemodynamic and electrocardiographic database – comprehensive collection of critical care waveforms," *J Clinical Monitoring*, vol. 7, no. 1, pp. 96–97, 1991.

[81] S. Leung and D. Lam, "Performance of printed polymer-based RFID antenna on curvilinear surface," *IEEE Transactions on Electronics Packaging Manufacturing*, vol. 30, no. 3, pp. 200–205, Jul. 2007.

[82] D. C. Brewster and et. al, "Guidelines for the treatment of abdominal aortic aneurysms: Report of a subcommittee of the joint council of the american association for vascular surgery and society for vascular surgery," *Journal of Vascular Surgery*, vol. 37, no. 5, pp. 1106–1117, May 2003.

[83] C. Assambo, A. Baba, R. Dozio, and M. J. Burke, "Determination of the parameters of the skin-electrode impedance model for ECG measurement," in *Proceedings of the 6th WSEAS international conference on electronics, hardware, wireless and optical communications, Corfu Island, Greece*, 2007, p. 90–95.

[84] L. Beckmann, C. Neuhaus, G. Medrano, N. Jungbecker, M. Walter, T. Gries, and S. Leonhardt, "Characterization of textile electrodes and conductors using standardized measurement setups," *Physiological Measurement*, vol. 31, no. 2, p. 233, Feb. 2010.

[85] M. R. Neuman, "Biopotential electrodes," in *The Biomedical Engineering Handbook, Second Edition. 2 Volume Set*, J. Bronzino, Ed. CRC Press, Dec. 1999.

[86] A. Albulbul and A. Chan, "Electrode-skin impedance changes due to an externally applied force," in *2012 IEEE International Symposium on Medical Measurements and Applications Proceedings (MeMeA)*, May 2012, pp. 1–4.

[87] V. Mihajlovic and B. Grundlehner, "The effect of force and electrode material on electrode-to-skin impedance," in *2012 IEEE Biomedical Circuits and Systems Conference (BioCAS)*, 2012, pp. 57–60.

[88] B. Taji, S. Shirmohammadi, V. Groza, and I. Batkin, "Impact of skin–electrode interface on electrocardiogram measurements using conductive textile electrodes," *IEEE Transactions on Instrumentation and Measurement*, vol. 63, no. 6, pp. 1412–1422, Jun. 2014.

[89] M. Puurtinen, S. Komulainen, P. Kauppinen, J. Malmivuo, and J. A. K. Hyttinen, "Measurement of noise and impedance of dry and wet textile electrodes, and textile electrodes with hydrogel," in *28th Annual International Conference of the IEEE Engineering in Medicine and Biology Society, 2006. EMBS '06*, 2006, pp. 6012–6015.

[90] T. Degen and H. Jäckel, "Enhancing interference rejection of preamplified electrodes by automated gain adaption," *IEEE transactions on bio-medical engineering*, vol. 51, no. 11, pp. 2031–2039, Nov. 2004.

[91] A. Calabria, "Understanding Lead-Off Detection in ECG," Texas Instruments, Tech. Rep., May 2012.

[92] I. G. Trindade, P. Spranger, F. Martins, R. Miguel, and M. S. Silva, "Fully integrated embroidery process for smart textiles," in *Proc. of the Nanotech conference*. Washington D.C., USA: Nanotech 2014, Jun. 2014, vol. 3, pp. 65–68.

[93] A. J. E. Salazar, J. Machado da Silva, M. Correia, and B. J. Mendes, "Built-in self-testing methodology and infrastructure for an emg monitoring sensor module," *IARIA International Journal On Advances in Systems and Measurements*, vol. 7, no. 1 & 2, 2014.

[94] S. Hao, "A self-calibration method for an implantable displacement sensor," in *Microwaves, Communications, Antennas and Electronics Systems (COMCAS), 2013 IEEE International Conference on*, Oct 2013, pp. 1–5.

[95] G. Lesbros and M. Sawan, "Wireless implantable sensing device for in-vivo monitoring of electrode-tissues contact variation," in *Computer Architecture for Machine Perception and Sensing, 2006. CAMP 2006. International Workshop on*, Aug 2006, pp. 67–68.

[96] C. C. Oliveira and J. M. d. Silva, "A fuzzy logic approach for highly dependable medical wearable systems," in *Mixed-Signal Testing Workshop (IMSTW), 2015 20th International*, Jun. 2015, pp. 1–5.

[97] M. Cinque, A. Coronato, and A. Testa, "Dependable Services for Mobile Health Monitoring Systems," *Int. J. Ambient Comput. Intell.*, vol. 4, no. 1, pp. 1–15, Jan. 2012.

[98] C. Oliveira and J. Machado da Silva, "Fault detection system for a stent-graft endoleakage monitor," in *Mixed-Signals, Sensors and Systems Test Workshop (IMS3TW), 2012 18th International*, 2012, pp. 17–21.

[99] M. Elgendi, B. Eskofier, S. Dokos, and D. Abbott, "Revisiting QRS Detection Methodologies for Portable, Wearable, Battery-Operated, and Wireless ECG Systems," *PLoS ONE*, vol. 9, no. 1, p. e84018, Jan. 2014.

[100] J. Pan and W. J. Tompkins, "A Real-Time QRS Detection Algorithm," *IEEE Transactions on Biomedical Engineering*, vol. BME-32, no. 3, pp. 230–236, Mar. 1985.

[101] M. Breeuwer, S. de Putter, U. Kose, L. Speelman, K. Visser, F. Gerritsen, R. Hoogeveen, R. Krams, H. van den Bosch, J. Buth, T. Gunther, B. Wolters, E. van Dam, , and F. van de Vosse, "Towards patient-specific risk assessment of abdominal aortic aneurysm," *Med. Biol. Eng. Comput.*, vol. 46, no. 11, pp. 1085—-1095, Nov. 2008.

[102] P. M. Nitzan, A. Babchenko, and B. Khanokh, "Verylow frequency variability in arterial blood pressure and blood volume pulse," *Med. Biol. Eng. Comput.*, vol. 37, no. 1, pp. 54—-58, Jan. 1999.

[103] J. J. Ricotta, J. Pagan, M. Xenos, Y. Alemu, S. Einav, and D. Bluestein, "Cardiovascular disease management: the need for better diagnostics," *Med. Biol. Eng. Comput.*, vol. 46, no. 11, pp. 1059—-1068, Nov. 2008.

[104] R. Kanagasabay, H. Gajraj, L. Pointon, and R. A. Scott, "Co-morbidity in patients with abdominal aortic aneurysm," *Journal of medical screening*, vol. 3, no. 4, pp. 208–210, 1996.

[105] N. Sakalihasan, R. Limet, and O. Defawe, "Abdominal aortic aneurysm," *The Lancet*, vol. 365, no. 9470, pp. 1577–1589, Apr. 2005.

[106] V. Riambau, R. J. F. Laheij, C. GarcSía-Madrid, and G. Sánchez-Espin, "The Association Between Co-morbidity and Mortality After Abdominal Aortic Aneurysm Endografting in Patients Ineligible for Elective Open Surgery," *European Journal of Vascular and Endovascular Surgery*, vol. 22, no. 3, pp. 265–270, 2001.

[107] K. Becker, B. Thull, H. Käsmacher-Leidinger, J. Stemmer, G. Rau, G. Kalff, and H.-J. Zimmermann, "Design and validation of an intelligent patient monitoring and alarm system based on a fuzzy logic process model," *Artificial Intelligence in Medicine*, vol. 11, no. 1, pp. 33–53, Sep. 1997.

[108] J. H. T. Bates and M. P. Young, "Applying Fuzzy Logic to Medical Decision Making in the Intensive Care Unit," *American Journal of Respiratory and Critical Care Medicine*, vol. 167, no. 7, pp. 948–952, Apr. 2003.

[109] M. Mahfouf, M. F. Abbod, and D. A. Linkens, "A survey of fuzzy logic monitoring and control utilisation in medicine," *Artificial Intelligence in Medicine*, vol. 21, no. 1–3, pp. 27–42, Jan. 2001.

[110] M. F. Abbod, D. G. von Keyserlingk, D. A. Linkens, and M. Mahfouf, "Survey of utilisation of fuzzy technology in Medicine and Healthcare," *Fuzzy Sets and Systems*, vol. 120, no. 2, pp. 331–349, Jun. 2001.

[111] L. A. Zadeh, "Fuzzy Logic," *Computer*, vol. 21, no. 4, pp. 83–93, Apr. 1988.

[112] M. F. Møller, "A scaled conjugate gradient algorithm for fast supervised learning," *NEURAL NETWORKS*, vol. 6, no. 4, pp. 525–533, 1993.

[113] L. Breiman, J. Friedman, R. Olshen, and C. Stone, *Classification and Regression Trees*. Belmont, CA: Wadsworth, 1984.

[114] V. M. Karjalainen J, "Fever and cardiac rhythm," *Arch Intern Med.*, vol. 146, no. 6, pp. 1169–71, Jun. 1986.

[115] H. G. Stratigopoulos and Y. Makris, "Error moderation in low-cost machine-learning-based analog/rf testing," *IEEE Transactions on Computer-Aided Design of Integrated Circuits and Systems*, vol. 27, no. 2, pp. 339–351, Feb 2008.

[116] F. D. dos Santos Alves, "Semi-passive tag sensor for wireless monitoring of endovascular stent-grafts," October 2015, faculdade de Engenharia da Universidade do Porto.

[117] "Directive 1999/519/ce, 12 july 1999," European Union Parliament and Council, Official Journal of European Community 7, 12 July 1999.

[118] SEMCAD X, "Reference manual for the semcad simulation platform for electromagnetic compatibility, antenna design and dosimetry."

[119] H. A. Wheeler, "Simple inductance formulas for radio coils," *Proc. Inst. Radio Eng.*, vol. 16, no. 10, p. 1398–1400, 1928.